Experimental study on the development of abrasion at offshore concrete structures in ice conditions

J.N.W. Tijsen

Delft University of Technology

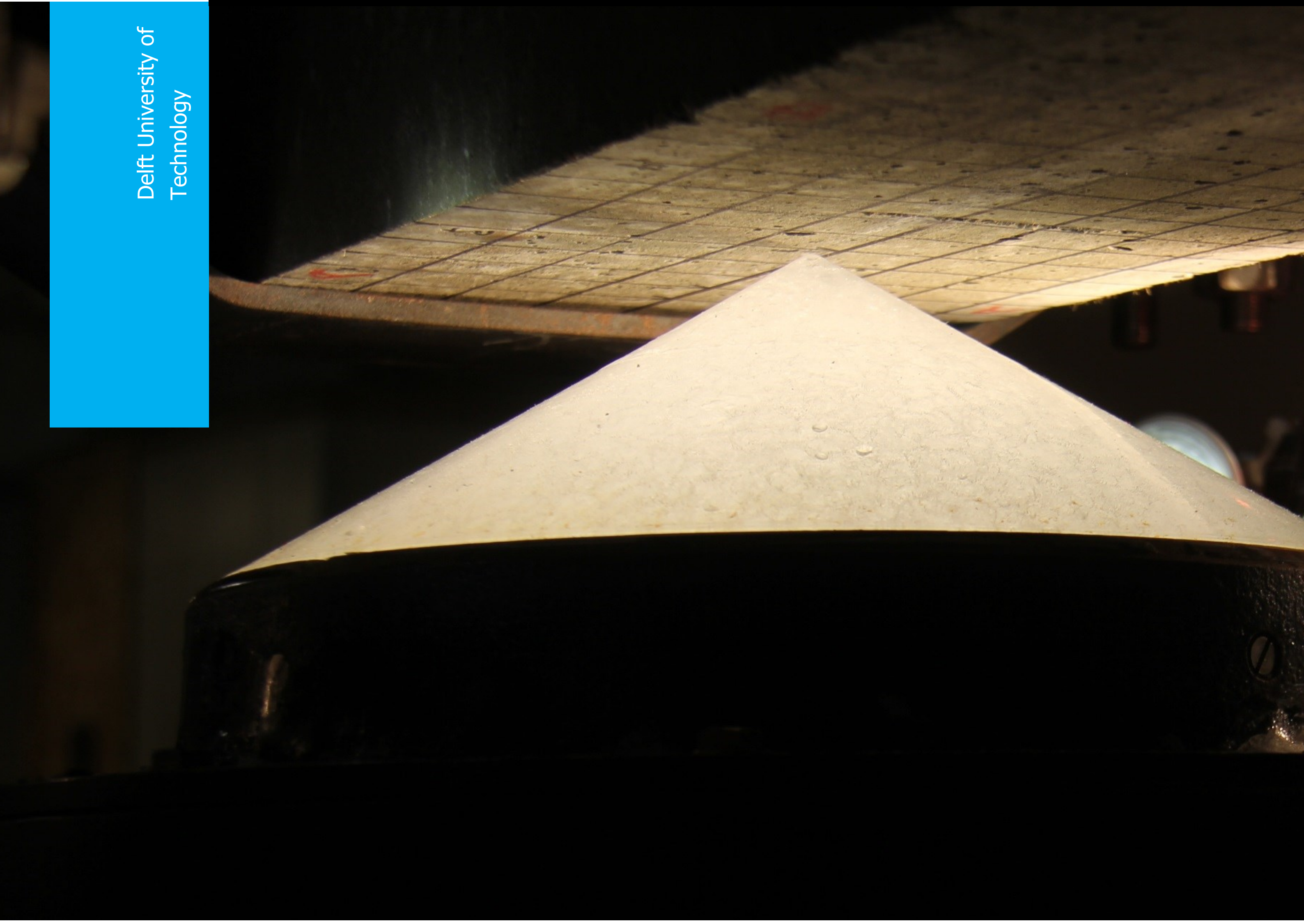

TU Delft
Delft University of Technology

STePS2

DELFT UNIVERSITY OF TECHNOLOGY

Experimental study on the development of abrasion at offshore concrete structures in ice conditions

Master of Science Thesis

For the degree of Master of Science in Offshore and Dredging Engineering

J.N.W. Tijsen

February 26, 2015

Faculty of Mechanical, Maritime and Materials Engineering (3mE),
Delft University of Technology

Delft University of Technology
Department of
Structural Dynamics

The undersigned hereby certify that they have read and recommend to the Faculty of Mechanical, Maritime and Materials Engineering (3mE) for acceptance a thesis entitled

Experimental study on the development of abrasion at offshore concrete structures in ice conditions

By

J.N.W. Tijsen

In partial fulfilment of the requirements for the degree of

Master of Science in Offshore & Dredging Engineering

Supervisor(s): Dated: February 26, 2015

____
Prof.dr. A.Metrikine

____
Dr. S.E. Bruneau

____
Prof.Dr.Ir. H.E.J.G. Schlangen

____
Dr. A.B. Cammaert

____
Ir. J.S. Hoving

Abstract

The oil and gas industry have an increasing interest to move their activities into the Arctic, because of the increasing demand for global energy and large amount of hydrocarbons available. These activities involve the construction of concrete structures, such as the gravity based structures at Sakhalin, in Eastern-Russia. Examples among civil structures are the Confederation Bridge in Canada or Sydostbrotten lighthouse in Sweden. Each of these structures experience severe ice conditions and abrasive ice loadings. Abrasion of Concrete structures in marine environments due to interaction with sea ice leads to erosion and damage.

Industry is interested in characterizing the ice abrasion phenomenon so that abrasion risk can be managed. The experiments conducted in this work have an exploratory character in order to identify the abrasion phenomenon and qualitatively observe the corresponding processes. The tests are a simulation of micro scale ice-structure interaction and involve the translation of concrete samples while subject to lateral impingement of conical ice samples. Loads in both axes are measured so that tangential and normal force relationships can be examined while the ice samples are catastrophically crushed. The paper divides the interaction into abrasive loading regions and loading orders intentionally to facilitate analysis of the abrasion process. The wear of the concrete surface is described using visual observation and surface feature measurements Concrete of varying mixtures has been examined and the effects on the concrete surfaces from repeated static ice-bonding and bond-breakage is analysed.

Figure 1 Experimental testing of ice-concrete abrasion

The results of experimental data indicate compression and tangential loading like dry and wet friction but also stick-slip loading. The data also indicates wear at the surface of the two concrete samples. The results in combination with literature lead to an identification of primary and secondary order of loading, and separation of loading regions at the structure. The report includes a case study of the construction of a concrete pile of for example an offshore platform which illustrates the risk of ice-concrete abrasion and the application of protective plating. Also, the report touches upon the numerical (lattice) models of ice and concrete. The experimental complement of the master thesis has been conducted under the flag of the STePS[2] research project within the laboratories of the Memorial University of Newfoundland, Canada.

Figure 2 Confederation bridge, Canada (left) and Sakhalin platform, Eastern-Russia (right) in ice conditions

PREFACE

Humans challenge nature by moving into the Arctic - one of the most extreme environments on earth and the ice abrasion phenomenon is a significant part of the challenge. Sometimes, the human exploration drift makes me wonder what comes after the Arctic.. Do you know? The exciting pioneering task drives me to research and contribute to beneficiary technology.

The report represents the completing piece of my Master of Science studies at the Delft University of Technology (DUT), the Netherlands. I wrote the report in two stages. The experimental stage from proposal to preliminary results within the STePS^2 research group at the Memorial University of Newfoundland (MUN), St. John's from May-August, 2014. The second stage, involving a full analysis at the DUT from September, 2014 - February, 2015. Industry's interest came from the ice abrasion phenomenon in the oil and gas industry, but the field of ice abrasion also applies on the civil industry, for example on bridges or lighthouses. The Arctic challenges are diverse and new terrain. My curiosity drove me to find out what the abrasion challenge truly means and I wrote a proposal with Dr. Steve Bruneau and Dr. Bruce Colbourne in May, 2014.

I also enjoyed the opportunity of publishing our experimental work to the POAC'15 conference (see Appendix VIII: Publication (POAC'15)), deliver a modest contribution to science and obtain experience on writing to the scientific community. Also, I hope my work can strengthen the bridge between the MUN and DUT.

ACKNOWLEDGEMENTS

My gratitude goes to Dr. Andrei Metrikine, Ir. Jeroen Hoving, Dr. Erik Schlangen, Dr. Gus Cammaert and Dr. Steve Bruneau for being part of my graduation committee and their helpful guidance on the study, special appreciation goes to Dr. Steve Bruneau and Dr. Gus Cammaert who were fantastic daily supervisors, mentors along the lines of progress in St. John's, Canada and Delft, The Netherlands.

I'd like to thank Dr. Bruce Colbourne at the Memorial University of Newfoundland, for his enthusiasm, fruitful thoughts on the experimental study and contribution on the paper submission to the POAC'15 conference. Lots of thanks goes to Jake Harris, my buddy and support during the execution of the experiments, and limitless effort to keep up with testing. I thank Dr. Bruce Quinton on his guidance on the operations of the bi-axial apparatus also known as the Quintonator. Also, I'd like to thank Dr. Amgad Hussein and Dr. Assem Hassan at the Memorial University of Newfoundland for their guidance on the concrete mixture design. My thanks goes to Ir. Sander Dragt on his willingness to support and discuss the data on crushing, the report includes his contribution. Definitely not to forget, much appreciation goes to all staff within the laboratories of the Memorial University of Newfoundland who were very helpful, among them Craig Mitchell, Matt Curtis, Shawn Organ and Mark Pope.

My thanks goes to the STePS^2 research group for support and funding. Last but not least, my gratitude goes to my family and loved ones for their support during the study and writing, from scratch to full report.

TABLE OF CONTENTS

NOMENCLATURE

Symbol	Meaning	Unity
a	Angle of contact	Degrees (˚)
β	Ice cone angle	Degrees (˚)
Φ	Angle of external friction	Degrees (˚)
s_c	Global compression pressure	MPa
s_v	Global compression pressure	MPa
s_{global}	Global compression pressure	MPa
s_{local}	Local compression pressure	MPa
τ	Local shear stress	MPa
μ_d	Dynamic friction coefficient	-
a_i	Proportional amount of aggregates	-
A	Abrasion depth	mm
ABR	Abrasion rate	mm/km
A_n	Contact area	mm2
b	Abrasion rate of cement stone	mm/km
E_c	Energy per crushed volume	MPa
F_{mean}	Mean force	kN
F_n	Normal force	kN
F_s	Sliding force	kN
$f_{c,t}$	Tensile stress of concrete	N/mm2
f_{peak}	Peak frequency	Hz
h_m	Roughness average	μm
h_M	Roughness maximum peak heighth	μm
L	Abrasion loading	-
L_{cr}	Fracture length	μm
n_1	Number of ice impacts required for fracture	-
n_s	Number of ice impacts	-
p	Contact pressure	MPa
p_{crit}	Critical stress where fracture occurs	MPa
R	Abrasion resistance	-
R_a	Roughness average	μm
R_i	Aggregate radius	μm
R_p	Roughness maximum peak heighth	μm
S_r	Abrasion rate	mm/km
T	Temperature	˚C
V_c	Crushed volume	m3
v_n	Normal velocity	mm/s
v_s	Sliding velocity	mm/s
v_{ice}	Ice velocity	mm/s
W_n	Work in normal direction per sliding distance	J/mm

W_s	Work in sliding direction per sliding distance	J/mm
W_{total}	Total work per sliding distance	J/mm
x	Indentation (normal direction)	mm
z	Sliding distance (tangential direction)	mm

1. INTRODUCTION

Ice crushing and grinding along concrete structures threaten severely the structural integrity of the concrete. Long distances of ice may slide along structures exposed in harsh cold environments and abrade any layer of material in contact with ice. Thick steel shields at the Sakhalin platform are torn apart by hundreds of kilometres of crushing and grinding level ice as is shown in Figure 3.

FIGURE 3 (LEFT) STEEL SHIELDS AT SAKHALIN, RUSSIA (KIRHAUG J., 2013) AND (RIGHT) 8 YEARS CONCRETE ABRASION AT CONFEDERATION BRIDGE, CANADA (JACOBSEN S. ET AL., 2012)

Industry identifies the abrasion phenomenon and likes to characterise abrasion such that they are able to develop abrasion resistant materials.

1.1 PROBLEM DESCRIPTION

The main concrete abrasion process involves a high level of complexity, because ice is a heterogeneous material as is the composite concrete. The large number of variables makes it difficult to predict a trustworthy ice-concrete abrasion rate and thus estimate sufficient ice abrasion resistance in any concrete design. The high number of parameters makes it interesting to touch upon an effect analysis on the abrasion rate.

The abrasive process is driven by ice forces exerted on a concrete structure and makes one to focus on ice-structure interaction first. The combination of crushing and sliding is a particular failure mechanism of ice on offshore structures. Practically level ice on offshore structures is the main concern for general concrete abrasion, but other types of ice as iceberg grade ice or fresh water ice shouldn't be forgotten as potential concrete loading either. Ice loading itself is likely to be very dominant in a concrete abrasion rate, but other loadings as waves, current and wind may put ice loading in perspective. Also, freeze-thaw cycles and chloride migration may influence the mechanical properties of concrete and thus the abrasion rate as well. Last, the abrading and changing concrete surface affect the ice loading over the structure's lifetime and in return affect the concrete abrasion rate.

Besides that, concrete abrasion mainly occurs below water level, because above water level ice adheres to the concrete and act as protective layer. Below water level one is able to speak of wet abrasion conditions. The transition from wet to dry zone (splash zone) is disputable which conditions prevails. Dry abrasion condition does not mean no abrasion occurs and the 'protective' ice layer requires further investigation. High local pressures and scouring processes in the interface layer may reduce the protective effects of any adhered ice layer.

1.2 Purpose and objectives

The main objective is: Assess how the concrete abrasion initiate and develop due to ice-structure interaction. The investigation will result into an in-depth description of the problem. The information will be useful for application onto mitigation methods to reduce the abrasion risk or defining the interface of a numerical model.

Sub-objectives:

1. Identify the types of relevant ice-structure interaction for concrete abrasion.
2. Determine what type of mechanisms can deteriorate the concrete surface.
3. Determine what type of factors affect the concrete abrasion resistance.
4. Specify the threat of concrete abrasion to offshore structures.
5. Recommend a strategy to measure and reduce the risk of concrete abrasion.

The report intends to better define abrasive ice loading. Ice and concrete also share an interesting interaction property. They both tend to easily form hydro bonds and can create large adhesive forces. The ice loading definition is relevant in order to understand and simulate the ice abrasion process. Also, the report intends to better define concrete abrasion resistance. The separation in abrasion loading and resistance simplifies the problem. Loading depends on ice parameters and resistance on concrete parameters.

1.3 Methodology

The exploratory character makes the methodology slightly different from conventional routes of experimental work. Exploratory implies in this work, explore variation of several parameters without a hypothesis and observe the outcome. The reason to have this experimental work in place is to tune follow-up experiments with hypothesis and get a head start in the line of research.

Memorial University Newfoundland possesses a bi-axial apparatus in a large coldroom (-10 Celsius) as is shown in Figure 4 for an experimental program that previously investigates moving ice loads on steel panels. The apparatus has been adapted for ice-concrete tests and can simulate a combination of crushing and grinding conditions as in particular ice-structure interaction. The system has been designed to behave as stiff as possible, but under extreme values involved with ice loading, stiffness should be treated carefully in the data.

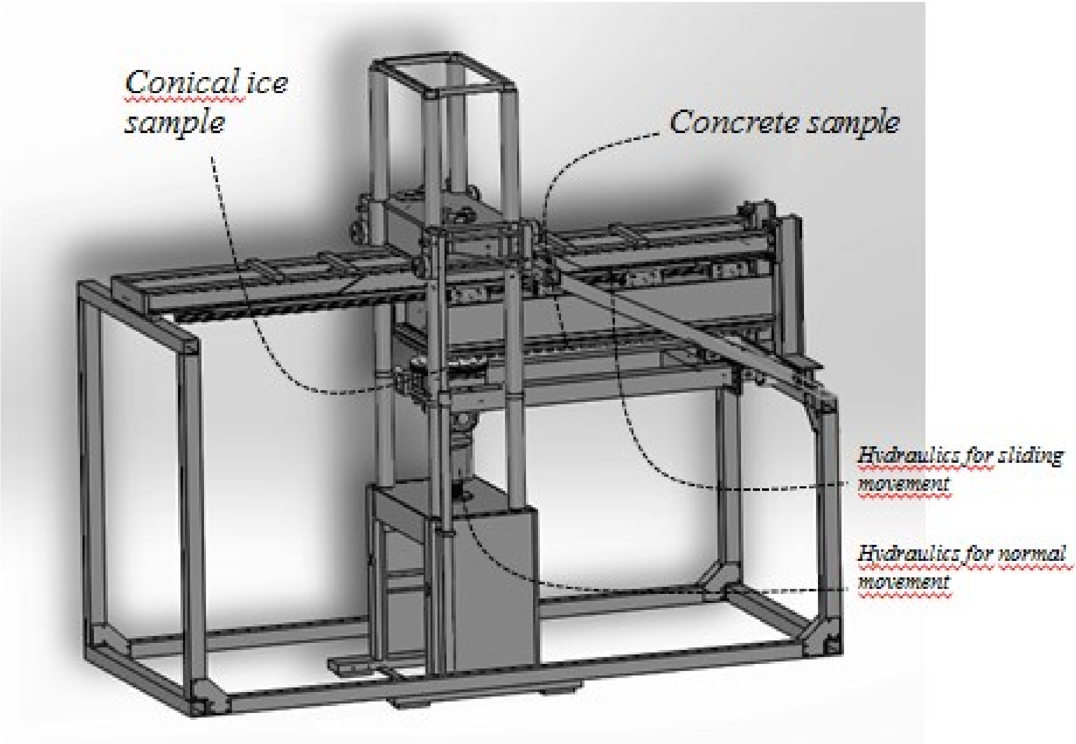

FIGURE 4 IMPRESSION OF BI-AXIAL APPARATUS

The system is able to simulate a microscopic process on a set point at the structure. The ice velocity and angle of contact will define the settings of the test apparatus. A schematization of the real scale situation is shown in Figure 5.

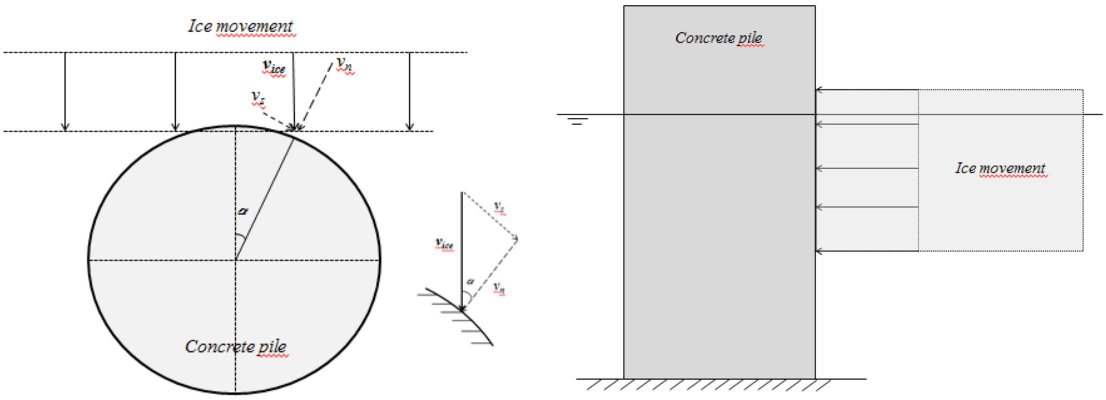

FIGURE 5 SCHEMATIZATION OF ICE LOADING, TOPVIEW (LEFT), ZOOM OF TOPVIEW ICE LOADING (MIDDLE) AND SIDEVIEW (RIGHT)

Conventional conical ice samples as used in this testing emphasizes simulation of iceberg grade ice. The ice samples are even of stronger quality due to strict procedures for fabrication, but main reason of following these procedures is to achieve a consistent ice quality over all of the ice samples. The consistency makes comparison between tests possible and more useful.

The very new way of ice-structure simulation allows one to better investigate ice loading in the laboratory and also its effects on for example a concrete surface. Crushing and grinding of ice over concrete may form a key to high similarity in abrasive processes projected from reality. Data output from these tests may provide new exciting insights in ice-structure interaction at micro level. The report will treat intentions, laboratory facilities and setups first, and steadily move to data output, discussions and conclusions.

1.4 SCOPE

The methodology is to theoretical explain the phenomenon concrete abrasion due to ice action on real-scale. Relate this to the exploratory experimental work done and come up with some relevant description of the data. The outcome of this report is not meant to achieve to be able to reduce the abrasion risk, but may provide an indication of the influence of several parameters. The scope is visualized in Figure 6.

The scope primary consist of the ice abrasion problem, but also consist of some pages on ice-concrete adhesion. Adhesion is a specific type of abrasion loading and is relevant contributor to abrasion under low ice velocities.

The primary order of abrasion loading is part of the scope and not the secondary order. The secondary order loading effects affect the long term abrasion resistance. Concluding insights from macroscopic to microscopic scale will improve the understanding and reduce the risk of the abrasion threat at the level of ice-structure interaction. A case study and a physical basis for a two materials lattice model illustrates the state of the art theory of abrasion.

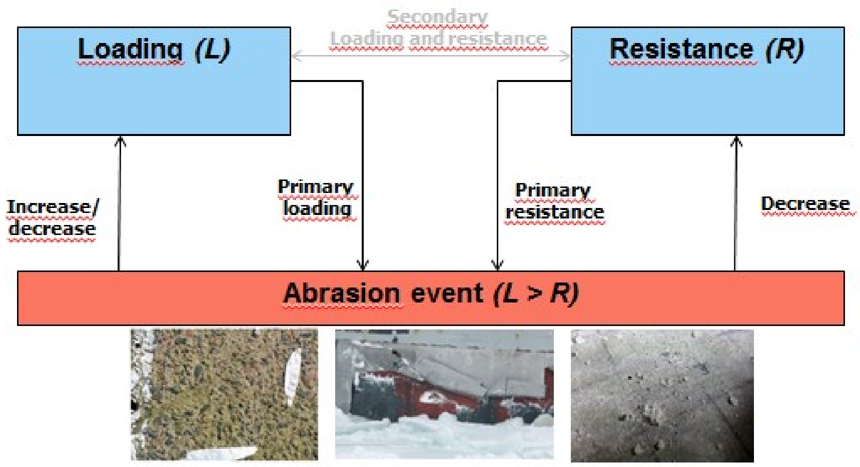

FIGURE 6 SCHEMATIZATION OF THE SCOPE. AN ABRASION EVENT CONSIST OF EXCEEDANCE OF THE ABRASION LOADING (L) OVER RESISTANCE (R). THE SECONDARY ORDER OF LOADING IS NOT PART OF THE SCOPE.

2. Theory of abrasion

2.1 Definition: Abrasion

The definition of concrete abrasion can vary per author and one should treat this values carefully. Abrasion is loss of surface material due to external loading. Important is to agree on a definition which suits for showing variation in loss of surface material reasonable well. Some authors measure surface material loss as weight and others attempt to characterize the spatial surface elevation. The use of abrasion definition by diverse industries should also increase caution on what is truly mend and captured with these values. The acceptation of a standard definition in the scientific world is thus a first step of developing standardization procedures as determination of abrasion sensitivity in cold environments. Higher detail of the texture changes provide insight in how the abrasion process affects the concrete surface, still, one must decide which parameters can characterize abrasion best. Abrasion might affect the shape of asperities, but might also increase the average abrasion depth and the first one is not visible in only an average surface elevation.

The most common definition is the integral of the surface elevation over a certain spatial area is zero (equal area above as under the line of average surface elevation), see Figure 7. The change of average surface elevation over time is defined as the abrasion rate. The average surface elevation does not provide any information about the height of asperities, thus sometimes a maximum (or minimum) value of the surface elevation has been added. The two parameters don't provide any information about the concentration of asperities or the shape of the asperities.

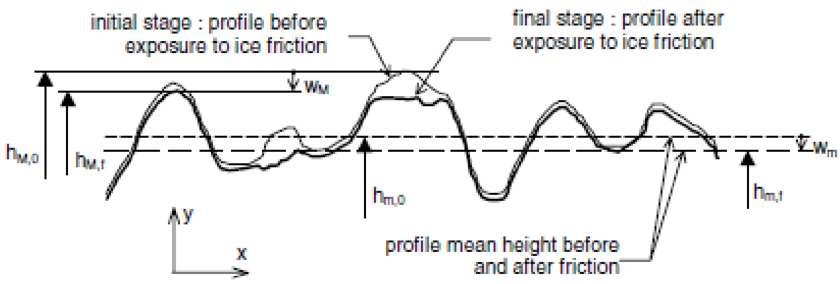

Figure 7 Maximum (h_M) and mean (h_m) height of a profile and calculation of the maximum (w_M) and mean (w_m) abrasion amount.

The derivation of the abrasion amount (or in general the average surface elevation) also varies per author and can be a certain line measurement (Itoh Y. et al., 1988) or a spatial measurement (Kirhaug J., 2013). The spatial measurement provides more representative values, but suitable measuring devices might not have been available for all authors. Two type of measuring methods are common: Contact and non-contact methods. Contact methods often uses a device with a needle or tiny point in a local reference system as shown in Figure 8. A large drawback of the contact method is potential damage on the concrete surface due to the grinding needle. The needle moves along a line and captures surface elevations at micro level.

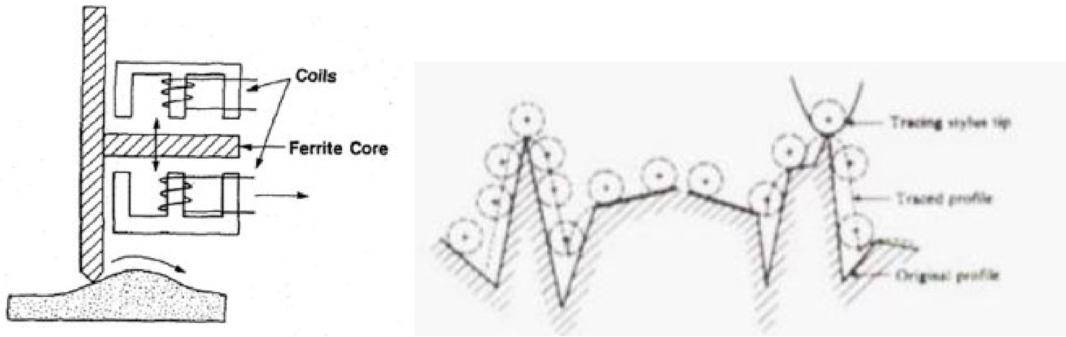

FIGURE 8 (LEFT) SCHEMATIC DIAGRAM OF LVDT STYLUS AND (RIGHT) DEVIATION IN MEASUREMENTS OF STYLUS TIP SIZE (KOBRICK R., ET AL., 2011)

The non-contact method uses for example radiation and reflection to capture the surface. The advantage is one is able to characterize a concrete surface area and delivers fast a high detail surface profile without any damage. The disadvantage is the datasets requires some experience to handle.

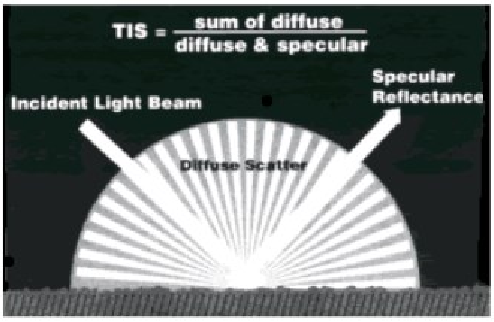

FIGURE 9 PRINCIPLE OF PHOTOGRAMMETRY. LIGHT IS BEING PROJECTED ON A SURFACE AND THE REFLECTION IS CAPTURED (KIRHAUG J., 2013)

The definition in the report prefers to characterise abrasion over an area, but the available devices limits the measurements to qualitative descriptions of the abrasion process.

2.2 Phenomenon: Ice-concrete abrasion

Ice loading is an important contributor to concrete abrasion, but also other factors are worth considering. One can distinguish three known types of damage (or abrasion) on the concrete surface:

- Mechanical
  - Ice crushing: Forces due to compression loading
  - Ice friction (dry and wet): Forces due to tangential loading.
  - Adhesion between ice and concrete: Forces due to hydro bonding between surfaces
- Physical
  - Indentation pore pressure
  - Freeze-thawing cycles: Internal pressure of freezing water present in the concrete. This can lead to microcracking.
  - Concrete shrinkage
  - Thermal gradients: Internal stresses due to temperature variation. This can lead to cracks and exposes the concrete to penetration of moisture and salts.
- Chemical
  - Chloride migration
  - Dissolving of lime

Mechanical loading and freeze-thawing are most important contributor to concrete abrasion (Huovinen S., 1990). The abrasion mechanism is thus more complex than barely friction. The discussion section will propose a separation of primary and secondary order of loading types. The method simplifies the abrasion loading versus resistance and allows to indicate the severity of the abrasion rate.

2.3 Location of maximum abrasion

2.3.1 Lateral location

Ice conditions are important, but even ice parameters are under control of environmental parameters. The environmental parameters influence thus ice, but very likely affects the concrete abrasion resistance as well. The prevailing environmental parameters can be, but not limited to air temperature, sea water temperature, salinity, wind velocity, current velocity and tides.

Ice conditions depends on environmental processes and require careful approach in design load for every new location in the cold. Level ice has been observed to be a relevant ice feature regarded ice-concrete abrasion (Janson J., 1988). The ideal local pressure distribution is for a circular concrete pile in a homogeneous continuum of ice is shown in Figure 10.

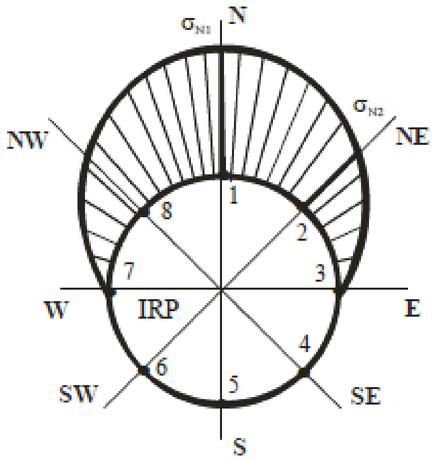

FIGURE 10 CONTACT PRESSURE DISTRIBUTION FOR ICE FLOW FROM THE NORTH AT AN ICE RESISTANT PLATFORM (IRP) (BEKKER A ET AL., 2003)

The local pressure is according to this ideal distribution maximum at the perpendicular face relative to the ice flow. Lab studies indicate increasing concrete abrasion with increasing contact pressure (Itoh et al., 1988), in other words concrete abrasion is maximum at point 1 and largely affected by ice crushing processes. Contact pressure is required for active concrete abrasion, the backside of structure without any active pressure does not show significant traces of ice-concrete abrasion in the field studies. Two ice flow parameters on mega-scale are thus important to estimate accurately in prediction of concrete abrasion rate:

- Direction of ice flow
- Duration of ice flow

The parameters determines the lateral location with maximum abrasion on the structure and helps to determine the design abrasion rate (Vershinin S. et al., 2006)

2.3.2 VERTICAL LOCATION

The vertical location depends on water level variation over time, for example tidal effects (Takeuchi et al., 2005). Maximum abrasion occurs at the maxima and minima of the tidal wave. The change of surface elevation naturally slows down when the tide turns and thus concentrates abrasive loads at the minima and maxima.

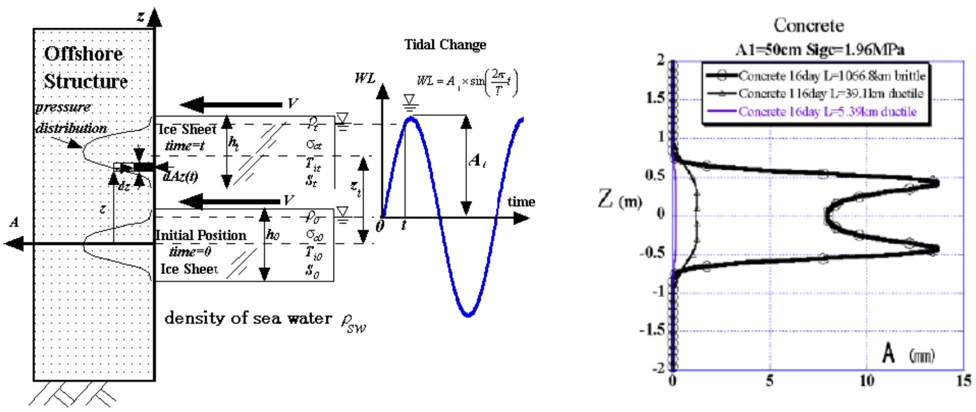

FIGURE 11 SCHEMATIZATION OF THE EFFECT OF TIDAL CHANGE ON THE ABRASION DEPTH A (MM). LEFT FIGURE IS THE SCHEMATIZATION OF THE TIDAL PROCESS AND RIGHT FIGURE SHOWS THE EFFECT ON THE ABRASION

Abrasion can occur above and under water, in other words in dry, wet or transitional conditions. Although, one observes larger abrasion amounts under water than above (Janson J., 1988). The effects of liquid like layers at the ice-concrete interface on the abrasion rate have not been studied yet.

2.3.3 Influence geometry

The failure mechanism of ice acting on a concrete structure depends on the geometry. Most observed structures with abraded surface are vertical surface, thus ice crushing and grinding are dominant failure mechanisms. The bridge pier in Figure 12 shows largest abrasion rates at position 2 above water level.

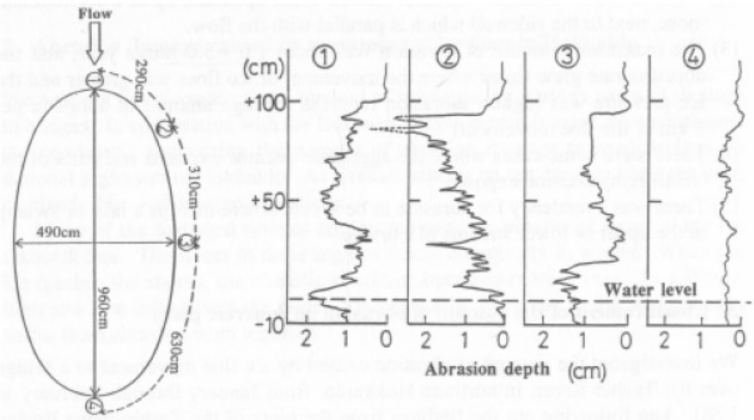

Figure 12 Cross section of bridge pier and abrasion depth (Hara F. et al., 1995)

Figure 12 shows the geometrics affect the location of the abrasion rate. The geometric configuration directly affect the pressure distribution and the number of contact events between the ice and structure. The significance of the geometrics requires further investigation.

2.4 ICE ABRASION LOADING

Contact pressure, ice temperature and impurities in the ice have been proven in field and lab studies to directly affect the abrasion rate, but also indirect factors like physical or chemical factors (see section 2.2). The definition of abrasion loading is the set of factors which cause concrete abrasion.

The abrasion rate behaves proportional to the sliding distance as is shown in Figure 13. The sliding depends on ice velocity driven by environmental parameters. The results in Figure 13 are from lab results with other parameters kept constant. The sliding distance indicates the number of contact events and also seems to indicate the accumulation of abrasion events (abrasion depth).

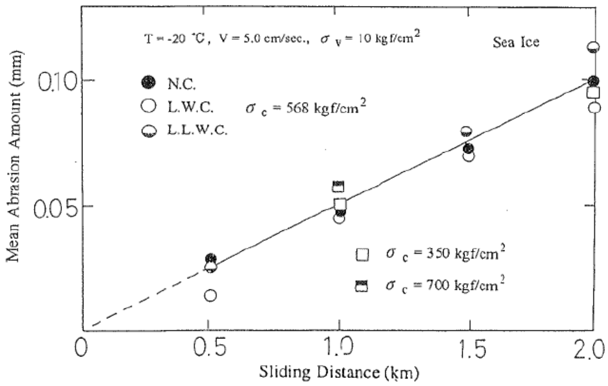

FIGURE 13 RELATION SLIDING DISTANCE AND ABRASION, THE FIGURE SHOWS A LINEAR RELATION BETWEEN THE SLIDING DISTANCE AND THE ABRASION DEPTH (ITOH Y. ET AL., 1988)

2.4.1 CONTACT PRESSURE

Contact pressure is the compressive pressure which the ice mass exerts on the concrete surface. The contact pressure definition depends on the scale. Global pressure involve an average pressure on an area and local pressure is commonly the meso- or microscopic pressure. The choice of global and local depends on the design purpose. Determination of shear and overturning moments will suffice with global pressures, but strongly depends on the weakest spot in the ice. Global pressure will not fully suffice in the explanation of concrete surface deterioration, local pressure becomes more relevant instead. The spatial distribution of local pressure does strongly depend on for example the distribution of mechanical properties in the ice material as is shown in Figure 14 and are thus difficult to predict without any a-priori information.

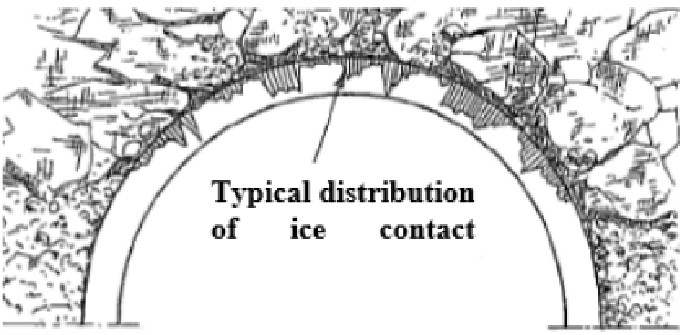

FIGURE 14 TYPICAL DISTRIBUTION OF ICE CONTACT PRESSURE ON THE CONCRETE SURFACE (JANSON J., 1988)

Contact pressure is an important factor to the abrasion rate as is shown in Figure 15 and shows the contact pressure relate reasonable linear to the abrasion rate. The contact pressure logically increases the number of contact events and thus the abrasion rate.

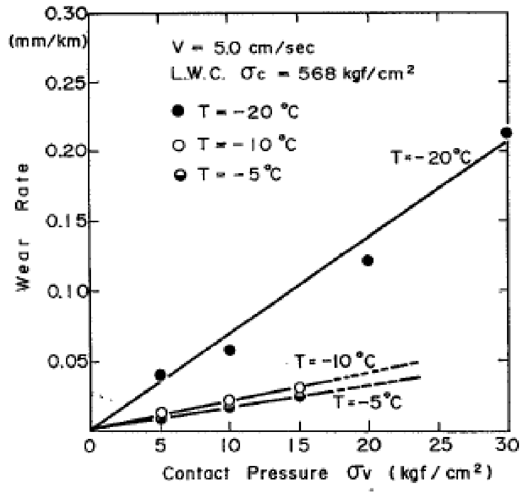

FIGURE 15 RELATION CONTACT PRESSURE AND ABRASION DEPTH (ITOH Y. ET AL., 1988)

The exact mechanism is not clear yet, because the contact pressure also relates proportionally to the shear stresses. The contact pressure is thus (directly or indirectly) proportional to the abrasion rate. Lab data consists in all tests of average contact pressures, although the contact area is relatively small most measured contact pressures are considered as global pressures. The formula for global pressure is:

$$\sigma_{global} = \frac{F_n}{A_n}$$

Where σ_{global} is the global pressure (MPa), F_n the normal load (kN) and A_n the nominal area (mm^2). However, global pressure is directly dependent on the local pressures, so the data can reveal some correlation between the local pressure and ice-concrete abrasion rate. The global pressure can also be written as:

$$\sigma_{global} = \int\int \sigma_{local}(x,y)\ dxdy$$

Where x and y are spatial variables of a specified area in a continuum. The global pressure describes the average pressure over an area. Assume the contact area maintains constant, but the global pressure increases. The local pressures will thus increase as well, but can also take on higher and lower pressure values. The local deviation relative to the average pressure is assumed to be an important loading effect on the concrete abrasion mechanism. The local pressure might even exceed the compression strength of the concrete in some cases. Perhaps, the loading can be simplified to a cyclic impulse loading over time.

The contact pressure depends on the weaker material, ice in this case. The ice compression strength limits in other words the contact pressure. The ice compression strength directly depends on the ice velocity and also thus on the corresponding shear stress and abrasion rate. Commonly, the global compression strength of ice is in the range of 2 – 5 MPa (Hoving J., 2015), but decreases with contact area (size effect) as is shown in Figure 16. For example a contact area of 1 m^2 seem to induce a compression stress in the range of 10 MPa, but an contact area of 10 m^2 in the range of 1 MPa.

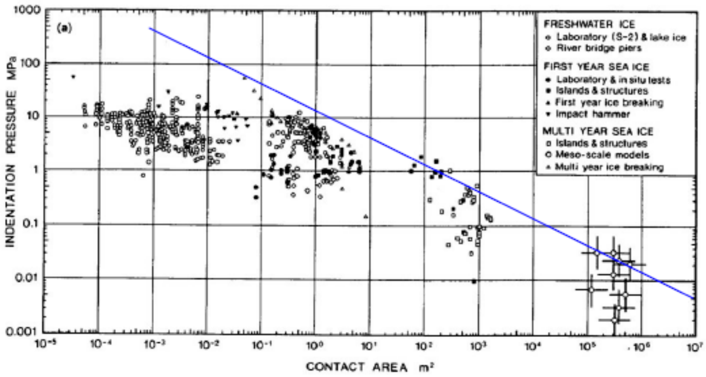

FIGURE 16 RELATION OF PRESSURE AND AREA (SANDERSON T., 1988)

The size effect got two explanation. Firstly, the statistical size effect assumes the ice feature is as strong as its weakest link, failure of the weakest 'link' cause the entire ice feature to fail. Practically in agreement with Figure 16 an increasing ice feature (contact area) the decreases the compression strength. Secondly, the energetic size effect assumes fracture initiation in the weakest 'link' and under continuous loading the fractures propagate and relief the peak stresses. The stress redistribution due to fracture is independent of the size of the ice feature. Ice is thus a quasi-brittle material considering the size effect.

Slow ice velocity cause a ductile behaviour within the borders of the viscoelastic strains – Stresses can relax and the global pressure can develop very high values. Also, adhesion is more dominant in slow ice velocities. The faster ice velocities, which are more common, cause a brittle failing behaviour and fracturing dominates the force build-up. The latter crushing mechanism is a non-simultaneous process illustrated by Figure 17 and can initiate extreme local pressures for a short amount of time (order of milliseconds) due to the formation of stress concentrations. The term for this phenomenon is also high pressure zone (HPZ).

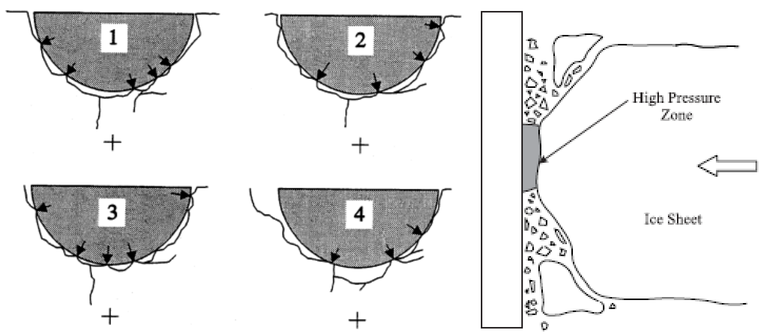

FIGURE 17 NON-SIMULTANEOUS ICE FAILURE BY TESTS ON BRITTLE WAX (ASHBY M. ET AL., 1986) AND SCHEMATIZATION OF ONE THE HIGH PRESSURE ZONE DURING A CONTACT EVENT, SIDE VIEW (JORDAAN I., 2001)

High pressure zones tend to locate in zones of high confinement, away from free surfaces, but spalls and rubble can fill up the free surfaces and involve some local ice pressures. The high pressure zones seem to occur at various places at the structure, the values of the loading involves large uncertainties still (Jordaan I., 2001). The level of local loading on real scale is interesting in determination of the ice abrasive loading.

The high pressure zones transfers the gross of the total force to the contact material. The local pressures within HPZ for multiyear sea ice can occur as high as 60 MPa (Masterson D. et al., 1993) and for medium-scale indentation tests up to 80 MPa (Frederking R. et al., 1990). Ship ice ramming into multiyear sea ice got up to pressures of 70 MPa (Glen I. and Blount H., 1984). Small-scale indentation tests on polycrystalline freshwater ice at -10 Celsius, pressures greater than 100 MPa occurred over areas of a few mm^2 while overall pressure were over 35 MPa (Mackey T. et al., 2007). The HPZ occurences are dynamic processes, they continuously change in number and location and thus lead to large fluctuation in load and pressure.

2.4.2 Extrusion due to crushing

An additional section as follow up on the contact pressures section treats extrusion briefly. Extrusion is a mechanism which can cause high shear stresses on the concrete and can cause significant ice abrasion on concrete. Extrusion involves fixation of ice material at the ice-concrete interface corresponding to large shear up to the static bounding limit is reached. Then, crushed ice material starts to move under slip and release the compressive shear stresses. Schematization of the process is shown in Figure 18.

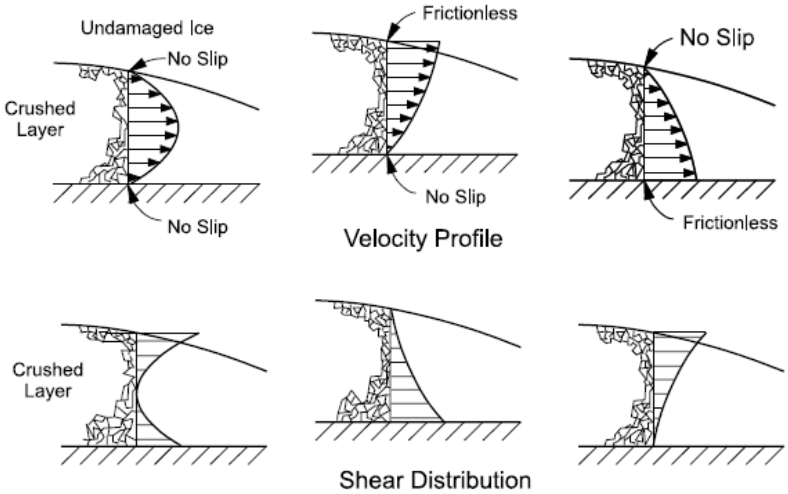

Figure 18 Development of shear and slip conditions, left sketches show no slip, middle sketches slip on the ice surface, right sketches slip on the concrete surface (Jordaan I., 2001)

The driving factor is ice compression and involves often saw-tooth curves corresponding to the stick-slip (compression – extrusion) process as is shown in Figure 19.

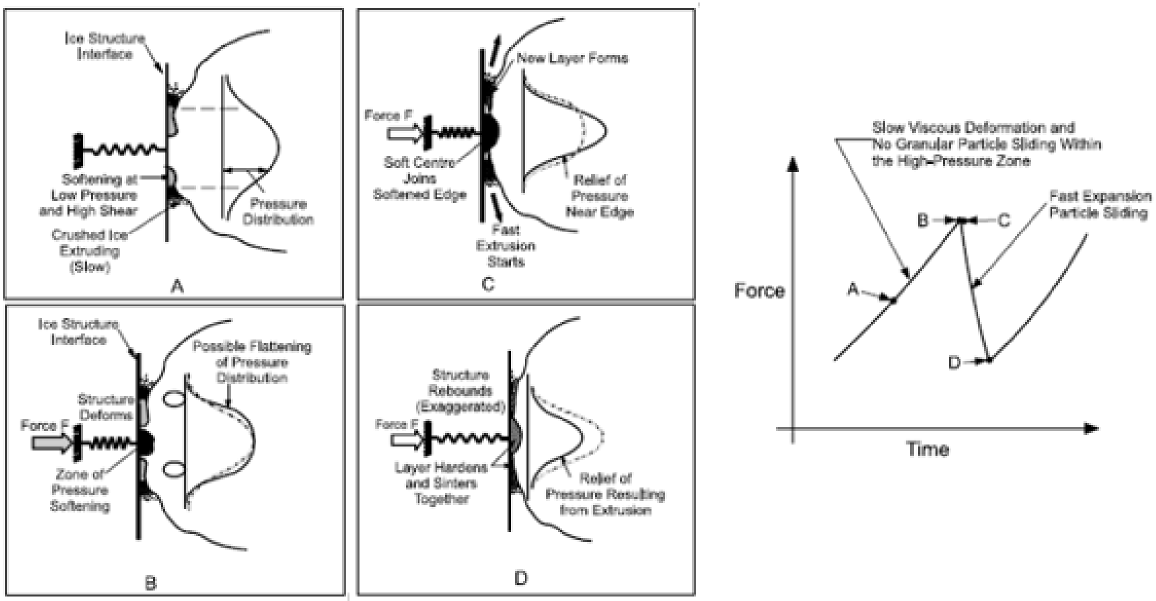

Figure 19 Schematization of extrusion process under existence of high pressure zone (Jordaan I., 2001)

The extrusion process as is shown in Figure 18 and Figure 19 involve a transition of movement under slip from an ice particle flow with a viscous character to an ice flow with a more granular character (Jordaan I., 2001).

Basically, the shear stresses on the concrete surface under slip conditions originate from fundamental different ice particle flow regimes. Also, relieve of compression pressure drives the ice particle flow and increasing confinement increases the compression stress build-up and thus, increases the kinetic energy of the ice particle flow. Commonly, concrete has a larger static bond to ice than steel, thus logically confinement is larger for concrete than for steel. The compression stress is higher and also, the kinetic energy of the ice particle flow. The abrasion rate depends on the local shear stresses and thus directly on confinement. The slip condition is disputable for high compression stresses, for low compression stresses with increasing relative velocity seem to affect the abrasion rate hardly (Hara F. et al., 1997).

2.4.3 Ice temperature

Ice temperature is the temperature of the ice at the location of contact. The ice temperature is a second important factor for ice-concrete abrasion (Itoh Y. et al., 1988). The ice temperature depends on the thermodynamic history of an ice feature. An iceberg shows for example different temperature distributions than level ice, because of the different freezing process during its life.

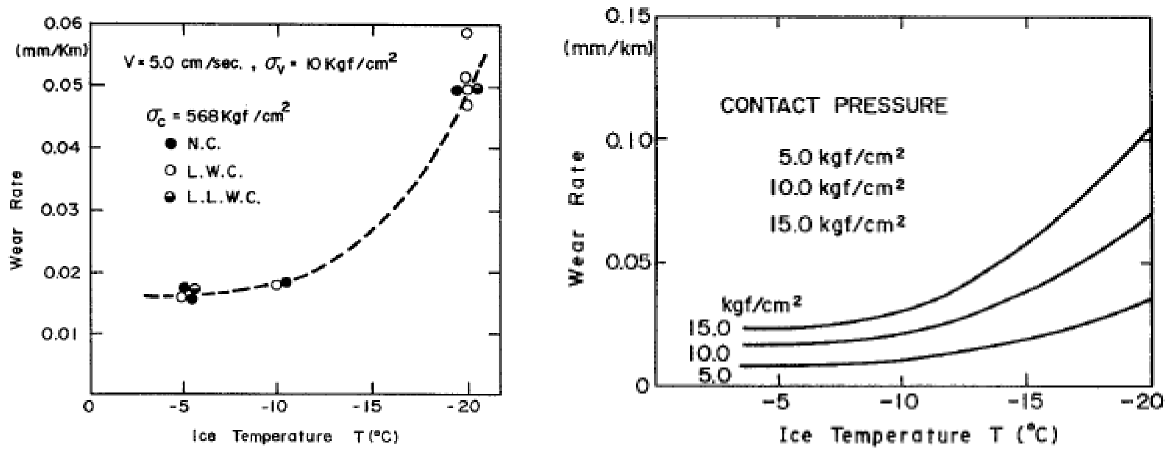

Figure 20 Relation between ice temperature and wear rate, the right graph also varies on contact pressure (Itoh Y. et al., 1988)

Figure 20 shows that decreasing ice temperature increases the abrasion rate. The thermodynamic ice property is thus able to change the mechanical interaction such that it affects the abrasion rate. The temperature depends mainly on the sea water temperature and the air temperature. The air temperatures vary over the seasons as is shown in Figure 21 and ice temperature profile in Figure 22.

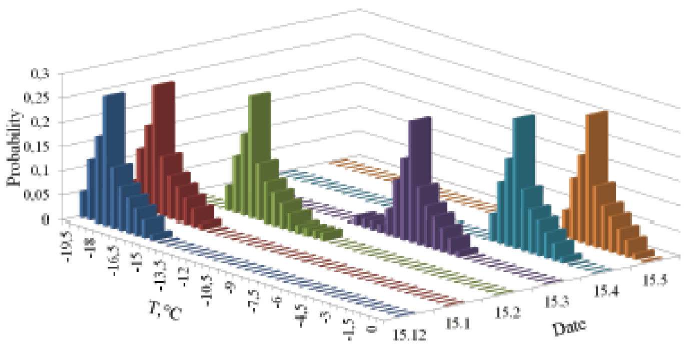

Figure 21 Example monthly temperature distribution per 15th of each month (Bekker A. et al., 2010)

The ice structure of sea ice varies of granular to needle like from top to bottom. The local pressure due to varying ice structure and temperature will affect both the concrete abrasion rate over the ice thickness. Abrasion rates increases with decreasing temperature, so the top layer has a larger effect on the abrasion rate than the lower layers of ice. The ice temperature of level ice varies over the thickness from water temperature to extremely cold air temperatures in the high Arctic, temperature differences of 30 Celsius are not uncommon in the high Arctic. A schematization of the temperature distribution over the ice thickness is shown in Figure 22

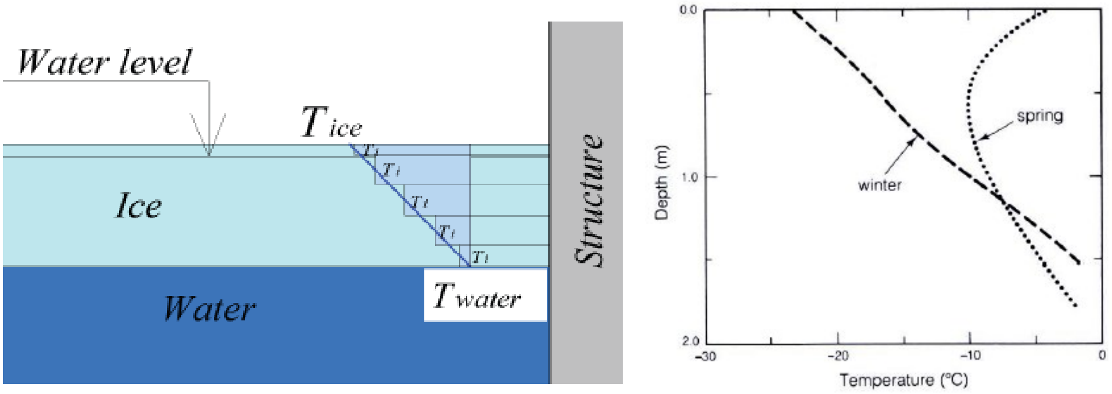

FIGURE 22 (LEFT) DISCRETIZATION OF TEMPERATURE VARIATION ON AN ICE DEPTH (BEKKER A. ET AL., 2010) AND (RIGHT) AN EXAMPLE TEMPERATURE PROFILE THROUGH ICE (DALEY C. AND COLBOURNE B., 2012)

The temperature dependency over the seasons should put under consideration in the assessment of the structural lifetime concerning abrasion, because the abrasion rate doubles (even more) from -10 ˚C to -20 ˚C (Daley C. and Colbourne B., 2012). The temperature of icebergs varies from the outer layers air temperature to a constant inner temperature of -15 to -20 Celsius. Besides that, the temperature might also change due to generation of frictional heat.

2.4.4 IMPURITY CONTENT

The impurity content of ice between the undamaged ice and concrete affects the concrete abrasion rate. The median diameter of sand, sand concentration and brine inclusion in the ice all affect the impurity content of ice. Concrete abrasion increases with increasing sand or brine content (Itoh Y. and Tanaka Y., 1994). The physical ice contact event with increasing impurity content becomes very intense on the concrete surface and will increase the concrete abrasion rate.

The ice impurity content also depends on the temperature. Brine pockets will eventually precipitate with decreasing temperature. The first precipitation occurs at -8.2 ˚C for $Na_2SO_4.H_2O$, second $NaCl.H_2O$ precipitates at -22.9 ˚C. The latter one is the dominant salt in sea water. Residual salts precipitate all out at -36.8 ˚C (Daley C. and Colbourne B., 2012). Decreasing temperature increases ice impurity content and thus increase the abrasion rate.

Sand inclusion also effects the ice impurity content and the abrasion rate. Sea ice possibly can contain sand or dirt due to sediment transport from rivers or shallow waters. Increasing concentration of sand particles increases the abrasion rate up to a certain maximum as is shown in Figure 23.

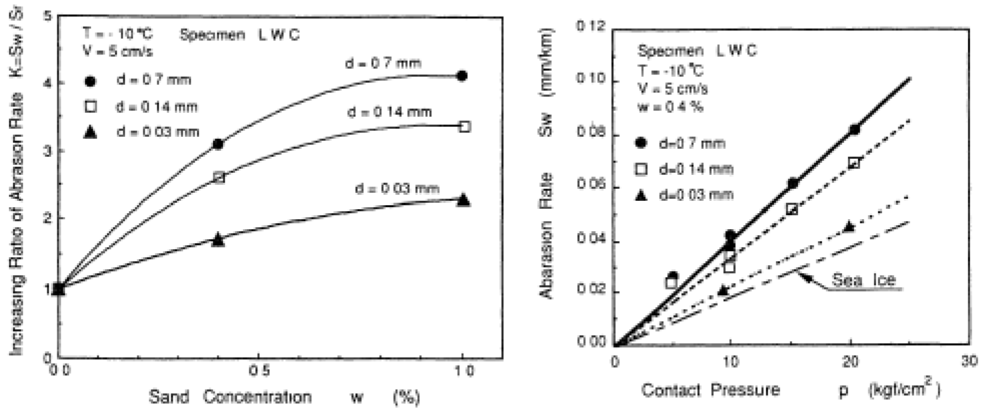

FIGURE 23 EFFECT OF SAND CONCENTRATION ON ABRASION RATE AND EFFECT OF SAND PARTICLE DIAMETER ON ABRASION RATE (ITOH Y. ET AL., 1994)

Figure 23 shows a trend as effect on the abrasion rate, the smaller diameter has less effect than the larger diameter. The expectation is that with increasing diameter an upper limit will be found where the abrasion rate not further increases.

2.4.5 ICE GRADE

The ice grade depends on the history of the ice material (Daley C. and Colbourne B., 2012). The thesis considers only three types of ice: First year fresh water level ice, first year sea water level ice, icebergs. Freshwater level ice freezes differently than sea water ice. Fresh water has a maximum density at 4 Celsius. A layer of cold less dense water lays on top and when the surface water temperature drops below the freezing point of 0 Celsius the top layer quickly freezes. The top layer does not mix with the lower warmer layers of water (4 Celsius) (Daley C. and Colbourne B., 20120). Freshwater ice is a relative strong ice grade.

Seawater ice freezes very differently when the temperature drops. The sea water undergoes an intricate mixing process. The top layers cool and become denser, so they sink until they reach equilibrium with lower layers. The upper layer gets replaced by warmer or less saline water from below. Generally the top 10-20 meters of sea water requires to cool down to its freezing point of -1.8 Celsius (for 35 ppm salinity) (Daley C. and Colbourne B., 2012). Sea water is a complex ice grade due to salinity, air entrapment and migration of those. The lower layers of sea water ice consist of needle-like layers and also involves a lower structural strength than the granular type of ice (Bekker A. et al., 2010).

Icebergs are made of freshwater ice. They are broken off ice material from a land-based glacier or ice shelf. Accumulating snow compresses the underlying layers to dense ice. The deep blue colour is the true colour of glacial ice where the bubbles forced out under compression and correspond to the deeper layers of the glacier. White iceberg ice contains bubbles corresponding with less compressed layers of the glacier. The density profile might also vary over the iceberg dimensions. The outer layers Firn can have densities of 400 kg/m^3, but can't be classified as ice. The Firn- ice (from 800 kg/m^3) transition is mainly 40 – 60 meters below the top surface for newly calved icebergs. The outer layers under melting are relatively warm ice material close to the melting point, but the inner strong layers commonly have temperatures of -15 to -20 Celsius (Daley C. and Colbourne B., 2012). The inner compressed ice layers are commonly one of the strongest natural ice grades.

2.5 CONCRETE ABRASION RESISTANCE

Concrete material exists in numerous compositions with each unique performance and the next step consist of an investigation in the concrete abrasion resistance. The concrete abrasion resistance depends on the microscopic failure mechanisms. Abrasion is generally speaking the result of failing concrete and observations often describes traces of abrasion, not the abrasion event itself. Some failure mechanisms are shown in Figure 24 and the abrasion resistance expression should include the resistance to at least these material failures.

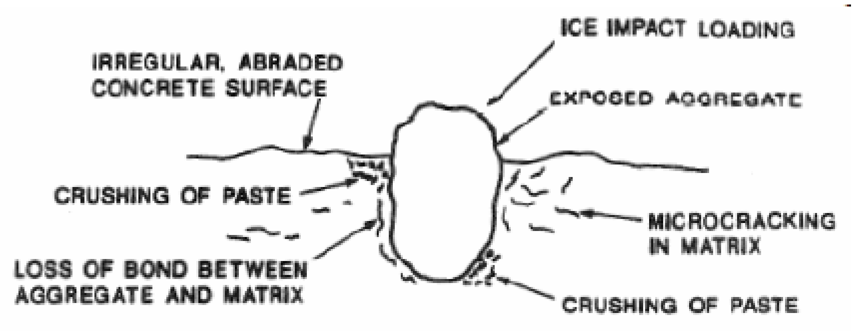

FIGURE 24 FAILURE MECHANISMS ASSOCIATED WITH ICE ABRASIVE LOADING

2.5.1 ABRASION PROCESS

Abrasion is not a constant process, but will evolve over the abrasion depth. The abrasion rate depends on the heterogeneous concrete material and thus changes at larger abrasion depths. Figure 25 shows three zones, surface region, transition region and stable region, where the latter two involves aggregate exposure.

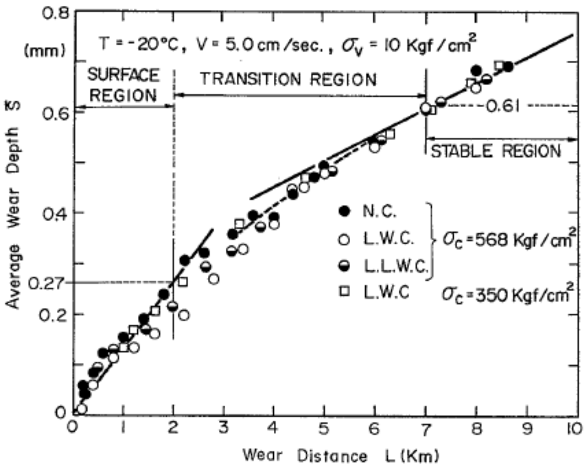

FIGURE 25 RELATION BETWEEN ABRASION DEPTH AND ICE SLIDING DISTANCE (WEAR DISTANCE) (ITOH Y. ET AL., 1988)

(Huovinen S., 1990) verifies the three stages in Figure 25 and explains the physics. The three stages correspond with physical failure mechanisms and depends on the appearance of cement and aggregates at the concrete surface, see Figure 26.

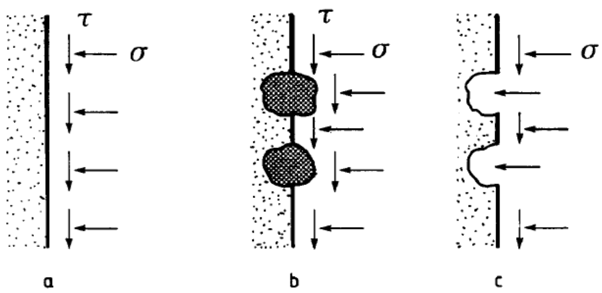

FIGURE 26 STAGES OF CONCRETE ABRASION. (A) LOOSENING OF CEMENT STONE, (B) SECOND ABRASION OF CEMENT STONE PLUS LOOSENING OF PROTRUDING AGGREGATE STONES AND (C) ABRASION OF CEMENT STONE AFTER LOOSENING. (HUOVINEN S., 1990)

The first stage of abrasion consist of cement wear and structural strength of the cement governs the abrasion resistance. The second stage involves loosening of protruding aggregate stones and the abrasion rate decreases over this stage. The influence of aggregates-cement strength increases on the abrasion rate. The last stage always occurs in combination with the second stage. The protruding aggregates loses, but meanwhile other aggregates just reveals.

(Itoh Y. et al., 1994) came up with an empirical formula to describe the abrasion rate:

$$S_r = p(9.708T^2 + 1295.7) * 10^{-6}$$

Where S_r is the abrasion rate per sliding distance in km, T is the temperature in Celsius and p is the contact pressure in kgf/cm^2. The formula provides reasonable estimations within the borders of the experimental data and correspond to one unique concrete type, but is not easily expandable to other concrete types.

2.5.2 Fracture

(Huovinen S., 1994) considers stage 2 and 3 as most relevant. The schematization of the ice loading on the concrete in that stages is shown in Figure 27. Note the clear separation of the normal and shear component. The components also induce a rotating moment on microscopic level.

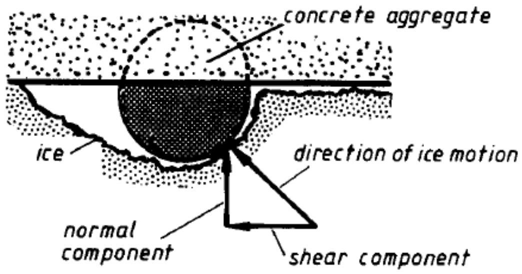

Figure 27 Forces against protrudent aggregate stones (Huovinen S., 1994)

The local loading consist of compression and shear according to (Huovinen S., 1994). The ratio of shear and compression depends partially on the microscopic surface geometry of the concrete and partially on the angle of contact (see section 1.3). The relevant microscopic surface parameters are asperity shape and height. The local ice-concrete friction factor thus provides information about the average loading angle on a concrete asperity. For example the friction coefficient of 0.1 (-) indicates an loading angle of 5.7° relative to the normal direction. (Huovinen S., 1990) zooms in onto the local fracture mechanics of the aggregate-cement binding, see Figure 28.

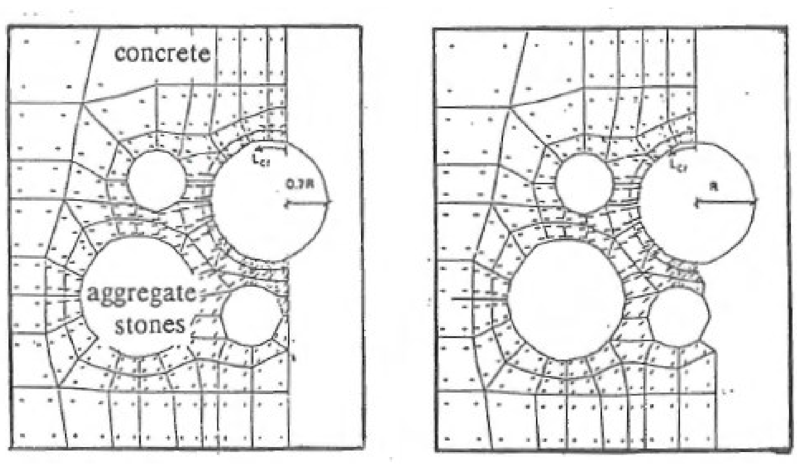

Figure 28 FEM of concrete surface material (Huovinen S., 1990)

The basis of the failure condition is the loosening of a protruding aggregate due to fracture, the loosening event occurs when the radius of the aggregate (R) exceeds the fracture length (L_{cr}). The following formula indicates the abrasion depth from the criterium.

$$ABR = \sum_{i=1}^{n} a_i \frac{\log(n_s)}{\log(n_1)} R_i + (1 - a_i) * b$$

Where a_i is the proportional amount of aggregates of radius R_i, n_s the number of ice impacts during ice movement s, n_1 is the number of ice sheet impacts required for R to exceed the fracture length L_{cr}, and b is the abrasion rate of cement stone. Notice the superposition of cement abrasion and aggregate abrasion. Superposition requires each variable to be independent, but the independency of cement and aggregates within the concrete material is disputable. Table 1 shows a series of concrete samples which were put under testing in the laboratory and indicates compressive strength and addition of Silica Fume seems to affect the abrasion favourable.

TABLE 1 VARYING CONCRETE MIXTURES (HUOVINEN S., 1990)

No	Material	f_c [MPa]	w/b	Exposure	Abrasion (mechanical)
1	ND Concrete	60	0,27	Freeze-thaw (50 cycles) + abrasion (mechanical)	6,2
2	ND Concrete	60	0,28		5,4
3	ND Concrete	60	0,31		9,3
4	ND Concrete	40	0,41		10,8
5	ND Concrete	40	0,36		9,1
6	ND + Silica Concrete	60	0,31		2,6
7	ND + Silica Concrete	60	0,31		4,8
8	LW Concrete	30	0,35		11,2
9	LW Concrete	30	0,35		11,5
10	ND Slag Concrete	60	0,29		4,5
11	ND Slag Concrete	60	0,29		7,1

The addition of very fine material like Silica Fume or Blast Furnace will improve the fracture resistance of concrete, because the matrix bond increases – the very fine particles will fill up the spaces between the smallest grains.

The water cement ration (w/c factor) is an important mixture parameter. Commonly, an increasing w/c factor correspond with a decreasing compression strength. Also, an increasing w/c factor increases the abrasion rate as is shown in Figure 29.

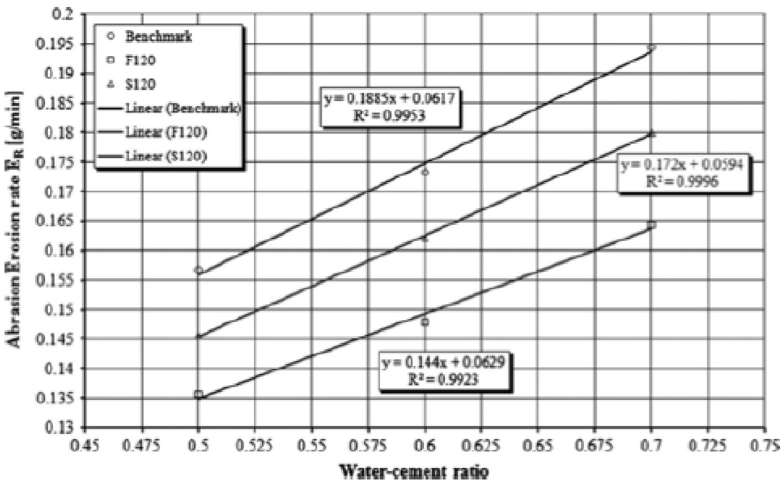

FIGURE 29 RELATION BETWEEN W/C FACTOR AND ABRASION RATE. THE BENCHMARK IS WITHOUT FIBRE REINFORCEMENT, THE F120 AND S120 ARE WITH DIFFERENT TYPES OF POLYPROPYLENE FIBRE REINFORCEMENTS (GRDIC C. ET AL., 2012)

Concrete reinforcement with basalt fibres, but also with polypropylene fibres (Figure 29) increases the abrasion resistance. The abrasion resistance of basalt fibre reinforced concrete seem to correlate with the flexural concrete strength rather than with the compression strength. An increasing flexural strength decreases the abrasion rate as is shown in Figure 30.

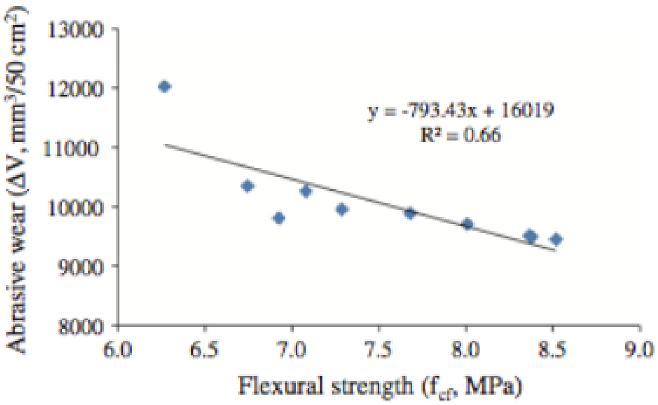

FIGURE 30 RELATION CONCRETE FLEXURAL STRENGTH AND ABRASION RATE (KABAY N., 2014)

The flexural strength relates often to the tensile strength in concrete material. Tensile stresses in concrete easily induce fracture and will put underlying concrete layers at risk. Fibre reinforcement of concrete will reduce fracture propagation. Fracture is an important mechanism for abrasion (Huovinen S., 1994) and thus addition of fibres will increase the abrasion resistance.

2.5.3 COMPRESSION STRENGTH

The compression strength often represent the global resistance to compression loading like through a cylindrical compression test. An increasing global compression strength increases the concrete abrasion resistance as is shown in Figure 31. The cylindrical compression strength does not represent the local compression strength. Local means on microscopic level.

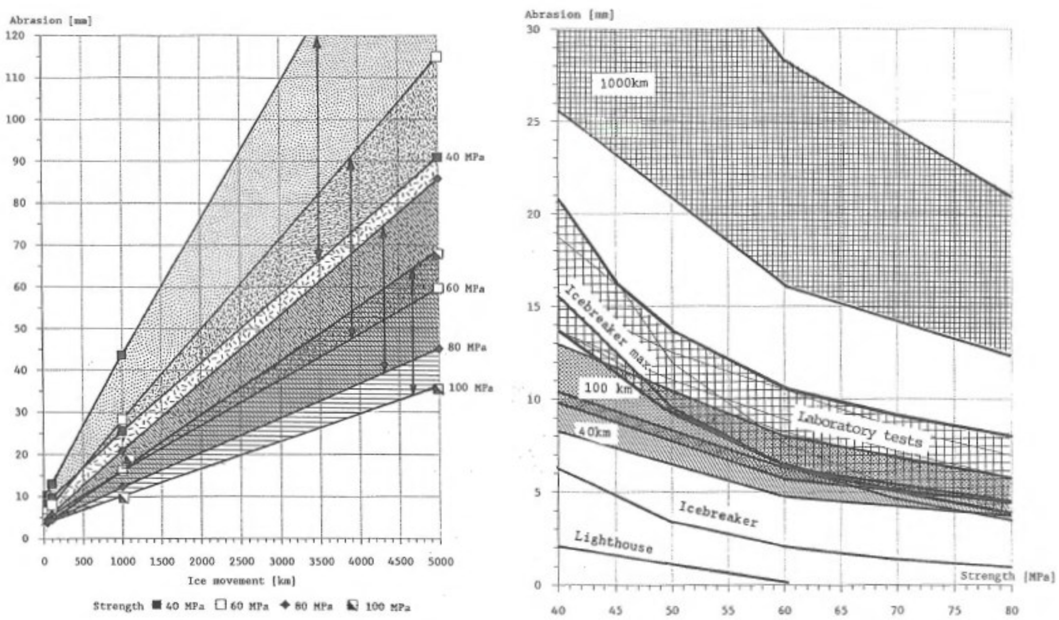

FIGURE 31 (LEFT) RELATION OF ICE SLIDING LENGTH AND ABRASION DEPTH. (RIGHT) RELATION OF CONCRETE COMPRESSION STRENGTH AND ABRASION DEPTH (HUOVINEN S., 1990)

An increasing compression strength often increases the fracture resistance (stronger matrix strength) and reduces the fracturing of concrete. An increasing fracture resistance decreases the abrasion rate (Huovinen S., 1994) and thus an increasing compression strength decreases the abrasion rate. Figure 32 shows the relation between the ice sliding distance and abrasion rate for five materials. Andesite and sandstone have the largest abrasion resistance in the sample range. Tuff and granite the lowest.

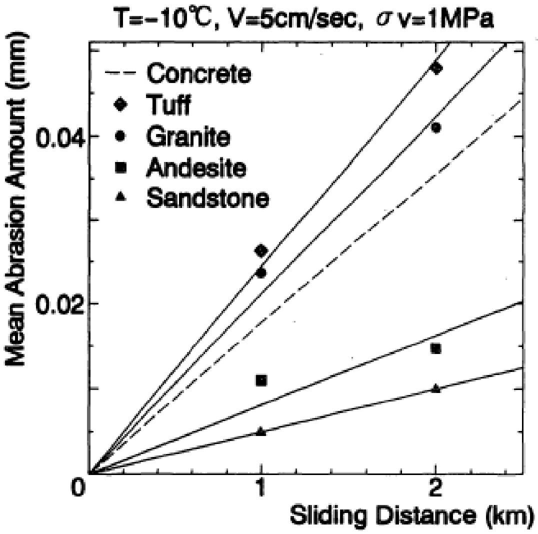

Figure 32 Relation between sliding distance and abrasion (Hanada M. et al., 1996)

2.5.4 Freeze-thaw

Freeze-thaw cycles induce stresses due to freezing of the aqueous pore solution in the concrete material. ice will form in the saturated pores when the ambient temperature drops below the freezing point of the pore solution. The pore size distribution of the material directly affect the ice formation process, because the water expels from the pores or attracts to the ice crystals in the pore structure (Zuber B. and Marchand J., 2000; Powers T. and Helmuth R., 1953). The water movements induces internal stresses and might exceed the tensile strength of concrete (Helmuth R. , 1961). Fracture and surface scaling (see Figure 33) are typical forms of frost damage. Surface scaling often involves the presence of salts, for example in a marine environment. (Jacobsen J. et al., 2006) describes the characteristics of internal and surface frost damage.

Figure 33 Concrete surface scaling (Concrete construction magazine)

Freeze-thaw cycles often result into a loss of cement material, in other words concrete abrasion. The rate of scaling depends on the air void system and concrete compression strength (Marchand J. et al., 2005). The scaling rate depends on more compounds like the nature of minerals, chemical additives and admixtures. The effect of compounds on the capillary system explains the scaling resistance further. Scaling occurs mainly on the concrete surface and thus reduce the strength (and abrasion resistance) of the upper concrete layers (Marchand J. et al., 2005). Also, bleeding, casting conditions, workability and curing operations reduce the concrete strength (and abrasion resistance) in the upper concrete layers. Specifically, the deterioration processes affect the mechanical properties and microstructure at the concrete surface (Hooton R. et al., 1997). (Marchand J. et al., 1998) suggests no significant scaling occurs below -10 ˚C. The duration of the freezing period appears to be more important than the cooling rate below a critical temperature (Marchand J., 1993). The pressure develops due to ice growth in the pores and then, exerts hydraulic or osmotic pressure on the pore walls. Also, possible effects of the crystallization of salts increases the pressure (Marchand J. et al., 1994).

2.5.5 Temperature fluctuations

Temperature fluctuations induces large internal stresses. The tidal zone on the structure is the main concern, especially during very large temperature difference between the air and sea water temperature. The thermal stresses decrease the abrasion resistance and thus increases the probability on ice abrasion – a secondary order of loading.

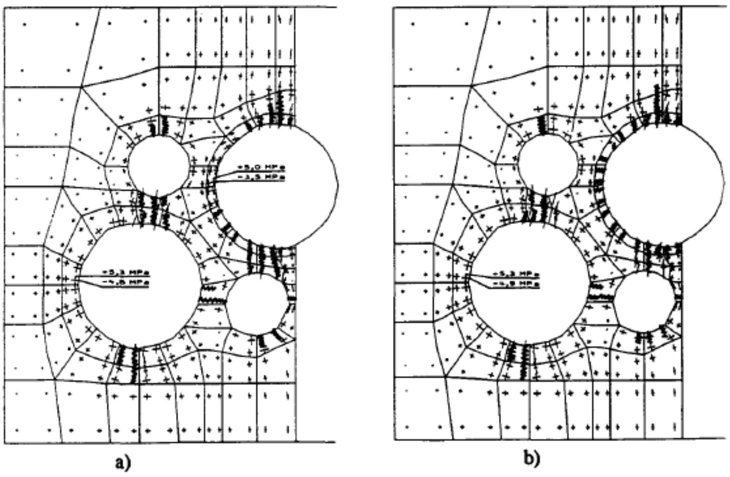

Figure 34 Greatest stresses and cracks at a concrete temperature of-30 °(dT = -40 °C) and tensile strength of the transition layer f_{AB} = 6 MPa (a-figure) and f_{AB} = 2 MPa (b-figure) (Huovinen S., 1992)

Figure 34 shows large thermal stresses due to casting and hardening during pouring. The peak stresses seem to concentrate around the boundaries between the cement and aggregate. The cement material seem to spread the residual stresses easily through the material.

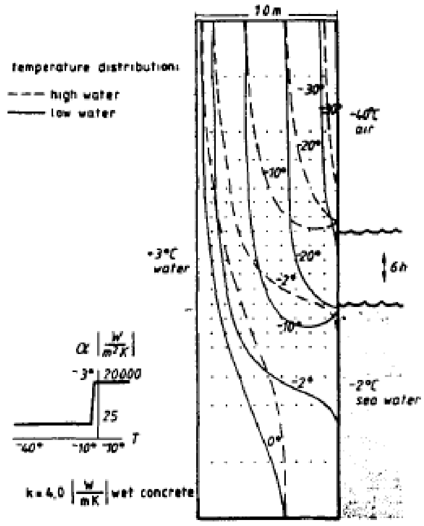

Figure 35 Temperatures during water level fluctuations, air temperature -40 °C and sea water temperature -2 °C (Huovinen S., 1992)

Figure 35 shows the tidal effect on the temperature fluctuation. The temperature fluctuates with a period of 12 hours. An decreasing period often increases the local temperature gradient. The effect of the tide on local temperature gradients requires more investigation. The abrasion resistant design requires sufficient resistance concerning the temperature fluctuation.

(Jansson J., 1988) claims the temperature gradient plays a minor role on fracturing. The temperature below/above water could be 30 Celsius in the Baltic region of interest and the tidal exposed area on the lighthouse structure is thus expected to show fracture due to thermal stresses. However, no fracture was found and the effect of thermal stresses on the concrete abrasion resistance is not expected to play any major role.

2.5.6 Indentation pore pressure

Abrasion also occurs due to indentation pore pressure. Hydraulic pressure loads the pore walls and introduces compression and tensile stresses. Indentation pore pressure occurs during an ice impact on the concrete asperities under wet conditions. Water comes from the sea or the liquid-like-layer (LLL) at the ice. Frictional heat only increases the water content at the interface. Commonly, ice fails in brittle conditions and initiates large contact pressures (see section 2.4.1).

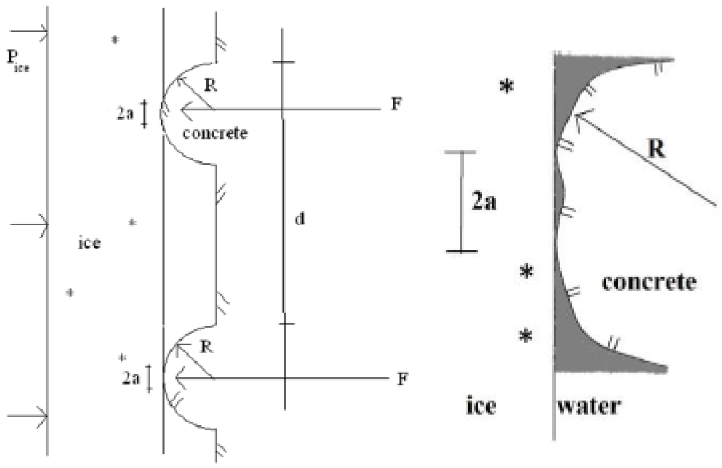

FIGURE 36 (LEFT) PLANE ICE SURFACE (LEFT) MOVING WITH AVERAGE PRESSURE, P_{ICE} TOWARDS ROUGH CONCRETE SURFACE WITH ASPERITIES RADII R, SPACING D, REACTION FORCES F AND CONTACT RADII A. (RIGHT) WATER TRAPPED IN THREE PHASE INTERFACE, R = 0.01 – 10 MM (JACOBSEN J. ET AL., 2010)

Fracture occurs when the tensile stress exceeds the tensile strength (Jacobsen J. et al., 2010).

$$p_{crit} = f_{c,t} \leq p_{eff} \approx (p_m - p_{ice})$$

Where p_{crit} is the critical stress where fracture occurs. The importance of the failure mechanism has not been very clear yet, (Jacobsen J. et al., 2010; Bekker A. et al., 2012) suggests the mechanism is responsible for just 0.15% of the cases with a numerical model in the background. However, the exceedance of concrete tensile strength by hydraulic pressure might participate as an relevant part in the ice-concrete interface and should get some more verification.

2.5.7 CHEMICAL ABRASION RESISTANCE

The most important chemical abrasion resistance consist of resistance to alkali-aggregate reactions, chloride penetration and carbonation. Alkali (basic or basal salts)-aggregate (for example silica compound) reactions can cause serious fracture in the concrete. Cement products are of rich alkali material while substances of the aggregates can possibly react with them. Commonly this does not occur at a very high rate, because the aggregate compound requires to dissolve in the pore water first. However, the dissolving process reduces the concrete strength, but requires a water rich environment and the presence of fractures only accelerates the process (Marchand J. et al., 1998).

Chloride penetration and carbonation are not a direct threat to the concrete material but rather to the concrete reinforcements. The reaction product, tricalcium aluminate (Ca_3Al) reacts with chlorides and result in chloro aluminates (Justnes H., 1998). Carbonation decreases the pH and releases the chlorides from the chloro aluminates. The increasing chloride in comparison to the OH^- ions can exceed the tolerance limits of the reinforcement steel and progressively corrode. The structural designer should be aware about the corrosion threat and eventually manage it.

2.6 ABRASION RATES

The abrasion rate often is an expression of mm average surface roughness change over the relative ice movement. Assuming the relative ice movement involves a constant ice grade over movement. Second, the abrasion rate does not describe the microscopic processes of abrasion very well. Figure 37 shows a first set of measurements of the abrasion rate - a block of sea ice grinded km's forth and back over a concrete sample whereas the ice block is replaced regularly. An abrasion measurement represents the average of five line measurements of the surface topography. The abrasion rate varies between 0.14 – 0.05 mm/km dependent on the surface material under a vertical pressure of about 1 MPa (10 kgf/cm²).

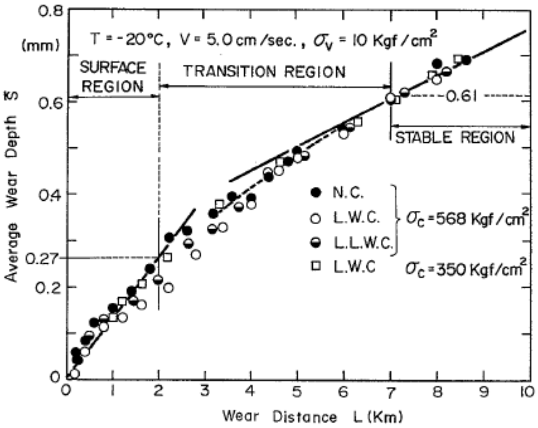

FIGURE 37 AVERAGE ABRASION DEPTH OVER ICE SLIDING DISTANCE (ITOH Y. ET AL., 1988). CONCRETE TYPES WITH A COMPRESSIVE STRENGTH OF 568 KGF/CM² (57 MPA) AND 350 KGF/CM² (35 MPA). THE ABRASION RATES ARE 0.14 MM/KM IN THE SURFACE REGION, 0.14 – 0.05 MM/KM IN THE TRANSITION REGION AND 0.05 MM/KM IN THE STABLE REGION

Figure 38 shows the reduction of the concrete on the abrasion rate due to surface treatment. The abrasion rates are all in the stable region (see Figure 37), because it represents the steady state abrasion rate. The application of polyurethane resin lining improves the abrasion resistance with 550% or resin mortar lining with 323%, but surface treatment as polymer impregnation with steel fibre reinforcement reduces the abrasion resistance with 41%.

Specimen	Wear Rate (mm/km)
L.W.C. (σ_c = 568 kgf/cm²)	0.055
Polyurethane Resin Lining	0.010
Resin Mortar Lining	0.017
Polymer Impregnation	0.055
Polymer Impregnation with Steel Fiber Reinforcement	0.094

FIGURE 38 EFFECT OF SURFACE TREATMENT (ITOH Y. ET AL., 1988)

Table 2 shows the effect of various materials on the abrasion rate. Remarkable is the difference of the abrasion rate for concrete material in comparison with (Itoh Y. et al., 1988) within the identical experimental setup, most likely (Hanada M. et al., 1996) tests another type of reference concrete.

TABLE 2 ABRASION RATES OVER ICE SLIDING DISTANCE FOR VARIOUS MATERIALS (HANADA M. ET AL., 1996)

T= -10℃, σ v= 1MPa	
materials	abrasion rate (mm/km)
	sea ice
concrete	0.0178
steel	0.0030
polyurethene	0.0030
zebron	0.0078
LDPE	0.0022
sandstone	0.0049
tuff	0.0251
pyroxene andesite	0.0084
dacite A	0.0065
dacite B	0.0177
granite	0.0216

Table 2 shows that steel (83% improvement), polyurethane (83% improvement) and LDPE (88% improvement) have very good abrasion resistances in comparison to the reference concrete. Also, zebron (56% improvement), dacite A (63% improvement), sandstone (72% improvement) and pyroxene andesite (53% improvement) have good abrasion resistance.

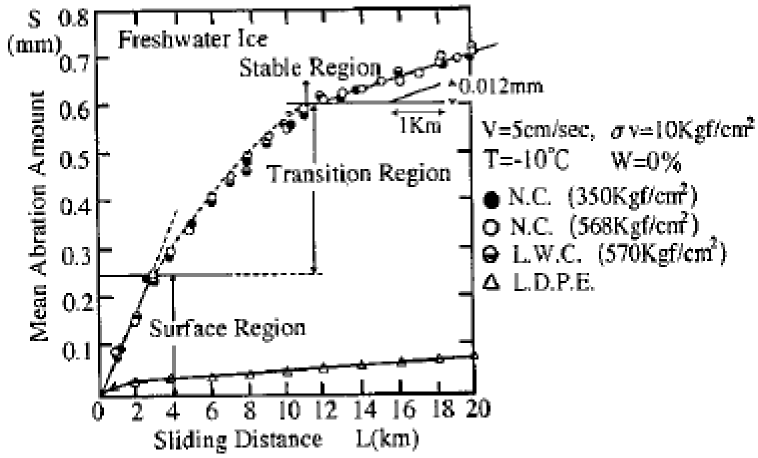

Figure 39 Abrasion depth over ice sliding distance for concrete types (Hara F. et al., 1997). The abrasion rates are 0.085 mm/km in the surface region, 0.044 mm/km (average) in the transition region and 0.012 mm/km in the stable region.

Figure 39 shows the abrasion depth and correspond to an abrasion rate of 0.012 mm/km in the stable region. Also, with the same experimental setup only much lower abrasion rate than (Itoh Y. et al., 1988) and reasonable lower than (Hanada M. et al., 1996). The reason is freshwater ice with no saline and sand contents in comparison to sea ice, the impurities serve as sandpaper and increase the abrasion rates.

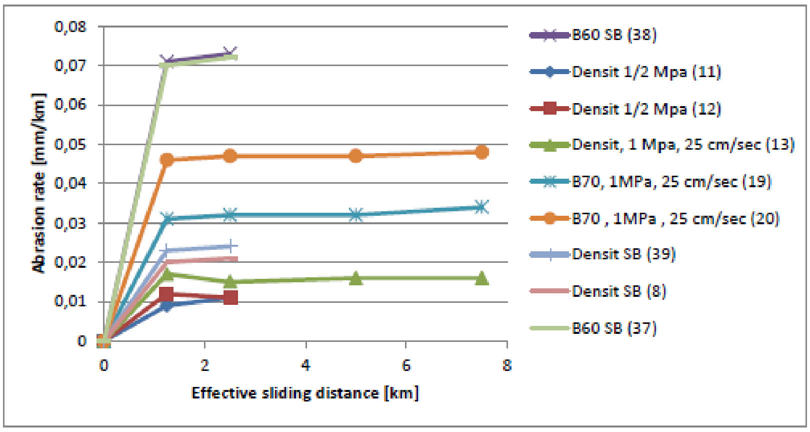

Figure 40 Average abrasion rate developments for tested specimens (Kirhaug J., 2013)

Figure 40 shows the test results of various abrasion tests within the NTNU Norway. The test apparatus does still shove a block of ice forth and back, but the system setup is an independent system design with other ice block dimensions (cylinder shape instead of block shape). Second, the measurement of abrasion are areal non-contact measurements instead of contact measurements over a line. Having said that, the abrasion rate values of (Kirhaug J., 2013) do fall within the borders of the experimental setup of the predecessors (Itoh Y. et al., 1988; Hanada M. et al., 1996; Hara F. et al., 1997) in the 80's and 90's. (Kirhaug J., 2013) shows lower abrasion resistance for the B60 concrete over the B70 concrete and agrees with (Huovinen S., 1990) on the favourable effect of increasing compression strength. The densit sandblasted mortars (repair material) behave reasonable well (about 0.02 mm/km) within the border of the B70 concrete grade (0.03 – 0.05 mm/km). The abrasion rates of the densit mortar under ½ MPa (about 0.01 mm/km) normal pressure should be normalized to 1 MPa by multiplication of 2 according to the proportionality of the abrasion rate to normal pressure and result into about 0.02 mm/km.

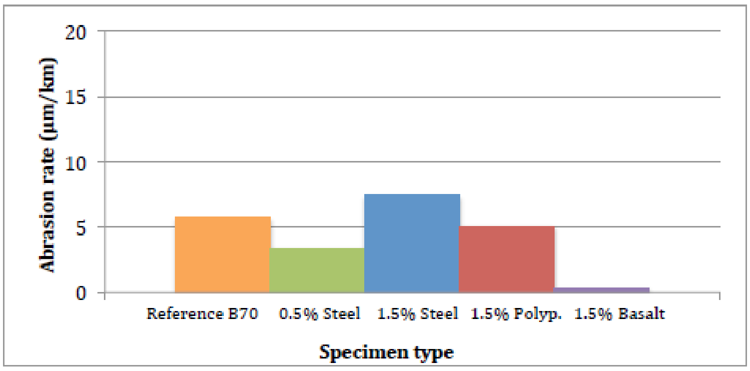

FIGURE 41 ABRASION RATES AND REINFORCED CONCRETE SPECIMENS WITH STEEL, POLYPROPYLENE AND BASALT FIBERS (SÆTRE K., 2014)

Figure 41 shows the follow-up of the work of (Kirhaug J., 2013) with the same testing equipment within NTNU Norway, an investigation in steel and basalt fiber reinforcements as measure to increase the abrasion resistance. The abrasion rates reduces for all reinforced specimen except for the 1.5% steel and 1.5% propylene fibers. The basalt fibers seem to extremely improve the abrasion resistance, but the abrasion rate includes also an average of two negative abrasion rates which falls outside the abrasion definition within the report. The average abrasion rate of the basalt fibers without the outer layers between 0.003 – 0.005 mm/km and is still an improvement on the abrasion resistance in comparison to the B70 concrete.

The abrasion rates in the lab vary between 0.003 – 0.14 mm/km under 1 MPa normal pressure and different concrete compressive strengths. The observations in the field vary between 0.3 – 11.6 mm/year (Janson J., 1989; Hara F., 1995). Observation suggest around the Sydostbrotten lighthouse 700 – 800 km ice sliding distance (Janson J., 1989). The corresponding abrasion rate varies between 0.00038 - 0.017 mm/km. The ranges differ a factor 10 smaller on real scale than on lab scale and most likely originate from areal pressure effects. The global contact pressure at the concrete surface is 2 -5 MPa, but the global contact pressure decreases with increasing area due to the size effect (see section 2.4.1). The extreme local pressures over 70 MPa (see section 2.4.1) in real scale.

Concluding, the data from the laboratory provides indicative abrasion rates on material abrasion on macro scale. The lab data only differ a factor 10 to real-scale data. Meso- and microscopic processes as fracturing or chemical loading within concrete abrasion require further research. The data can be valuable input for the evaluation of mitigation (see section 5.3.2) or basis for numerical simulation (see section 6).

3. EXPERIMENT

3.1 TEST SETUP

3.1.1 APPARATUS

The bi-axial apparatus is an MTS machine with expansion frame. The MTS machine drives the hydraulics in normal direction and the expansion frame drives the hydraulics in tangential direction. Moving loads on steel plating was the initial purpose of the apparatus. Steel plates were put with steel bolts in the apparatus. The threads are still visible in Figure 42. The concrete sample is strapped with two relative thin steel straps to the carriage with two bolts. The left photo in Figure 42 shows on the topside of the photo the steel straps.

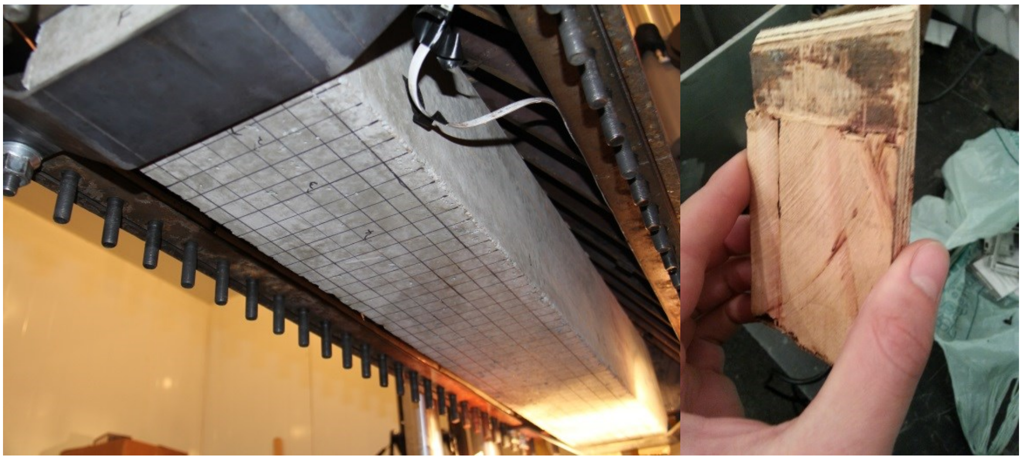

FIGURE 42 STRAPPING AND WEDGING OF CONCRETE BEAM

The straps tension the beam vertically to the carriage and prevent vertical displacement. The tension in the straps also keep the concrete sample in sideward position by dry friction. The concrete sample has 5 mm margin in longitudinal direction due to installation tolerances and also requires fixation. The wooden wedges (see right photo in Figure 42) provide tight fixation of the concrete sample in longitudinal direction, two wedges were hammered in the gap. The installation of the concrete sample is an intensive operation and requires at least two man in order to do it safely. Two manual cranes with synthetic straps support the lifting operations.

Figure 43 illustrates the lab simulation of the real scale situation. Also, in order to determine the input parameters for the experiment it’s crucial to understand the schematization.

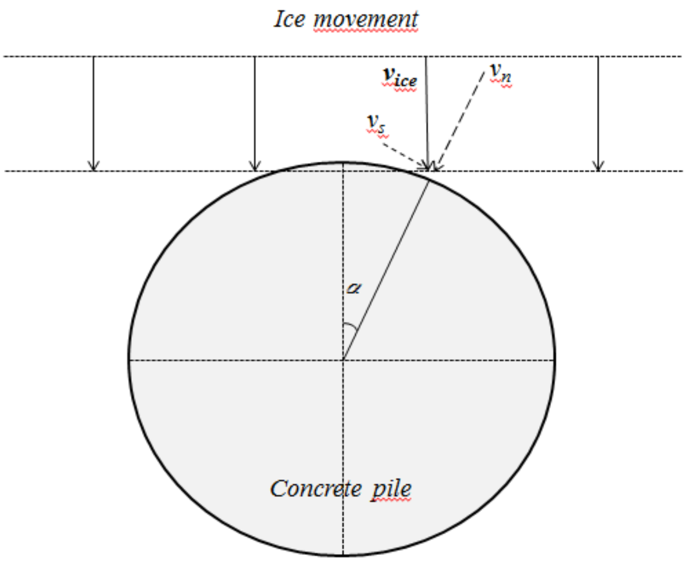

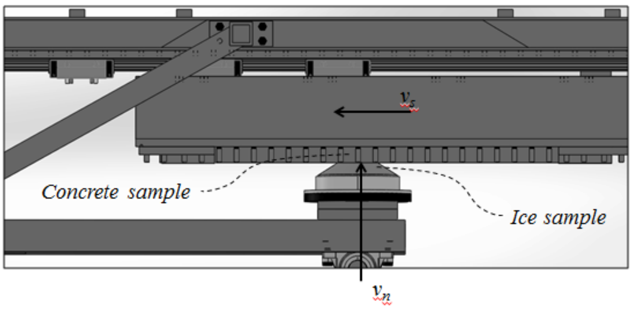

FIGURE 43 ICE-STRUCTURE INTERACTION (UPPER FIGURE) SIMULATION IN THE LABORATORY (LOWER FIGURE). THE UPPER FIGURE SHOWS AN INCOMING SHEET OF LEVEL ICE WITH ICE VELOCITY (V_{ICE}) INTO A CIRCULAR CONCRETE PILE AT A POINT OF CONTACT. THE SYSTEM HAS TWO DEGREES OF FREEDOM: ICE VELOCITY (V_{ICE}) AND ANGLE OF CONTACT (α) , TOGETHER DEFINE THE NORMAL VELOCITY (V_N) AND SLIDING VELOCITY (V_S). THE LOWER FIGURE SHOWS THE IMPINGEMENT OF THE CONICAL ICE SAMPLE (V_N) AND SIMULTANEOUS SLIDING OF THE CONCRETE SAMPLE (V_S).

The input for the test settings consist of a normal and sliding velocity. The definition of the normal velocity (v_n) is:

$$v_n = v_{ice}\cos(\alpha)$$

The definition of the sliding velocity (v_s) is:

$$v_s = v_{ice}\sin(\alpha)$$

Concrete abrasion often involves a combination of numerous factors under the varying parameters and initiate a need to separate the loading types. The advantage of bilateral simulation is to simulate in future settings certain abrasive loading types and zoom in onto the corresponding abrasion mechanics.

3.1.2 DATA STREAMS

Concrete abrasion due to ice action requires to monitor and record the loading processes well. Also, visual data indicate high detail material and supports the physical description of the loading process. A number of measurements streams have been set up (see Table 3), because the experiment got an exploratory character. The movie cameras have been put from four different angles, among them a high speed camera to enable dynamic analysis of the ice action. The thermal camera observes any potential heat traces due to frictional heat. The amount of visual output allows to describe the interface layer very well. The testing involves an extra thermocouple as cross reference for the thermal imagery. Also, the thermocouple is within the vision range of the thermal camera.

TABLE 3 TYPE OF MEASUREMENTS

Unity	Tool
Vertical force	Load cell under MTS moving unit
Horizontal force	Two load cell symmetrical aligned at the back of the swing arm, the horizonta force is the summation of these two load cells.
Vertical displacement	- , very accurate
Horizontal displacement	Jojo pod, a wire under tension by a spring determines the position of the carriage. Structural vibrations can disturb the measurement.
Video	Three go-pro's from three different angles
High speed video	Sideward pointed, FPS is variable dependent on duration of test (Type: Megaspeed)
Thermal video	Upfront, so one is able to observe heat traces after contact (Type: FLIR A65). Purpose identify heat gradients.
Photo	Before and after testing of concrete surface and ice cone. Also, with focus on abrasion traces.

3.1.3 MEASURING ABRASION

Section 2.1 shows two ways of measuring concrete abrasion: Mass loss and surface texture changes. Mass loss won't meet the demand of the experiment, because the goal is to investigate the concrete abrasion process and surface texture characterization is thus preferable. Capable devices were only limited available and this study explores four ways of quantification of concrete abrasion:

- Visual data by video and photo camera
- Surface roughness measurement device (up to 160 µm)
- Two identical test runs before and after a test sequence. Identify potential change of tangential forces due to the change of surface texture.
- Calliper (hole characterization)

The data outcome is able to reveal the visual aspects of the concrete abrasion process.

3.2 TEST SEQUENCE DESIGN

The experiment has an exploratory character. The intention is to explore the abrasion mechanism and simulate the ice-concrete abrasion process as best as the facilities allow. The settings of normal velocity (v_n) and sliding velocity (v_s) come resemble to a specific ice velocity (v_{ice}) and angle of contact (a) (see section 1.3). (Jansson J., 1988) reveals crushing is an important contributor to concrete abrasion and new ice-concrete crushing data can extent the crushing dataset of the STePS[2] crushing series at ice-steel. Three crushing tests at 0.1, 1.0 and 10 mm/s are the first testing part for each beam.

The second process to touch upon is ice sliding. Ice sliding causes shear stresses upon the concrete surface and can wear off aggregates. Few tests are designed such that ice slides under constant normal load (10 kN) over the concrete surface. The sliding rates are chosen at 1.8, 18.0 and 180 mm/s, but more important is that they resemble to the third part of testing.

Third test category is the actively driven shear stress. Simultaneous indenting and sliding initiate high contact pressures in both ductile and brittle failure region. The ductile and brittle indentation rates are known due to ice-steel crushing tests. The indentation rate resemble to the crushing tests and the sliding rates are set at 50%, 100%

and 1800% of the indentation rate, for example with 10 mm/s indentation rate, is the sliding rate respectively 5.0, 10.0, 180.0 mm/s.

The full test sequence is shown in Appendix VII: Test schedule.

3.3 TEST PROCEDURE

The concrete surface requires to be clean prior to testing. The operators requires to remove dust and loose material from the surface by compressed air. The dry abrasion conditions involve stuck ice after each test run. Stuck ice will act as protective layer. The ice remnants are carefully molten away by a heat gun and blown off by a compressor. The concrete surface remains without damage under the protocol.

Then, the ice cone will be put onto the MTS support by bolts. The bolting procedure requires care: Slow and equal tensioning of the bolts of the ice ring. Unequal tension at the bolts induces large internal stresses or fracture in the ice sample. The location of the tip of the ice cone requires to start every run at the same spot at the concrete surface. The vertical position of the tip requires to start such that the contact is almost achieved in order to avoid large impact loads. The initial position values are all noted. The computer controls the system during a test run and no people are allowed nearby the operating apparatus.

Post testing, the measurement devices are turned standby and the concrete surface (both with and without ice trail) and ice cone are taken on photo. The testing procedures are labour intensive and require two people to maintain a proper testing rate. Often one is archiving all data from the devices and the other is already preparing the concrete surface and placing another ice cone.

3.4 ICE AND CONCRETE SAMPLE

The ice strength is generally stronger than natural ice, but the quality of ice remains constant over a test sequence due to thorough fabrication procedure. The approximate ice crushing strength at low ice velocity (v_{ice} =*0.1 mm/s*) is about 20 MPa at an ambient temperature of -10 ˚C. The fabrication procedure and quality tests are shown in Appendix V: Ice sample fabrication.

The concrete samples consist of an high performance concrete sample with an average cylindrical compression strength at a concrete temperature of -10 ˚C of S_c = 73,0 MPa. The high performance concrete mixture includes the addition of Silica Fume (very fine grains) and very low w/c factor. The low performance concrete sample with an average cylindrical compression strength at a concrete temperature of -10 ˚C of S_c = 40,7 MPa. The low performance concrete mixture includes much aggregates in comparison to the high performance concrete mixture. The exact mixtures, fabrication procedure and validation tests are shown in Appendix VI: Concrete samples.

3.5 LIMITATIONS

The limitation of the experiment depends on the impact of errors. The following errors are mitigated:

- Angular deviation of impact: The swing arm forces the impact to turn around the turning point at the back of the structure and introduces an angle. The angular deviation introduces an increase in contact area and stress due to an eccentric moment. The correction of the contact area and corresponding moment are shown in
- Appendix I: Matlab code of single test
- Structural torsion of swing arm: The alignment of the horizontal load cells is imperfect installed and introduces an error in horizontal force measurements. The alignment has been mechanical improved and assumed to be negligible.
- Vibrating jojo-pod: The vibration of the jojo-pod wire introduces an error in the measurement of the horizontal displacement. The error increases if the structural vibration increases due to stick-slip. The

solution is an approximation on the horizontal displacement (*dz*) with a known time vector (*dt*) and known constant sliding rate (v_s), the formula is:

$$dz = v_s * dt$$

- Structural excitation around the Eigen frequency: The Eigen frequency is hard to determine in horizontal directions and is definitely of influence of the force measurements. The importance of dynamics decides whether to pursue the filter out the structural effects and it appears it is not sufficient relevant to put much effort in it yet.

Other errors of the simulation type are as follows:

- Ice sample quality in comparison with natural ice: Ice is in nature a heterogeneous material (see section 2.4.5) and in the experimental work one attempts to simulate that with the lab version of heterogeneous ice. Sea (level) ice is main contributor to ice-concrete abrasion problems and thus fundamentally different than the lab ice. However, the ice grade is pretty well controllable, consistent and is able to potentially reveal a common mechanism.
- Size effect: Ice appears to be much stronger in laboratory than in practice due to the size effect (see section 2.4.1).
- Absence of water: Literature observes that wet conditions appear to be more abrasion sensitive than dry conditions. The current testing compromises in capability and simulate dry abrasion conditions which are less realistic than wet condition due to formation of a protective ice layer and absence of a higher liquid content at the contact interface.
- Freeze-thaw cycles: Concrete in ice abrasion exposed environments are always exposed to freeze-thaw cycles (see section 2.5.4). Freeze-thaw cycles reduces the abrasion resistance of concrete and thus simulation of freeze-thaw cycles is crucial of simulation of the process. The freeze-thaw cycles have not been part of the experiment.
- Temperature gradients: Sea water and air temperature might differ over 30 degrees in the high Arctic and can cause large temperature gradients at the concrete which might also reduce the abrasion resistance (see section 2.5.5). The temperature gradient have not been part of the experiment.
- Chemical ingression and reaction of concrete composite with sea water elements (see section 2.5.7). Chemical ingression have not been part of the experiment.

Also, the structure is a 2D lateral simulation of a 3D real scale setting. Vertical (real) deflection of ice movement upward (weight) and ice movement downward (buoyant weight) are for the case of simplicity left out, but should not be forgotten in the end. The second drawback is fracturing, on both macro and micro scale. Fracturing and spalling reduces the interfacial area between the ice and concrete and affects directly the compression, shear stresses and adhesive bindings. The proportionality between the three forces correspond to the behaviour of the loading. The effect of fracture is an important aspect for further verification of the abrasion simulation and does not fall within the scope of this report. Third drawback is the absence of wet conditions. Literature identified wet conditions appears to increase abrasion in comparison with dry conditions. The mechanism is not certain yet, (Janson J., 1988) suggest the dry conditions obtain a protective ice cover sticking to the concrete and (Sistonen E. and Vasikari E., 2008) suggest wet conditions increase fracture effects like scaling or indentation pore pressure. Essence, is wet conditions are of increasing importance in determination of extremes at the concrete structure. The tests are only conducted in dry conditions due to practicability.

4. Results

The result section shows the results from the experiment shown in section 1.3 and 3. The section treats ice loading and abrasion traces from interaction.

4.1 Shear loading of ice

Shear loading induces concrete abrasion (Huovinen S., 1990) and gets attention in section 4.1. Shear loading involves dry, wet friction and adhesion. Adhesion seem to introduce a cyclic type of shear loading.

4.1.1 Effect of ice velocity

Ice velocity definition is the relative velocity between ice and structure. The ice velocity directly effects the shear load. Figure 44 shows the tangential load for ice velocities v_{ice}=1.8 and 180 mm/s .

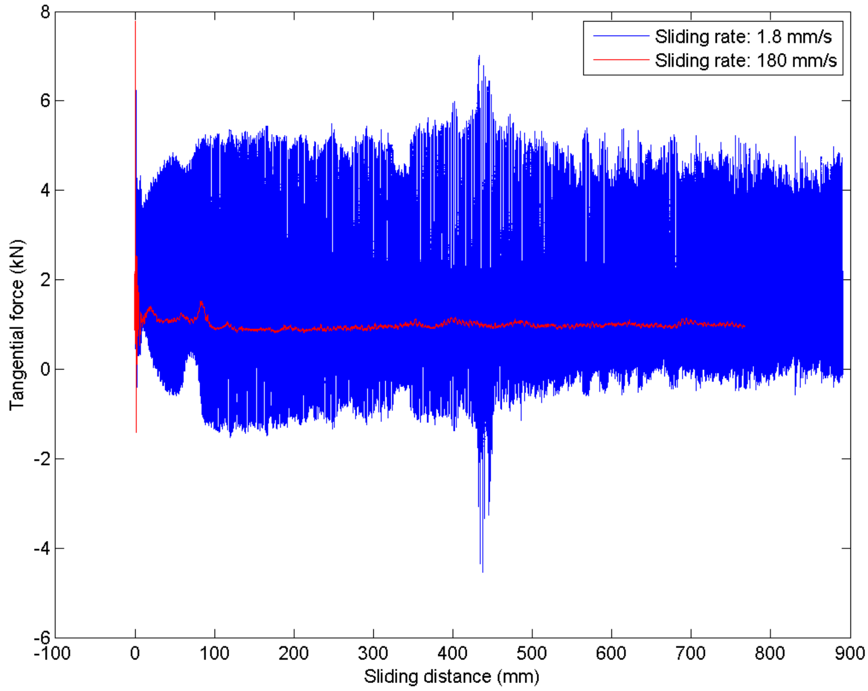

Figure 44 Tangential force for two ice velocities (sliding rates) (under F_N=10 kN – Concrete type I)

Slow ice velocity (v_{ice} = 1.8 mm/s) reveals stick-slip behaviour. Adhesion strengthen the tangential resistance with hydro bonding and makes it harder to maintain displacement for the control system. Figure 44 zooms in onto the cyclic loading by application of a Fast Fourier Transform (FFT).

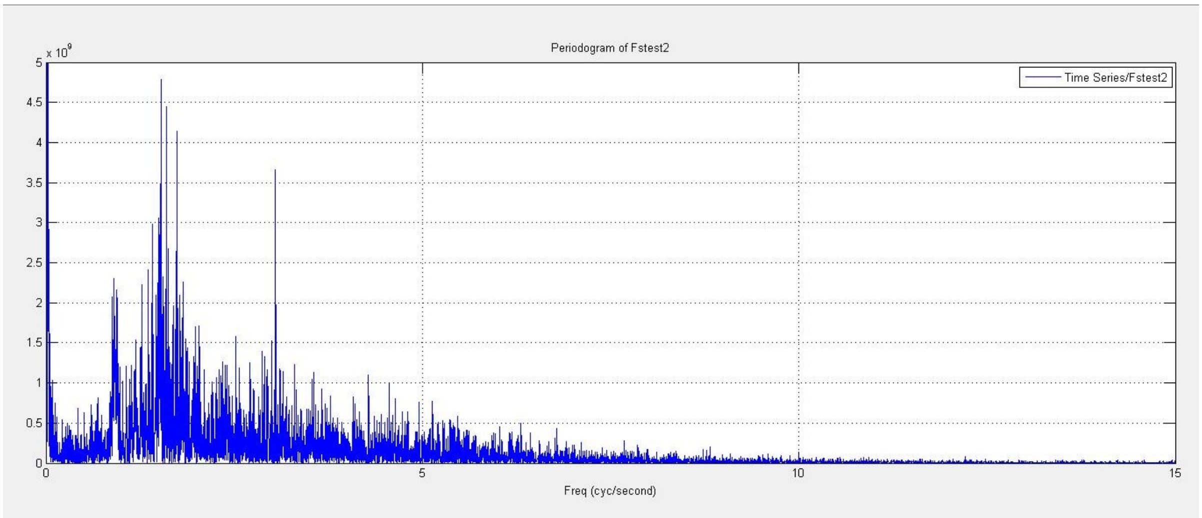

FIGURE 45 FFT OF THE SLOW TEST (V_{ICE} = 1.8 MM/S) FROM 0 – 15 HZ

Figure 45 shows the peaks in the frequency domain between 0 – 5 Hz, above the 5 Hz the peak frequencies are negligible. Figure 46 zooms in onto the frequency range from 0 – 5 Hz.

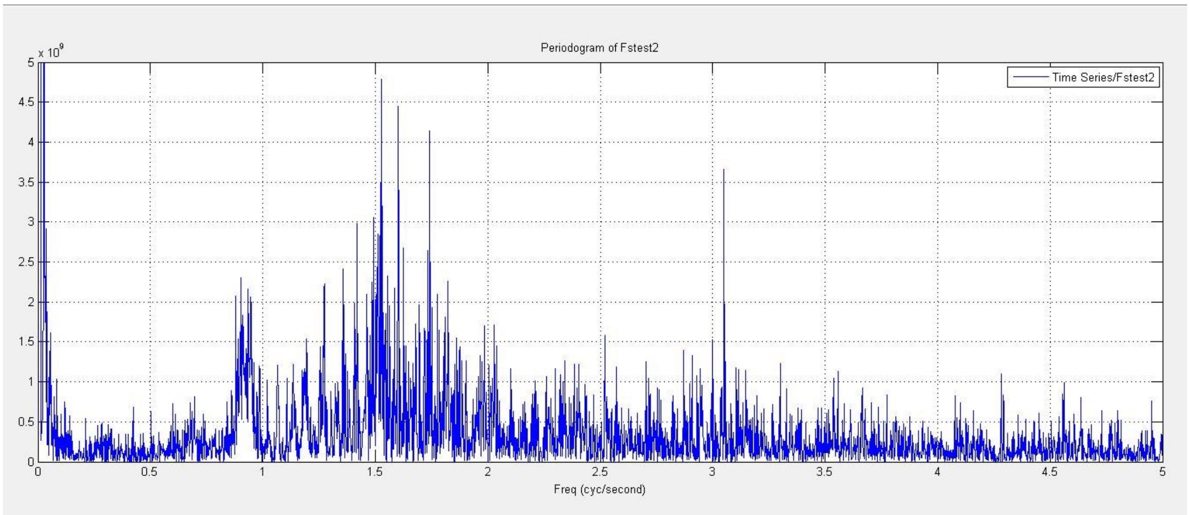

FIGURE 46 FFT OF THE SLOW TEST (V_{ICE} = 1.8 MM/S) FROM 0 - 5 HZ

The first peak is located around the 0.9 Hz, second around 1.5 Hz and the third around the 3 Hz. Most likely 1.5 and 3 Hz correspond with each other due to a mode of a structural vibration. The peak at f_{peak}=0.9 Hz seem to occur due to stick-slip, but Figure 47 proves that might not be entirely true.

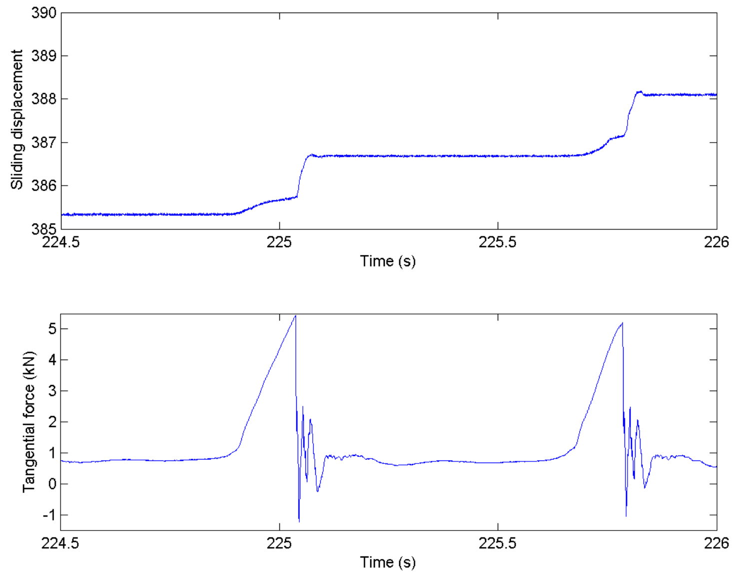

FIGURE 47 STICK-SLIP CYCLUS FOR 1.8 MM/S SLIDING RATE

Figure 47 shows a random chosen time interval in the slow test (v_{ice}=1.8 mm/s) and indicate a stick-slip period of approximate 0.75 second corresponding with 1.3 Hz. The frequency in Figure 47 does not resemble to a peak in the frequency domain in Figure 46. The hypothesis is stick-slip does not occur at solely one frequency.

The force build-up can be categorized in four stages:

1. The system sets a new desired position and tangential loading builds up, see triangular force build-up
2. The ice reacts with a viscoelastic strain and becomes stiffer with increasing load, but the adhesive bonding (plus friction) maintains in place.
3. The loading equals or overcome the adhesive resistance (plus friction) and adhesive bindings break
4. Movement starts and the new desired position has been reached (little overshoot due to jojo pod or elastic bonding of ice-concrete), load drops, adhesive bonding will rebuild and strengthen the tangential resistance. And another cycle initiates.

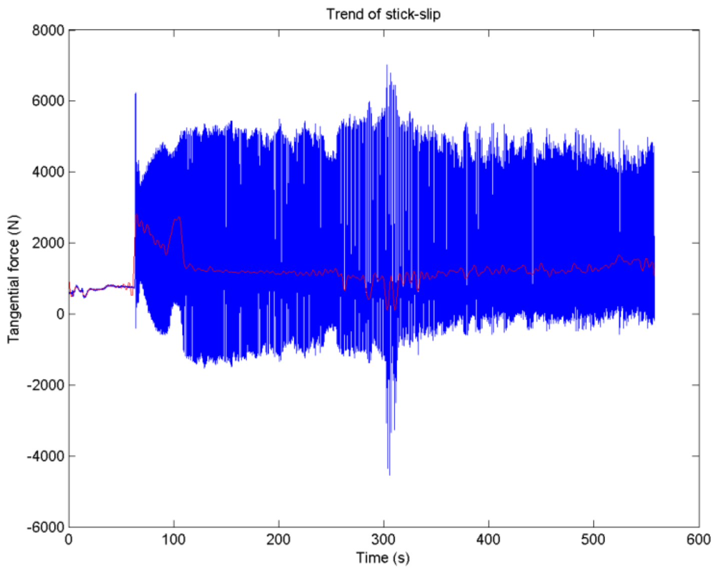

FIGURE 48 LOW PASS FILTER <0.2 HZ - TRENDLINE DURING STICK-SLIP AT AN ICE VELOCITY OF V_{ICE} =1.8 MM/S (F_N=10 KN / CONCRETE TYPE I)

Figure 48 shows the trendline of the slow sliding test (1.8 mm/s) and the mean is F_{mean}= 1.21 kN. The mean of the fast sliding test (180 mm/s) is F_{mean}= 1.24 kN. The contact load build-up naturally weighs more in a fast test than in a slow test, so the fast test may differ slightly more with the mean tangential load of the slow test. The major difference is the type of loading and time scale.

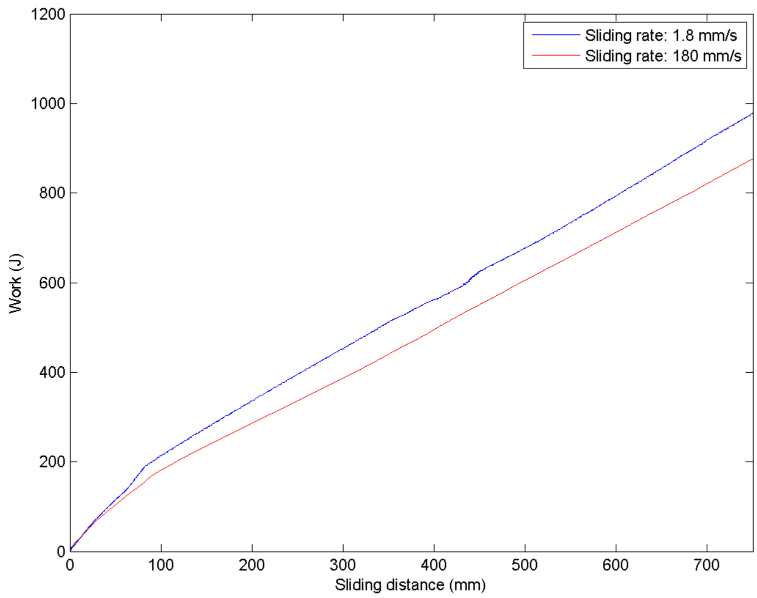

FIGURE 49 WORK EXERTION FOR SLOW (V_{ICE}=1.8 MM/S) AND FAST SLIDING (V_{ICE}=180 MM/S) (F_N=10 KN – CONCRETE TYPE I)

The slow sliding rate exerts slightly more work on the concrete surface than the fast sliding rate. Slow sliding goes with stick-slip cyclic loading with relative high peak loading (5 times mean value). The cyclic loading with the high peaks causes a larger slope in the work curve. The derivative of these graphs indicates work generation on the concrete surface over sliding distance (or time with a known sliding rate).

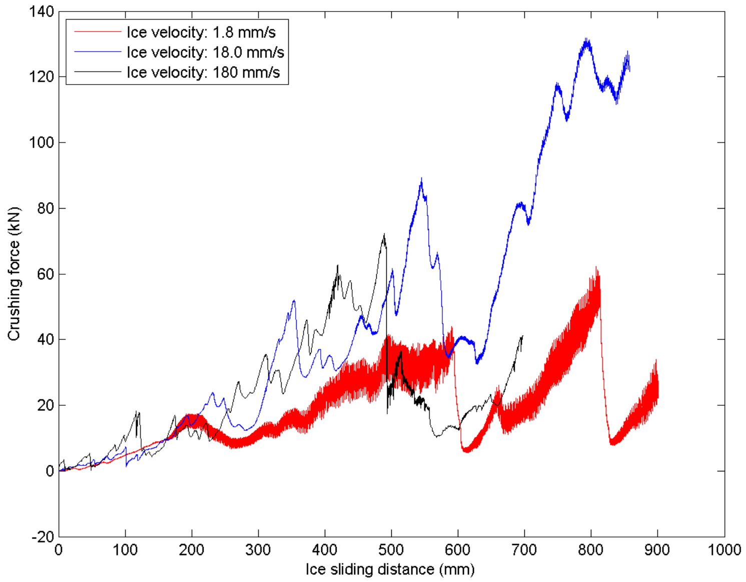

FIGURE 50 CRUSHING FORCE FOR THREE ICE VELOCITIES OF V_{ICE}=1.8/18.0/180 MM/S (AT A=86.6 DEG)

Figure 50 shows the curves of the crushing forces under three ice velocities. The slow ice velocity (v_{ice}=1.8 mm/s) shows stick-slip effect while the faster ice velocities (v_{ice}=18.0 and 180 mm/s) test do not. The slow ice velocity (v_{ice}=1.8 mm/s) shows even lower crushing forces than the faster ice velocities (v_{ice}=18.0 and 180 mm/s) tests. All tests show fracturing behaviour known as brittle ice failure.

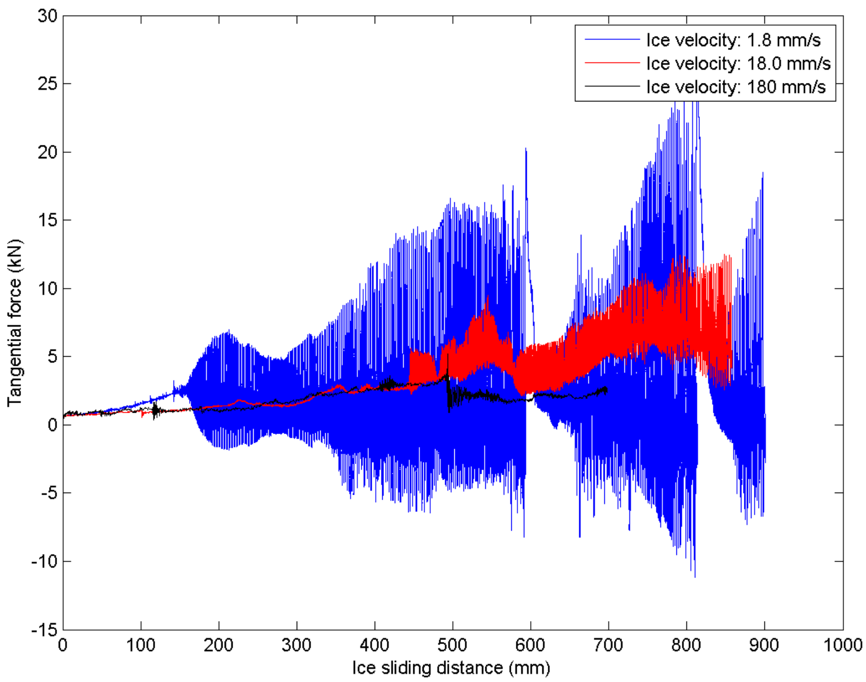

FIGURE 51 TANGENTIAL FORCE OF THREE ICE VELOCITIES OF V_{ICE}=1.8/18.0/180 MM/S (AT A=86.6 DEG)

Figure 51 shows the tangential force of the three ice velocities and indicate the stick-slip phenomenon. The ice velocity of v_{ice}=18.0 mm/s shows stick-slip from about the sliding distance of z_{sd} = 450 mm while the slow ice velocity of v_{ice}=1.8 mm/s got stick-slip during the entire test. Also the tangential force is much higher during the slow ice velocity than the faster ice velocity, although the steady state average does not differ significantly. The relevance of the friction factor becomes of increasing importance because it provides essential information about the functioning of the contact area during load transfer. The dynamic friction factor definition is:

$$\mu_d = \frac{F_s}{F_n}$$

Where μ_d is the friction factor (-), F_s is the tangential (sliding) force (kN) and F_n is the normal force (kN). The dynamic friction factor is the factor when the forces get into steady-state. The run-in region in the beginning of the experiment depends on the static friction factor and depends strongly on the bonding energy between the ice and concrete. The dynamic friction factor converges to a steady state value, because the duration of bonding is in balance with the ice velocity.

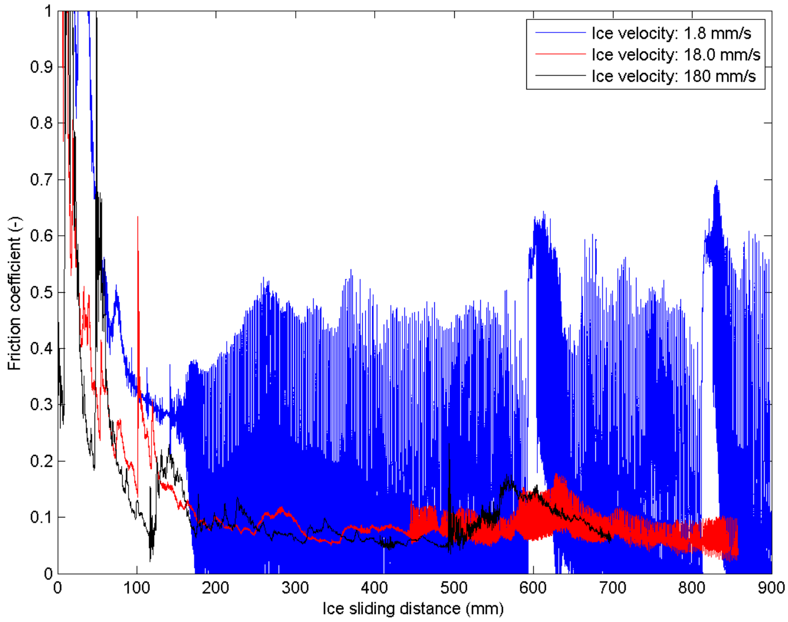

FIGURE 52 FRICTION FACTORS FOR VARYING ICE VELOCITIES (AT A=86.6 DEG)

Adhesion increases the static friction factor (μ_s) , but the effect reduces for increasing ice sliding velocity (v_{ice}) . The stick moment of the stick-slip cycle induces the peaks of the tangential force at the slow ice velocity of v_{ice}=1.8 mm/s. The friction factors seem to converge to a steady-state values of μ_d<0.1.

The loading onto the concrete requires a parameter is able to express the loading accumulation, because abrasion depth is an accumulation of resistance failure. Work is able to do that. The relation between contact pressure and abrasion is proportional (see section 2.4.1). Ice sliding distance and abrasion depth are also proportional (see section 2.4). Work is thus an excellent measure for concrete loading due to its proportionality to force and distance. Work describes the energy requirement in order to destruct a specified ice volume. The formula to calculate work due to the normal force is:

$$W_n = \int_0^x F_n(x)\, dx \approx \sum_i^{n-1} (x_{i+1} - x_i)(\frac{F_{n,i+1} + F_{n,i}}{2})$$

Where x is the indentation (mm), F_n the normal force (kN) and i the index number of a chosen sample. The formula to calculate work due to the tangential force is:

$$W_s = \int_0^x F_s(x)\,dx \approx \sum_i^{n-1} (z_{i+1} - z_i)(\frac{F_{s,i+1} + F_{s,i}}{2})$$

Where z is the sliding distance (mm), F_s the tangential force (kN) and i the index number of a chosen sample. The total work W_{total} is the summation of the work due to normal force and the work due to tangential force.

$$W_{total} = W_n + W_s$$

The discrete method in order to calculate the continuous integral is also known as trapezoidal integration. The advantage of using integration is to reduce the magnitude of time effects onto. The crushing history is in other words captured as a single value and simplifies comparison between tests. The crushing resistance of ice for three ice velocities of v_{ice}=1.8/18.0/180 mm/s in Figure 53.

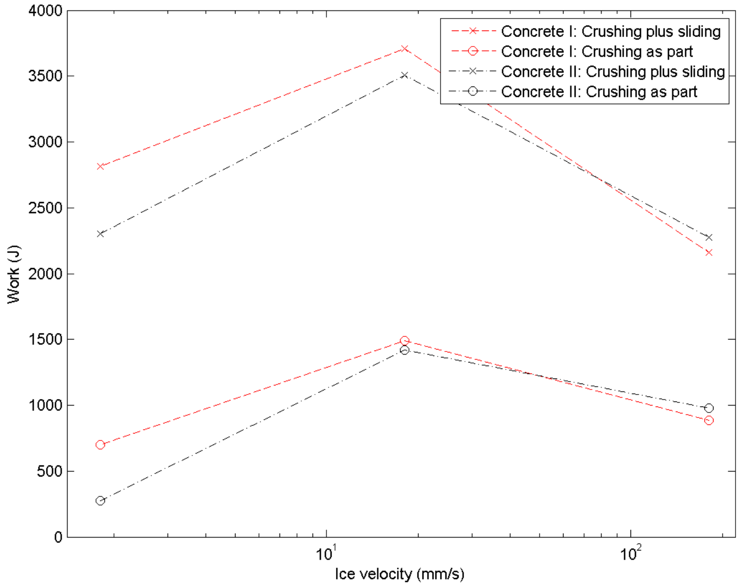

FIGURE 53 WORK FOR VARYING ICE VELOCITIES (1.8/18.0/180 MM/S) AT Α=86.6° – TWO CONCRETE TYPES

Figure 53 shows slow sliding test (v_{ice}=1.8 mm/s) exerts little work due to the stick-slip phenomenon, because the cyclic vibrations introduce fracture, reduce coherence of the ice material and reduce the concrete loading. Largest work appears at the transition ice velocity (v_{ice}=18.0 mm/s) with minor vibration but still with ductile force build-up. Work reduces for fast ice velocity (v_{ice}=180 mm/s), because the ice is not able to relax and increase the real contact area. Also, frictional heat increases and lubricates the interface.

4.1.2 EFFECT OF ANGLE OF CONTACT

The study likes to explore the various types of ice loading over various angles of contact (α). Especially considering the adhesion effects as stick-slip. The angle of contact (α) defines from which direction the ice exerts a load on the concrete surface. When α=0 degrees, the ice flow will collide on the perpendicular face of the structure relative to the ice flow and when α=90 degrees the ice flow will slide on a parallel face relative to the ice flow. See section 1.3 for more details on the simulation.

Stick-slip has been observed in two types of testing: Figure 54 shows grinding under constant normal load and under constant indentation, both during slow ice velocity (v_{ice} = 1.8 mm/s).

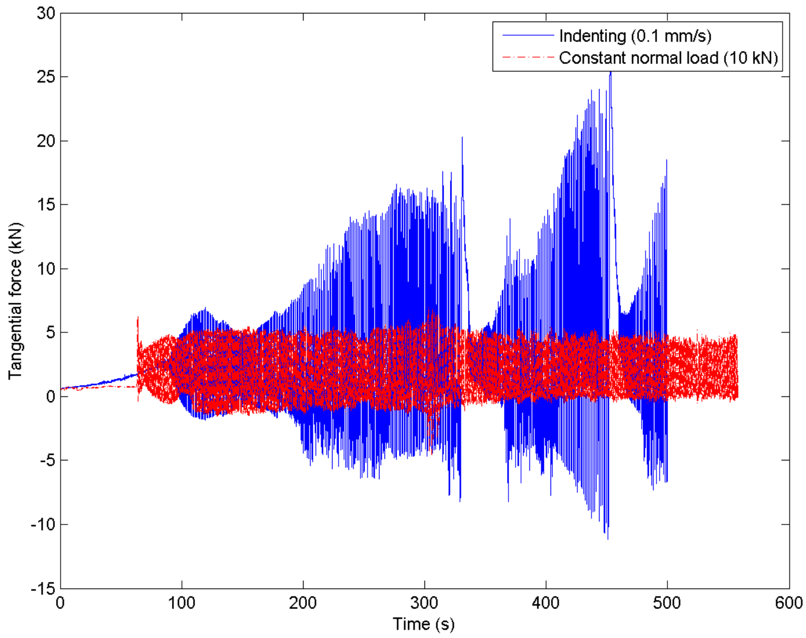

FIGURE 54 STICK SLIP AT SLIDING VELOCITY (V_S) OF 1.8 MM/S. CONSTANT INDENTATION VELOCITY (V_N = 0.1 MM/S AND A=86.6°) VERSUS CONSTANT NORMAL LOAD (F_N = 10 KN).

Constant indentation shows an increase of tangential force, but about t=340 s a large drop in tangential force occurs due to shearing off of a large ice piece. Figure 55 shows the fast Fourier transform (FFT) of the constant indentation test from Figure 54. Figure 56 shows the FFT of the constant normal force test from Figure 54.

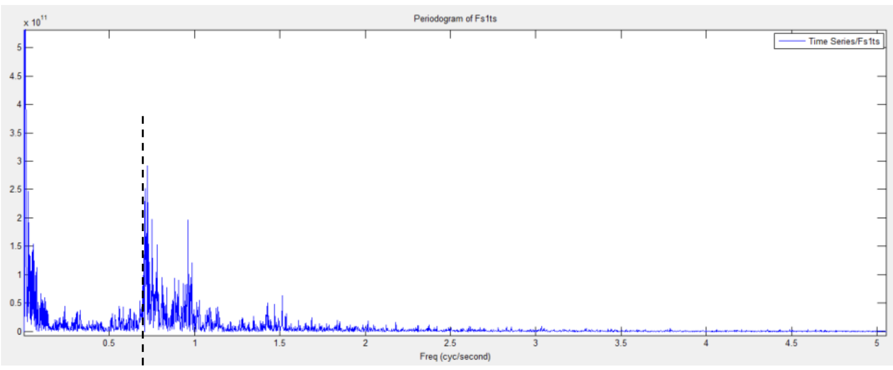

FIGURE 55 FAST FOURIER TRANSFORM (FFT) FROM CONSTANT INDENTATION TEST (A=86.6°) FROM FIGURE 54, FROM 0 – 5 HZ. THE PEAK FREQUENCIES OCCURS AT F_{PEAK} = 0.75 HZ.

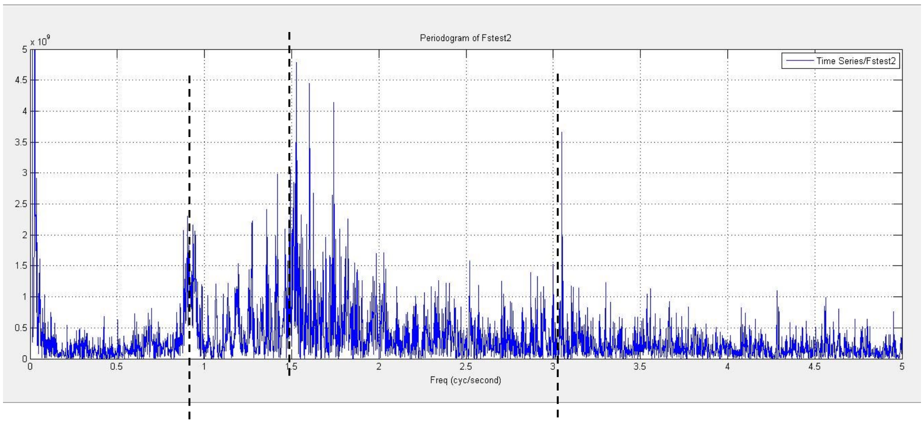

Figure 56 Fast Fourier Transform (FFT) from constant normal force test from Figure 54, from 0 - 5 Hz. The peak frequencies occurs at F_{PEAK} = 1.50 Hz, but also F_{PEAK} = 0.9 Hz amd F_{PEAK} = 3 Hz

Figure 56 shows peaks around 1.5 and 3 Hz, but Figure 55 shows other peaks about 0.7 Hz (T=1.4s). The peaks seem to correspond with stick-slip cycles (high speed footage), but the cycle period varies during the test. The stick-slip cycles contain high frequencies at low indentation (low contact area), but with increasing indentation (increasing contact area) the frequency decreases. Figure 57 shows the frequency is able to increase due to fracturing (decrease of contact area) and occurs often in the latter part of the test.

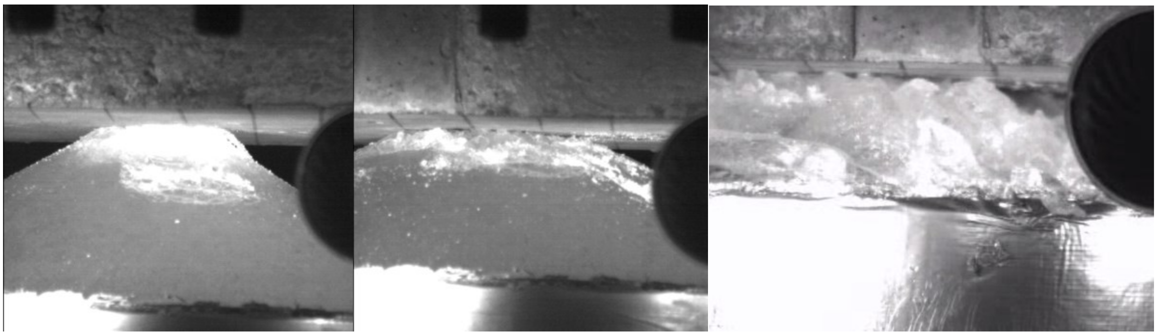

Figure 57 High speed imagery at varying contact areas, the screenshots show beginning test 1.5 Hz (left photo), halfway test 0.9 Hz (middle photo) and at the end of the test 1.1 Hz (right photo).

Ice sliding is the tangential movement of the ice relative to the concrete surface. An ice load is often a combination of crushing and grinding due to the normal and tangential component on the contact surface. The sliding effect on ice loading increases tangential stresses through the ice and concrete. The shear stresses on the contact surface may cause wear on the concrete surface. Sliding with wear is also named grinding. Grinding on the concrete surface may consist of a combination of dry and wet friction and adhesion.

4.2 Compression loading of ice

4.2.1 Effect ice velocity

Ice deforms as a nonlinear viscoelastic material during low indentation rates, also known as ductile failure and during higher indentation rates visco-plastic behaviour and fracturing occurs, also known as brittle failure. Brittle ice failure is most common in ice conditions offshore, but ductile rates result into larger forces than brittle rates.

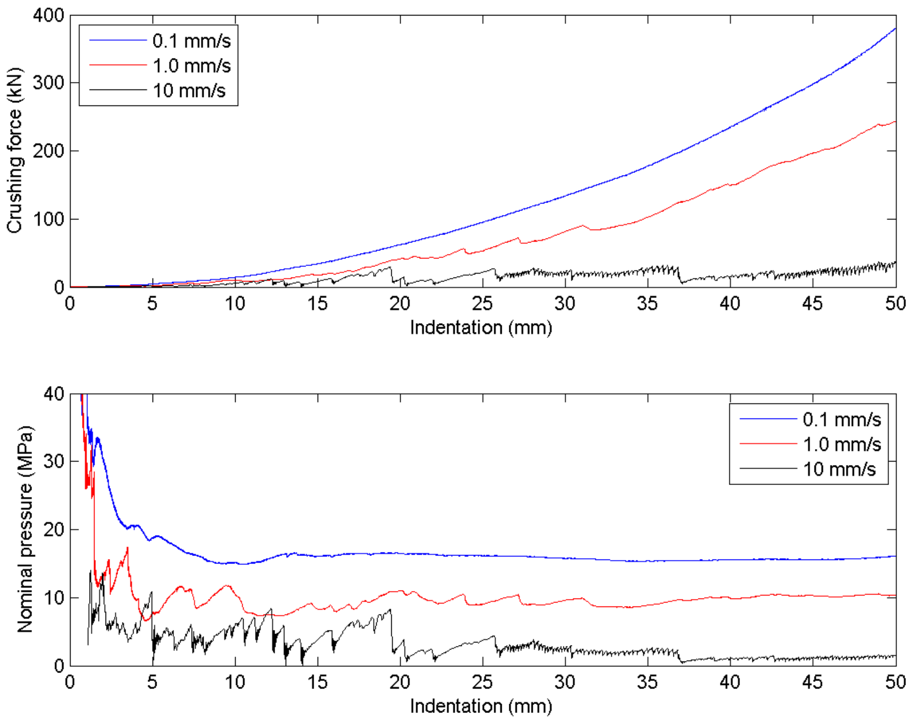

FIGURE 58 ICE-CONCRETE CRUSHING FORCE AND NOMINAL COMPRESSION PRESSURE FOR THREE ICE VELOCTIES V_{ICE}=0.1/1.0/10 MM/S (NO SLIDING / HP CONCRETE)

The crushing force behaves ductile or brittle dependent on the indentation rate and correspond to experimental work on ice-steel crushing (Dragt S., 2013; Dillenburg A., 2012). The slow ice velocity (v_{ice} = 0.1 mm/s) indicates a typical smooth, ductile force build-up. The fast ice velocity (v_{ice} = 10 mm/s) indicates brittle failure of ice. Also, ductile crushing forces are an order of 10 larger than brittle crushing forces. The intermediate ice velocity (v_{ice} = 1.0 mm/s) indicates the transitional region of ice failure under compression and indicates early brittle signatures.

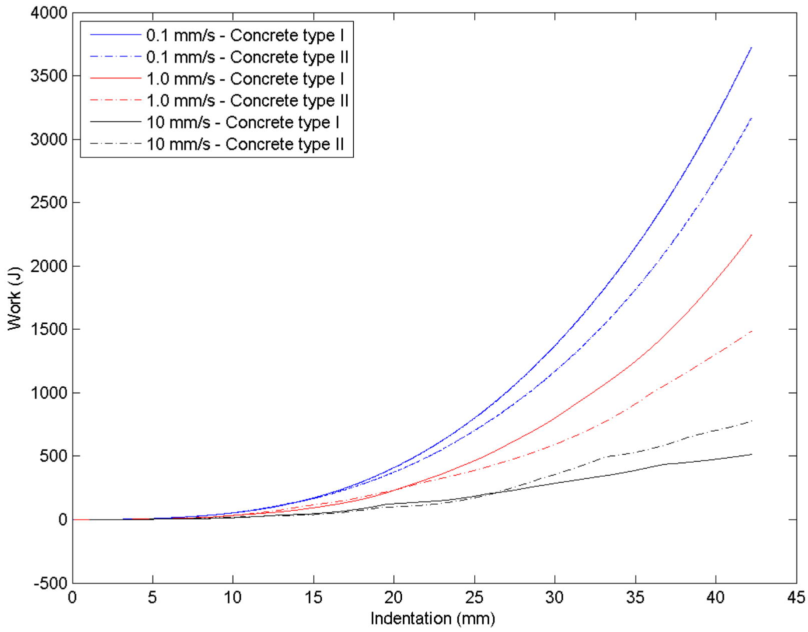

FIGURE 59 WORK CURVES FOR THREE ICE VELOCITIES ((V_{ICE} = 0.1/1.0/10 MM/S) AND TWO TYPES OF CONCRETE

Slow ice velocities (v_{ice} = 0.1 mm/s) exerts largest accumulation of ice loading onto the concrete surface, but are not very common ice velocities in the field. Increasing ice velocities (v_{ice} = 1.0/10 mm/s) decreases the accumulation of ice loading due to fracturing. The accumulation of ice loading concerns a global indication and not a local (read: microscopic) one, see section 2.4.1. Also, interesting is that concrete type I requires more destructive work than concrete type II in a slow ice velocity (v_{ice} = 0.1 mm/s), but concrete type I requires lower destructive work than concrete type II in faster ice velocities (v_{ice} = 1.0/10 mm/s). The exponential curvature originates from an increasing contact area over indentation, but is identical among all tests.

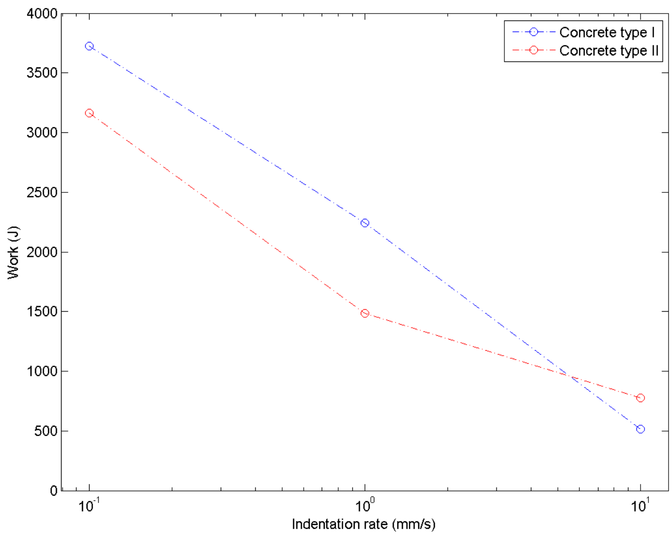

FIGURE 60 WORK FOR THREE INDENTATION RATES (FOR 42,2 MM INDENTATION)

Figure 60 shows the work required for destruction of a certain volume of ice material and thus serve as average strength over the volume.

4.2.2 Effect of material

The crushing data on concrete in comparison to (earlier work on) steel data requires to average the work (or energy) over the crushed volume.

$$V_c(x) = \frac{1}{3}\frac{\pi x^3}{tan^2(\beta)}$$

Where V_c is the crushed volume (m^3), x the indentation (m) and β the cone angle (degrees). The ice cone for the concrete test runs is always 30 degrees.

$$E_c = \frac{W_n}{V_c} * 10^{-6}$$

Where E_c is the energy per crushed volume (MPa), W_n work (or energy) (J). E_c is a reasonable measure for crushing resistance. Although, V_c represents the ideal conical volume and due to fracture the active volume can be smaller, but to globally examine the crushing mechanism E_c suffices.

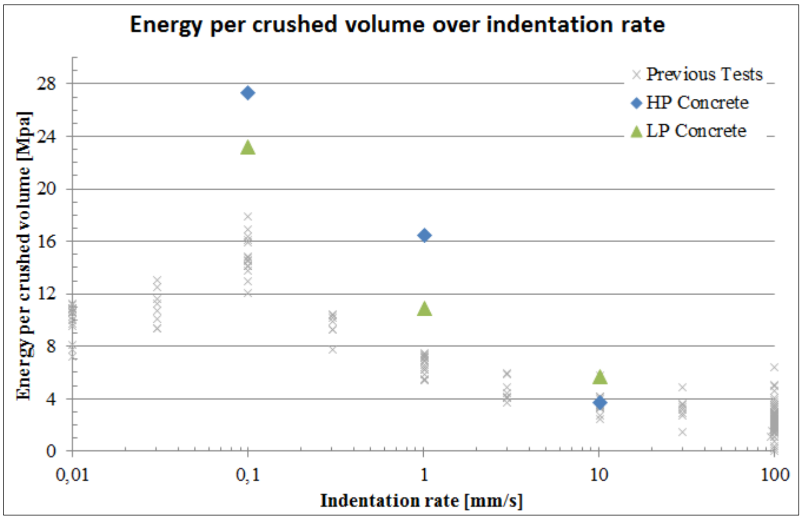

Figure 61 Comparison of ice-concrete crushing tests to ice-steel crushing tests (Dillenburg A., 2012; Dragt R., 2013)

Figure 61 shows previous data of the STePS[2] project on ice-steel crushing. The slow tests behave in the ductile regime and the fast tests in the brittle regime, and in the middle the transitional regime. Figure 61 clearly shows some observations as the concrete crushing tests indicate large energies (work) per crushed volume in comparison to the ice-steel crushing tests. Fast indentation rates (v_n = 10 mm/s) indicate no large differences between ice-steel and ice-concrete crushing tests. Adhesion and roughness with a concrete surface seem to involve a larger confinement and increases the ice crushing forces on concrete material in comparison to steel.

4.3 Concrete abrasion

The section shows evidence of abrasion on the concrete and ice.

4.3.1 Concrete indications

The starting point of the test runs have been classified as a crushing zone and transits gradually to a sliding zone. Typical features of this area after ice loading are holes and revelation of granular material on the surface. The cement particles have been removed. Indication of the concrete abrasion process are shown onto the surface by overview photos, but also with detail photos. The abrasion depth is an accumulation of abrasion events and relates to an accumulation of ice loading (see section 4.1.1 on the loading characterization).

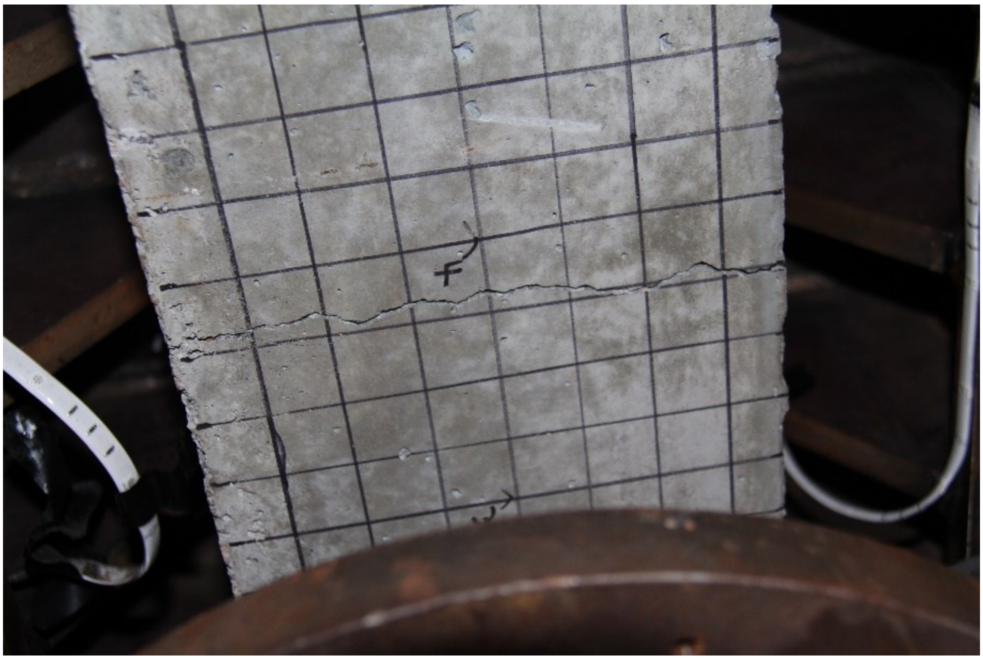

FIGURE 62 CONCRETE SURFACE PRIOR TO A TEST SEQUENCE

Figure 62 shows the surface of the concrete beam prior to a test sequence. The lower side of the photo shows the starting point of the beam (lower than crack). The concrete sample has been put into the apparatus and has a smooth surface. Silica fume decreases the surface roughness by filing up the smallest spaces in the concrete material. The number signs on the surface indicate the measurements of the surface roughness measurement device. The crack is unfortunate not part of the test, but due to a calibration error. The absolute location of the crack in sliding direction is 176.4 mm.

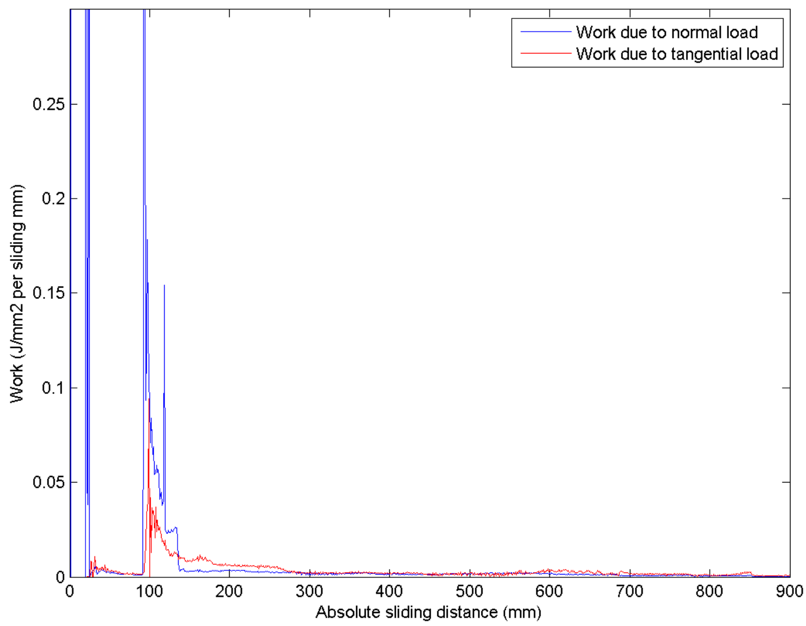

FIGURE 63 CONCRETE LOADING OVER TEST SEQUENCE

Figure 63 shows the ice loading in two direction on the concrete surface. The loading curve represents varying loading types (details about the test sequence in Appendix VII: Test schedule). The representation is thus rather a macroscopic than a microscopic approach and indicate the location of loading accumulation at the concrete sample. Figure 63 shows high activity around 100 mm sliding distance. Especially, due to normal load. The normal load (in work) is 5 times larger than the tangential load (in work). The loading decreases over the sliding distance, because the crushing without sliding tests only involve the starting point and no other locations. Figure 63 shows another peak loading at 40 mm absolute sliding distance, because the first tests started there. The starting location was changed to about 100 mm (93.4 mm) absolute sliding distance later, but the first slow test involves huge normal loading and is thus clearly visible in the loading graph (Figure 63).

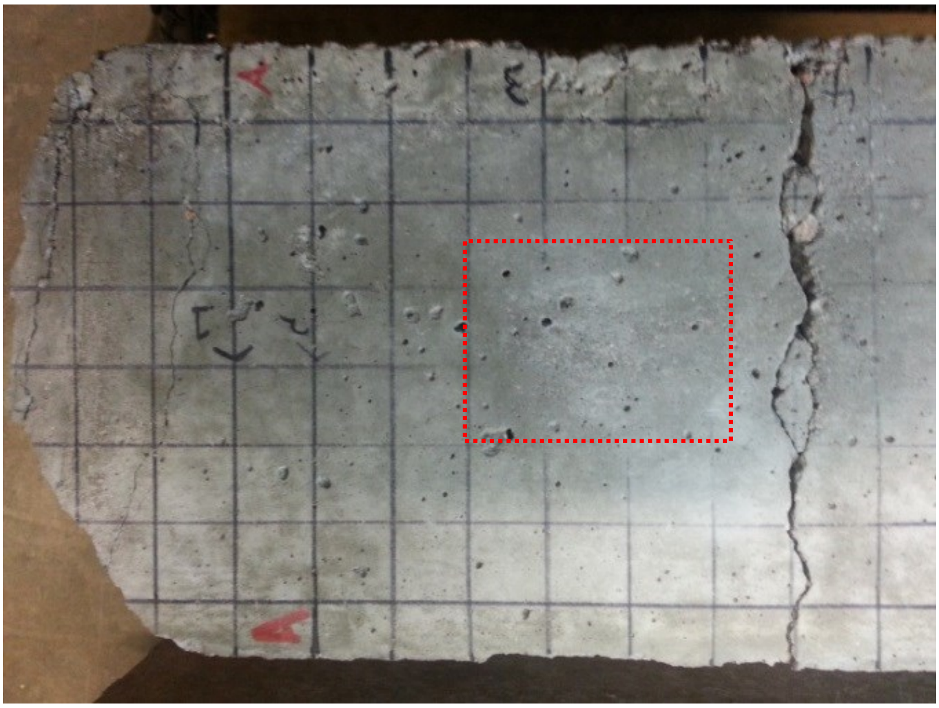

FIGURE 64 CONCRETE SURFACE AFTER TEST RUN 1B (POST-TEST SEQUENCE) - STARTING POINT

Figure 64 shows the high performance concrete beam post-test sequence. The shown area resembles to Figure 62 and clearly indicate surface wear. The grid lines got worn off and a number of holes became visible on the surface. Although the crack was not part of the test plan, it shows typical scour traces. The shallow surface crack seems to widen and the sharp corners got rounded shapes.

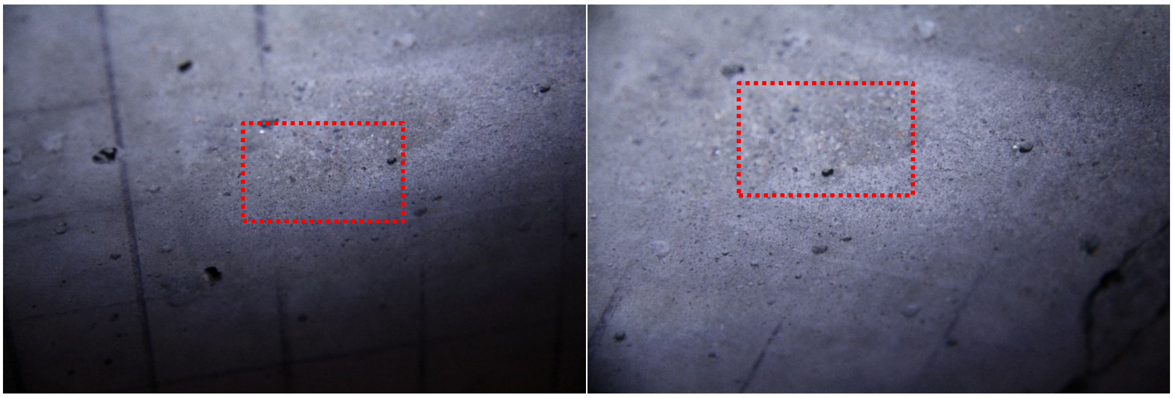

FIGURE 65 EXPOSURE OF AGGREGATES (AFTER TEST RUN 9B)

Figure 65 shows visible aggregates. The cement layers are torn off the surface and load the aggregate now. The material stage resembles to the initiation of stage II of the description of (Huovinen S., 1990). Aggregates stabilizes the abrasion rate as they involve a larger abrasion resistance. Removal of cement particles also involves an increasing roughness and thus increase shear stresses. Figure 66 shows global surface wear over a test sequence at the high performance concrete sample.

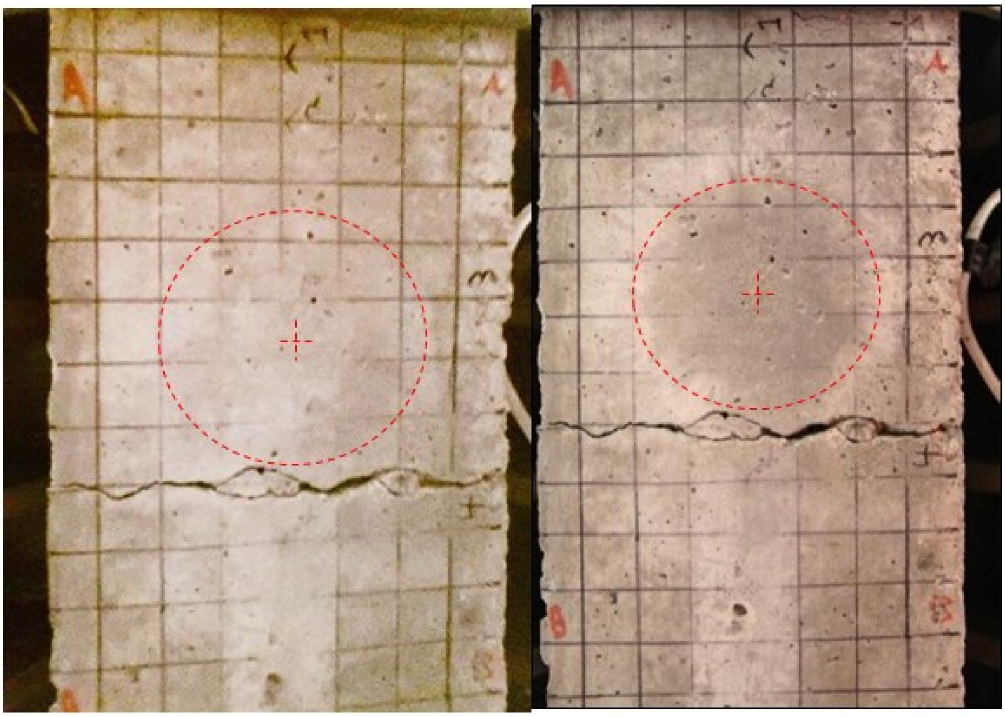

FIGURE 66 SURFACE OF HIGH PERFORMANCE CONCRETE SAMPLE BEFORE (LEFT) AND AFTER (RIGHT) SLOW CRUSHING TEST (V_{ICE} = 0.1 MM/S / $\alpha \approx 0°$). THE ABRASIVE LOADING OVER ONLY ONE TEST RUN IS ABOUT 1.95 J/MM^2 NORMAL LOADING AT THE REFERENCE CROSS. THE LOADING CORRESPOND TO A NOMINAL COMPRESSION PRESSURE OF ABOUT 20 MPA. THE CONCRETE AFTER THE TEST SHOWS SCOUR LIKE TRACES RADIAL ON THE CONCRETE SURFACE AND ALSO INVOLVES EXPOSURE OF SMALL AGGREGATES.

4.3.2 ICE INDICATIONS

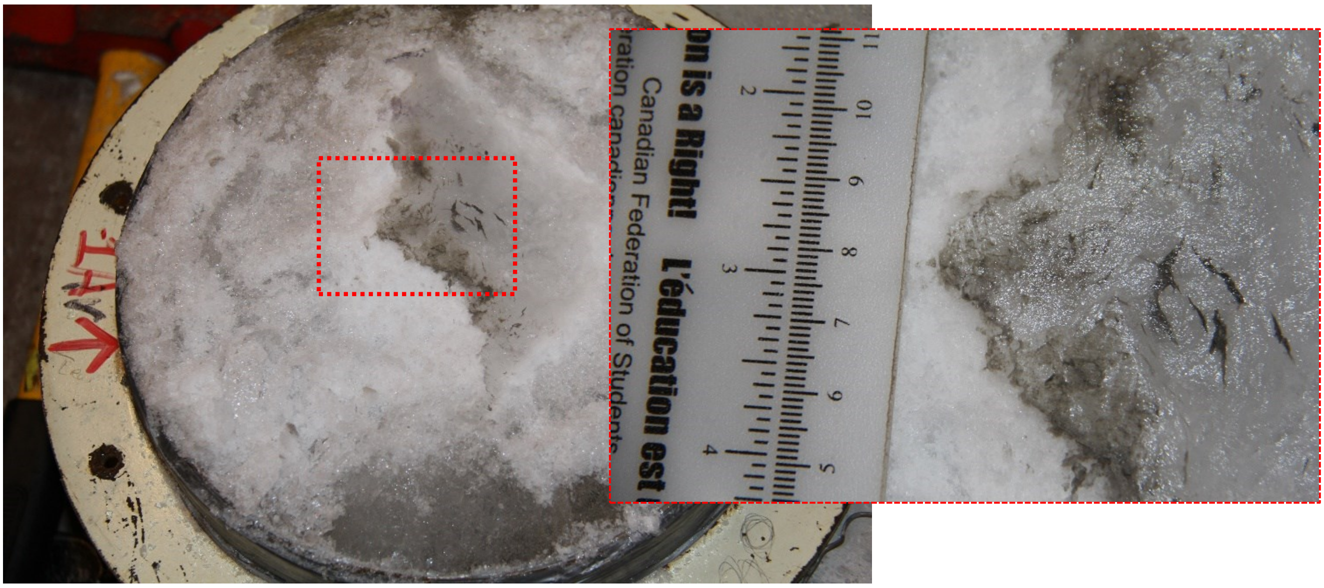

FIGURE 67 CEMENT PARTICLES AND DUST ENCLOSED UNDER THE ICE SURFACE AFTER TEST 1A (V_N=1.0 MM/S AND V_S=18.0 MM/S)

Figure 67 shows evidence of increasing impurity content due to concrete particle inclusion in the surface ice layer. An increasing impurity content increases the abrasion rate as is shown in section 2.4.4. Also, the photo reveals concrete particle concentrations along lines. The location of concrete concentrations might correspond to high pressure zones, because liquid like layers might be able to include the concrete particles and recrystallize after testing. Second theory, the high pressure zone forces the mixture of ice and concrete particles outward and concentrate them at the fracture lines of the high pressure zone. The zone at the front of the ice cone is typically shearing off ice. The shearing off occurs typically when the ice-concrete adhesion binding exceeds the internal ice cohesion binding along one of the shear lines in the ice cone.

FIGURE 68 ICE CONE AFTER (SLOW GRINDING) TEST 8 (1.8 MM/S) UNDER CONSTANT NORMAL PRESSURE (10 KN)

Figure 68 also shows concrete particles at the interface. Typical traces of concrete abrasion, even under passive sliding. The shear stress seems to exceed the shear resistance of few asperities and loose dust.

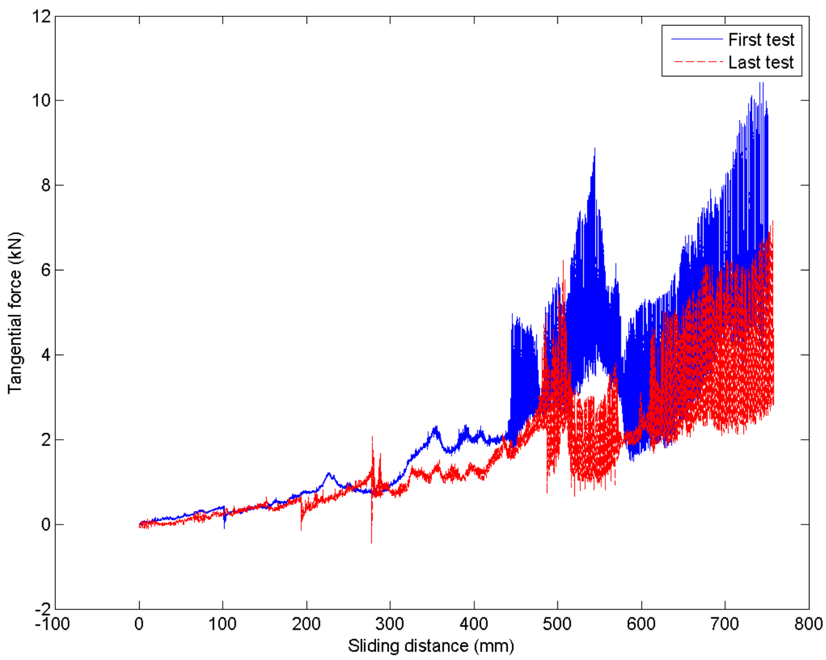

FIGURE 69 TANGENTIAL LOADING IN THE FIRST AND LAST TEST RUN ON THE HP CONCRETE BEAM (A=86.6 DEGREES AND V_{ICE}=18 MM/S)

Figure 69 shows the tangential forces of the first and last test run under identical settings. The first test results show larger tangential forces than the last test run. The results contradict abrasion causes increasing roughness and increasing tangential loading. Although no significant abrasion occurred from 100 mm sliding distance and thus no increasing tangential loading is expected. The minor variation is not significant in the graph.

4.4 CONCRETE GRADE

The two types of concrete have different proportions of components, see Appendix VI: Concrete samples. The abrasion resistant performance of the low- and high performance concrete are part of this section.

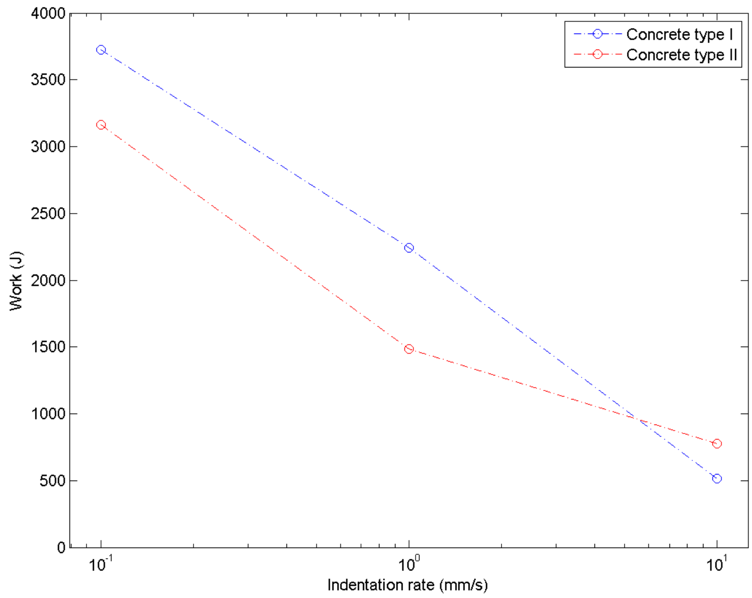

FIGURE 70 WORK FOR THREE INDENTATION RATES (FOR 42,2 MM INDENTATION)

Figure 70 shows work for two types of concrete. Concrete I is the high performance (70 MPa) smooth surface concrete, and concrete II low performance (40 MPa) rougher surface concrete. Figure 71 elaborates on loading in normal direction corresponding to Figure 70. The difference in loading for slow ice velocity (v_{ice}=1.8 mm/s) is due to a minor fracture event around 14 mm indentation, intermediate and fast velocity (v_{ice}=18.0, 180 mm/s) is not significant under brittle conditions.

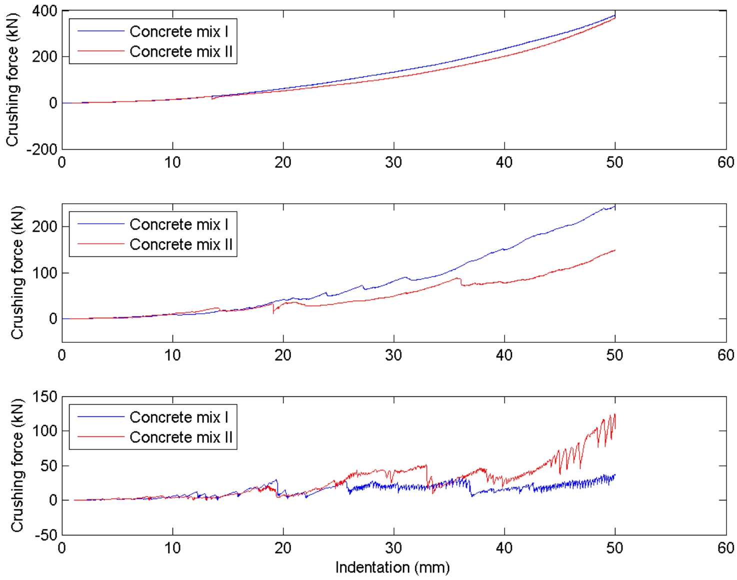

Figure 71 Comparison of the high (I) and low (II) performance concrete sample (Upper: Indentation rate 0.1 mm/s ; Middle: Indentation rate 1.0 mm/s ; Lower: Indentation rate 10.0 mm/s)

Figure 72 compare the tangential forces at a=86.6° , fast ice velocity (v_{ice}=180 mm/s) show slip (adhesion of minor influence) and slower ice velocities (v_{ice}=1.8, 18.0 mm/s) show stick-slip. The second observation in Figure 72 for intermediate ice velocity (18 mm/s) is stick-slip occurs halfway at an identical point in time for both concrete samples. Halfway the test the adhesive conditions are sufficient in order to form enough hydro bonds to show stick-slip. Increasing contact area (with indentation) increases the adhesive forces and under enough adhesive forces stick-slip occurs.

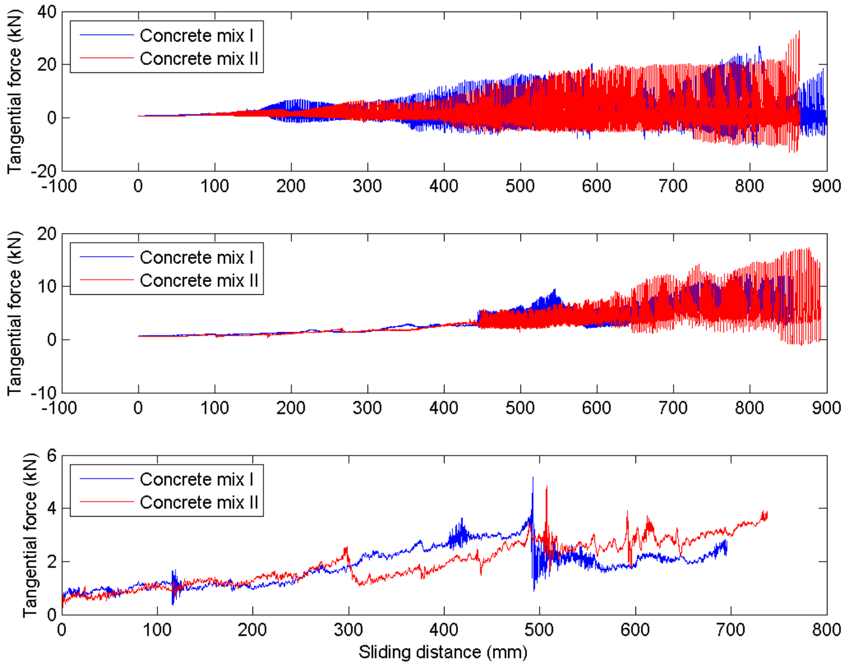

FIGURE 72 ICE-CONCRETE TANGENTIAL FORCES AT 1800% AT A=86.6 DEGREES FOR VARYING CONCRETE MIXTURES (UPPER: ICE VELOCITY 1.8 MM/S ; MIDDLE: ICE VELOCITY 18.0 MM/S ; LOWER: ICE VELOCITY 180 MM/S)

Figure 73 and Figure 74 show the frequency domain of both for low ice velocity (1.8 mm/s), because stick-slip sensitivity possibly varies per concrete.

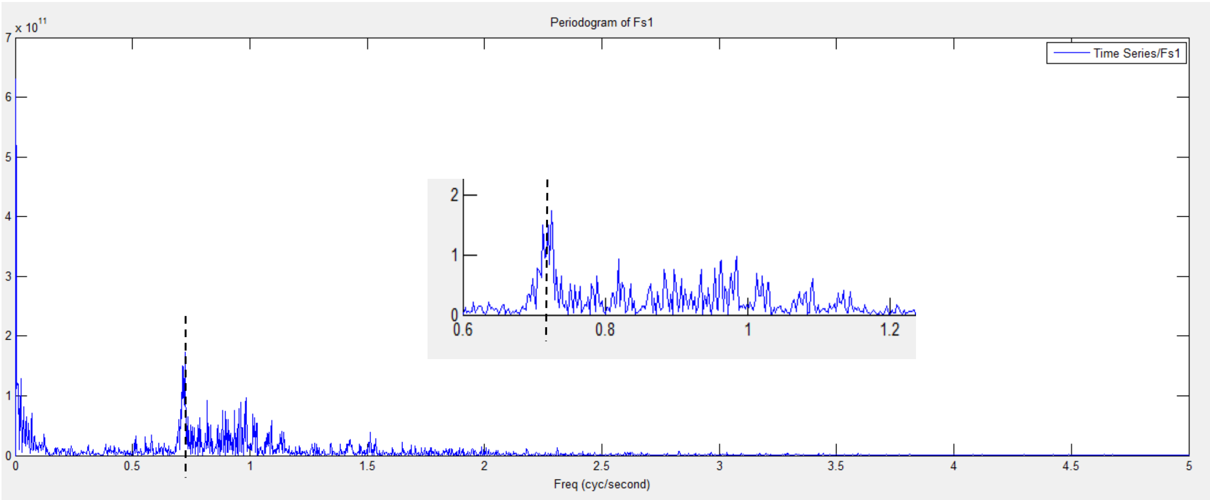

FIGURE 73 HIGH PERFORMANCE CONCRETE SAMPLE – FFT OF TANGENTIAL FORCE UNDER SLOW ICE VELOCITY (V_{ICE}= 1.8 MM/S) AT Α=86.6 DEGREES, FROM 0 – 5 HZ. THE PEAK FREQUENCY CONCENTRATES ABOUT 0.7 HZ.

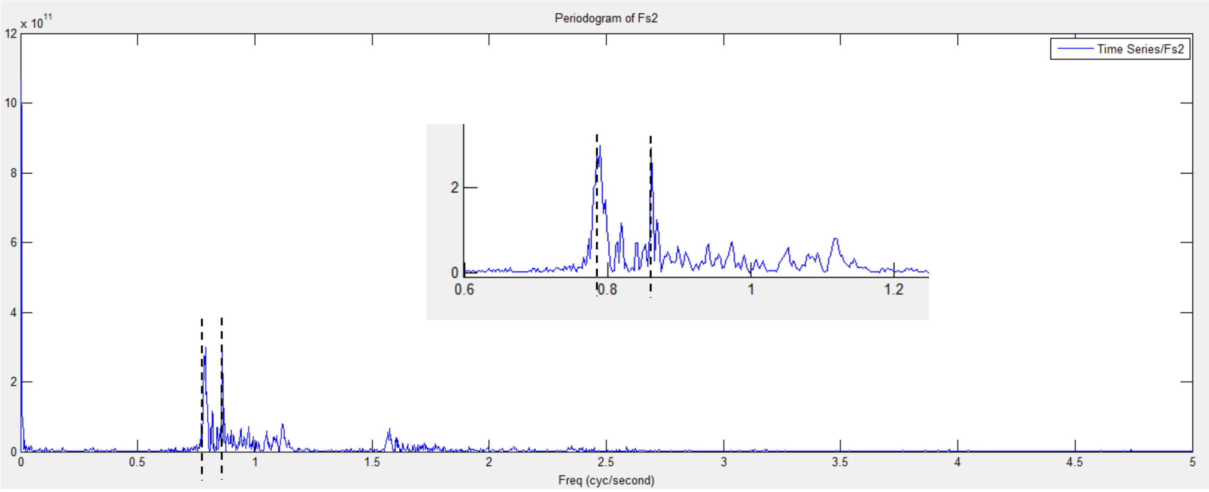

FIGURE 74 LOW PERFORMANCE CONCRETE SAMPLE – FFT OF TANGENTIAL FORCE UNDER SLOW ICE VELOCITY (V_{ICE}=1.8 MM/S) AT A=86.6 DEGREES, FROM 0 – 5 HZ. THE PEAK FREQUENCY CONCENTRATES AT ABOUT 0.78 – 0.85 HZ.

Figure 73 and Figure 74 show a slight difference in peak frequencies between 0.6 – 1.2 Hz. Figure 73 shows a peak about 0.7 Hz and Figure 74 about 0.8 Hz. The difference between cyclic loading might correspond to the difference in concrete surface roughness, but significance can't be proven with these data – especially not considered the uncertainty in ice sample quality. However, one can say the primary stick-slip cycles concentrate in a rough range from 0.5 – 2 Hz for both concrete types.

Figure 75 further illustrates Figure 53. Especially the low ice velocity (1.8 mm/s) indicates interesting behaviour, even with only one concrete data vector present. The drop in force seem to load the concrete surface periodically.

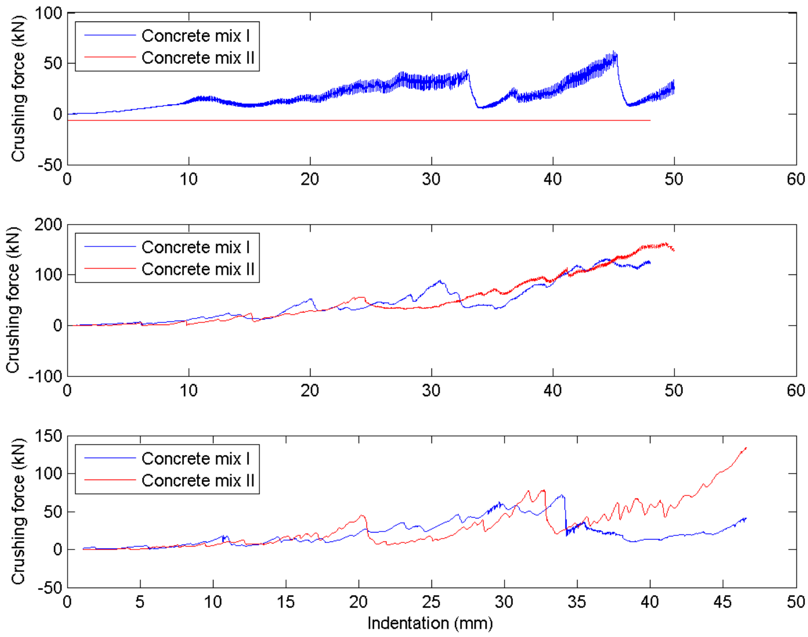

FIGURE 75 ICE-CONCRETE CRUSHING FORCES AT A=86.6 DEGREES FOR VARYING CONCRETE MIXTURES (UPPER: ICE VELOCITY 1.8 MM/S ; MIDDLE: ICE VELOCITY 18.0 MM/S ; LOWER: ICE VELOCITY 180 MM/S)

The periodic loading is a balance between ice shearing and ice-concrete adhesion. Figure 76 shows the spall stuck at the concrete surface (known sliding distance). Shearing off of the ice piece reduces the contact area and thus reduces the normal force (during constant indentation rate) in the upper Figure 75 (Upper graph - Slow test). Also, the reduction of contact area reduces the adhesive force between ice and concrete and only micro-shearing occurs. Meanwhile, the indentation increases, the contact area and adhesive forces also increases up to the point the adhesive forces exceed the shear strength of the ice and shearing off another ice piece occurs along the shear lines (Saeki H., 2010).

FIGURE 76 SHEARING OFF OF LARGE ICE PIECE - CRUSHING AND GRINDING (A = 86.6 DEG) – CONCRETE TYPE I

The abrasion after a test sequence for both concrete types is shown in.Figure 77.

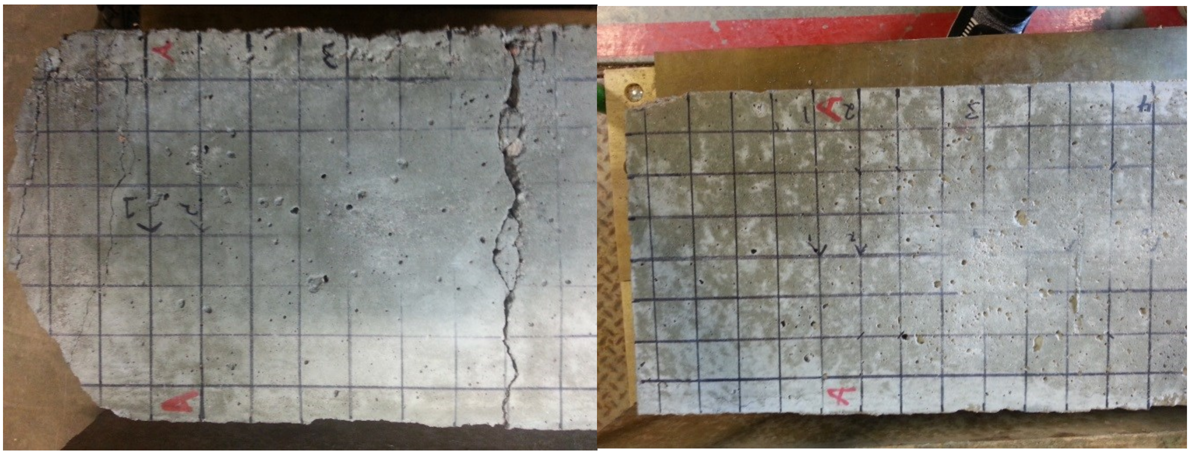

FIGURE 77 CONCRETE ABRASION FOR THE HIGH PERFORMANCE CONCRETE BEAM (LEFT) AND THE LOW PERFORMANCE CONCRETE BEAM (RIGHT) AT THE START LOCATION

The high performance concrete beam shows less abrasion under more ice loading than the low performance concrete beam. The low performance beam reveals much more aggregates than the high performance beam as is shown in Figure 78.

FIGURE 78 CONCRETE ABRASION ON THE HIGH PERFORMANCE CONCRETE SAMPLE (LEFT) AND LOW PERFORMANCE CONCRETE SAMPLE (RIGHT) OVER A TEST SEQUENCE. THE LOCATION IS AT THE STARTING POINT OF THE TEST RUNS AS SHOWN WITH THE CROSS IN FIGURE 66. THE LOADING ON THE HIGH PERFORMANCE CONCRETE SAMPLE IS MUCH HIGHER THAN FOR THE LOW PERFORMANCE CONCRETE SAMPLE. THE GRID LINES (20 MM DISTANCE) PROVIDE REFERENCE.

Carefully comparing the concrete types in Figure 78 due to the scale, the torn off aggregates are much large in the low performance beam. The aggregates hold better in the high performance beam, the matrix strength is thus larger. Second, scour traces around holes seem to develop much faster on the low performance concrete. The holes increase faster in lateral size, depth and expose the lower concrete material.

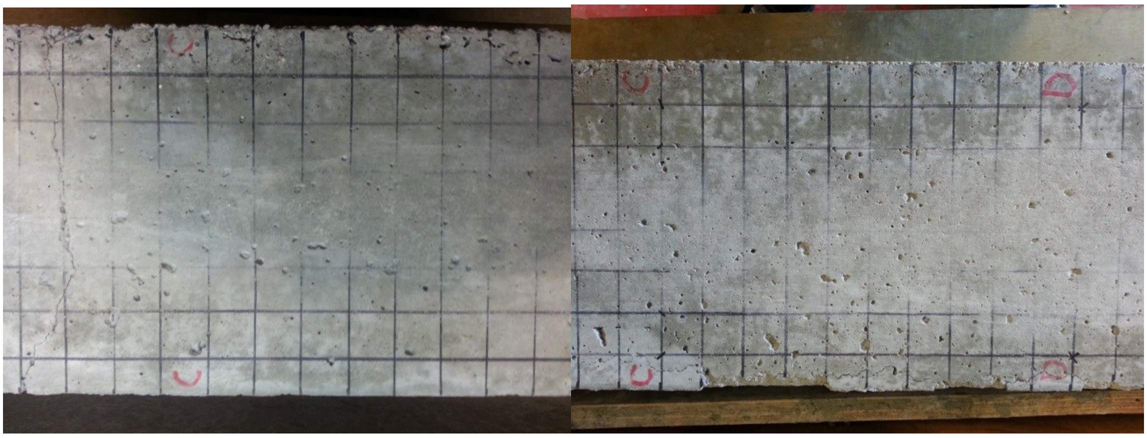

FIGURE 79 CONCRETE ABRASION FOR THE HIGH PERFORMANCE CONCRETE BEAM (LEFT) AND THE LOW PERFORMANCE CONCRETE BEAM (RIGHT) AT A GRINDING LOCATION (BETWEEN B AND C)

Figure 79 shows the two concrete beams at a grinding location, under only passive (under constant normal force) and active (increasing indentation) ice loading. The grinding location involves lower ice loading than the start location. The reference grid is worn off at both concretes and a trail shows up, but the abrasion shows no significant difference in both cases as is also shown in a Figure 80.

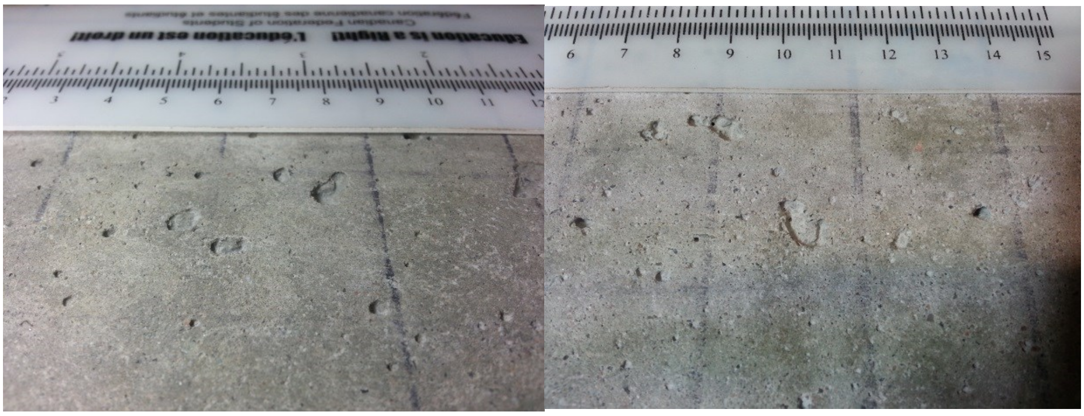

FIGURE 80 ABRASION TRACES ON THE HIGH PERFORMANCE CONCRETE BEAM (LEFT) AND THE LOW PERFORMANCE BEAM (RIGHT) AT A GRINDING LOCATION (BETWEEN B AND C)

4.5 INTERFACE LAYER

The interface layer has been defined as the layer between the surface of the ice volume and the contact surface, in this case concrete. The interface layer is affected by both ice rubble and concrete particles. The interface layer as system exchanges mass and heat with the surroundings. The processes within the interface layer are difficult to measure and therefore, evidences found are predominantly traces which may identify certain processes.

An attempt in this tests has been made to look after these processes by visual information. Different camera angles observe ice action related processes and a thermal camera identifies heat traces. The energy and mass balances may open a door to model the interface processes. Heat generation and absorption may not only affect friction factors and forces significantly, but also the molecular structure of the ice contact surface onto the concrete surface.

The measurements with the thermal camera FLIR A65 achieves a spatial accuracy of 50 mK and a temporal accuracy of 5 K. Any imagery over time doesn't make comparison useful, but over area with a reference point with known temperature does. The location of the reference point might be chosen at the outer points of the concrete, assuming the concrete material remains -10 Celsius (+- 1.5 Celsius).

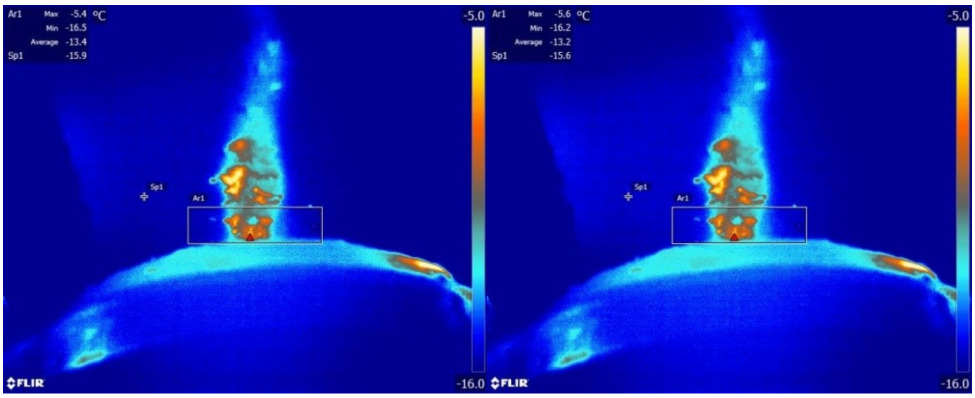

FIGURE 81 THERMAL IMAGE OF A CRUSHING AND GRINDING TEST (AT A=86.6 DEG AND ICE VELOCITY 18 MM/S) CONCRETE (EMITTANCE = 0.92 – LEFT PICTURE) AND FOR ICE (EMITTANCE = 0.96 – RIGHT PICTURE) TEMPERATURE DATA

Figure 81 shows a concrete temperature measurement of -15.9 Celsius. The real concrete temperature is assumed to be -10 Celsius (+- 1.5 Celsius) and the measurement value falls within the accuracy range of the temporal accuracy (5 Celsius). The ice trail material requires another correction for the emittance and thus another thermal image.

The maximum temperature of the ice trail surface is -5.6 Celsius as is shown in Figure 81 and result in a spatial temperature variation of 10.7 Celsius. The ice temperature is -10 Celsius (+- 1.5 Celsius) and thus the temperature of the ice trail surface approaches melting temperatures of the ice sample grade (0 Celsius). The interface might in other words consist of liquid and solid ice material. Second, the local temperature increments in the ice trail may introduce temperature gradients on the concrete surface below and can introduce local thermal stresses.

Third, the ice trail surface temperature measurements tend to concentrate at one side of the sliding side. Considering heat as direct dissipation of loading energy, heat spots provide qualitative data on the y-location (ice trail width) of interaction and peak contact pressures.

The heat dissipates relatively fast and is difficult to observe in slow test runs (ice velocity: 1.8 mm/s), heat dissipation does inevitably occur even in slow test runs but won't affect the interface much in that case. The heat can gradually conduct through the ice and concrete material, dissipate through convection of the air flow and won't be seen much through radiative measurement devices. The fast test are more sensitive to heat effects on the interface layer, because the trail (few seconds after interaction) is still radiating heat. Although the measurements indicate heat gradients, one should be careful with interpretation as the measurements can also include (minimal) heat reflection of surrounding objects.

5. ICE ABRASION

This section discusses the abrasion physics, investigates the threat and illustrates the risk by means of a case study.

5.1 LOCATION OF ABRASION

The test sequences align with the idea of three typical adhesive regions as shown in Figure 82, because three typical abrasive ice loading regimes occur over varying angles of contact (a) according to the experimental 2D simulation (see section 3).

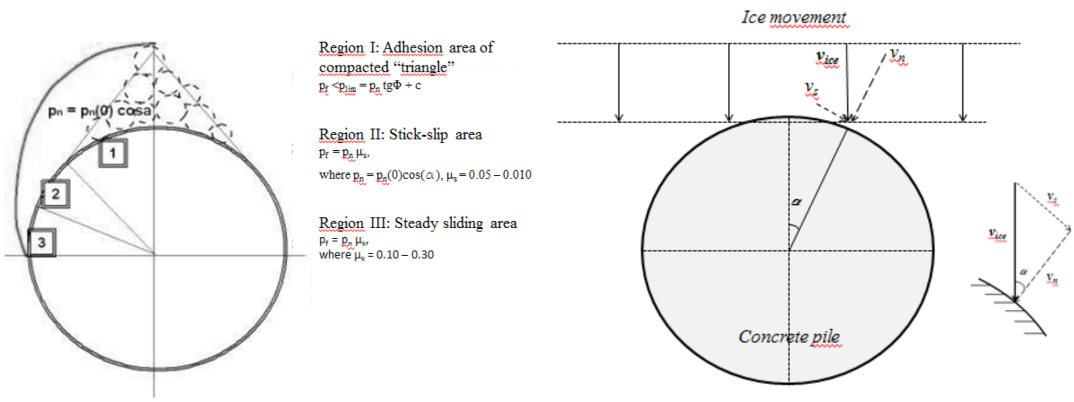

FIGURE 82 (LEFT) CONTACT REGIONS WITH DIFFERENT ABRASION MECHANISMS ACCORDING TO (JACOBSEN ET AL., 2012) AND (RIGHT) SCHEMATIZATION OF THE 2D LATERAL EXPERIMENTAL SIMULATION

The abrasion mechanisms globally consist of three categories: Solely crushing (a -> 0°), crushing and sliding (0°< a <90°) and solely sliding (a -> 90°) . These regions correspond to the three following modes of interaction:

- Region I 'Crushing and extrusion'
- Region II 'Stick-slip'
- Region III 'Slip'

The type of loading gets even more interesting on microscopic level, because each loading type may contribute in its own unique manner to concrete abrasion. (Itoh Y. et al., 1988; Huovinen S., 1990; Bekker A. et al., 2010; Sistonen E. and Vesikari E., 2008; Jacobsen et al., 2012) already identifies 9 abrasive loading types, which all contribute to abrasion according to the:

- Primary order of loading: Direct exceedance of abrasion strength by loading and physical deterioration of material surface occurs: Shear stress due to tangential forces (friction and adhesion).
- Secondary order of loading: Reduction of abrasion resistance and thus increasing the probability of physical deterioration of material surface: Stick-slip cycles, indentation pore pressure, freeze-thawing cycles, concrete shrinkage, thermal gradients, chloride migration, dissolving of lime.

The abrasion loading also changes with an abrasion depth. The shear stress will generally increase with increasing abrasion depth (roughness) under dry ice-concrete friction, but decreases if the troughs on the surface gets filled up with ice material. The ice material will stick to the concrete and induce ice-ice friction instead and decreases the shear stress. The effect of sticking ice in the troughs of the surface texture requires further investigation.

5.1.1 Region I 'Crushing and extrusion':

The location associated with Region I abrasion is around the structural face perpendicular to the ice movement and involves most critical ice abrasion on offshore structures (Janson J., 1989; Hara F. et al., 1995). The largest local compression (Bekker A. et al., 2003) and shear stresses occur in this region and result into exceedance of the abrasion resistance of the concrete. The local compression stress under brittle ice failure may reach, for very short periods, up to 60 MPa for multiyear sea ice (Masterson D. et al., 1993). In small-scale laboratory conditions over 100 MPa at areas of a few mm^2 (Mackey T. et al., 2007). The corresponding friction processes under these extreme pressures can thus induce large shear stresses. The observation of eruption of spalls during fast tests *(v_n > 1.0 mm/s)* resembles an extrusive processes under extreme compression stress (Jordaan I., 2001).

The abrasive ice loading quantity in this paper is work (or energy), because (Itoh Y. et al., 1988) indicates proportionality between concrete abrasion on the one hand and normal pressure and ice sliding distance on the other hand. Work includes force and displacement through a proportional relation and is thus able to indicate a global abrasive load. Also, one is able to determine the cumulative loading and compare it to the abrasion depth (see section 4.1.1 for the formula).

The unit of the abrasive loading is work over contact area J/mm^2 per mm absolute sliding distance, where absolute refers to the apparatus' reference system. The previously shown Figure 66 indicates the change of surface texture. Corresponding data on work shows the change of cumulative abrasive loading from tests. In these cases the ice was crushed against the concrete sample without lateral sliding, typically region I. The change in cumulative loading and abrasion reveals aspects of the abrasion process.

5.1.2 Region II 'Stick-slip':

The stick-slip region does not abrade the concrete in an early stage, but will reduce the concrete abrasion resistance over long time scales. Figure 47 shows a stick-slip cycle and indicates static friction up to half (5 kN) of the normal force (10 kN). The stick-slip region can abrade the concrete surface due to local fatigue issues (Huovinen S., 1990). Thus stick-slip loading falls partly under the secondary order of abrasive loading, because it does not exceed the nominal surface abrasion resistance but does tend to reduce it over time.

Figure 83 shows that the stick-slip character depends on ice velocity and the stick-slip region thus reduces with increasing ice velocity. However, slow ice velocities v_{ice} are of increasing importance for the local fatigue strength of the concrete surface.

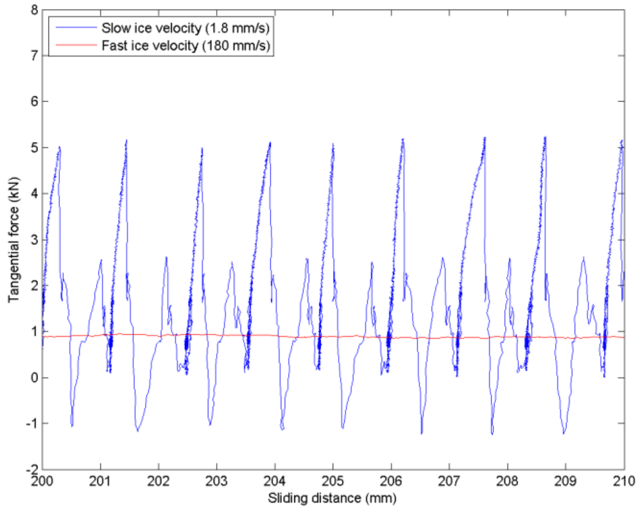

FIGURE 83 TANGENTIAL FORCE FOR SLOW (V_S=1.8 MM/S) AND FAST SLIDING (V_S=180 MM/S) UNDER 10 KN NORMAL LOAD – HIGH PERFORMANCE CONCRETE SAMPLE.

Figure 83 shows that the fast ice velocity is a very smooth sliding process in comparison with the slow ice velocity. The scatter of data points originates from the overshoot of the position in sliding direction. Figure 47 correspond with the slow ice velocity and illustrates the stick-slip cycle over time instead. The stick-slip cycle period not only depends on the ice velocity (v_{ice}) and angle of contact (a), but also on the concrete type. Note the stick-slip period also depends on the stiffness of the apparatus, but is the same for all tests. Figure 55 and Figure 56 are FFTs of the tangential loading in identical tests, but the two figures compare high performance and low performance concrete. The peak frequency and active frequencies vary (HP Concrete grade: f_{peak}≈0.7 Hz / LP Concrete grade: f_{peak}≈0.78 – 0.85 Hz), the LP concrete involve higher active frequencies than the HP concrete and indicate a variation in adhesive properties of the two concrete types. The (smooth) high performance concrete sample is more sensitive (lower active frequencies) for adhesion than for the (rough) low performance concrete sample. Adhesive bonding depends mainly on real contact area (Saeki H., 2010) and increases with increasing roughness. The adhesive forces seem to be larger on a smooth surface than rough surface over a test run, corresponding to observations on confinement in (Dragt R., 2013) for varying roughness' in ice-steel crushing tests. Ice seems to adhere between two asperities on the rougher surface and thus reduce the real contact area.

Figure 57 shows that the stick-slip period depends on fracture and thus on real contact area. High frequency motions correspond with low static binding and low frequency motions with high static binding. The ice sample in the right photo shows reduced real contact area due to fracture and spalling, and the stick-slip frequency is thus increased.

5.1.3 REGION III 'SLIP':

The slip region does not critically affect the abrasion risk of the concrete significantly. Low stresses and large sliding velocities characterize the region barely leaving any abrasion traces behind. However if we consider that the first two regions do not govern the design abrasion loading, then ice sliding can cause abrasion over long sliding distances as is shown in (Itoh Y. et al., 1988) and (Bekker A. et al., 2011). An abrasion event still does require sufficient compression stress in order to occur, for example due to enclosed ice spalls and rubble at the free surfaces between ice sheet and structure. The slip region only has to overcome the dynamic ice-concrete friction during large ice velocities and the tangential force consists of a combination of wet and dry friction. The slip region changes into a stick-slip region for lower ice velocities.

5.2 Abrasion physics

5.2.1 Theoretical abrasion

Concrete abrasion resistance implies the strength of the concrete material to any loading. Initial abrasion resistance is governed by cement properties as they fully cover the concrete surface, but after some surface abrasion the abrasion resistance dependence shifts to a combination of cement and aggregate properties. (Huovinen S., 1990) definition of surface characteristic stages over abrasion spans has been applied in this paper as is shown in Figure 84.

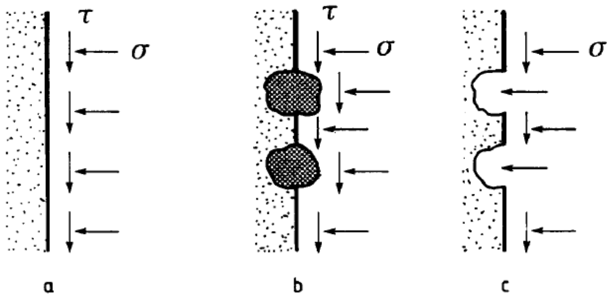

Figure 84 Schematization of concrete abrasion (Huovinen S., 1990)

Abrasion only due to exceedance of the abrasion strength falls under the primary order of abrasion. Primary abrasion resistance depends on local concrete and geometrical properties as already shown in the numerical model of (Huovinen S., 1990) but also in (Hanada M. et al., 1996). Material properties affect the location of local peak stresses and geometrical properties affect the extreme value of stress. Also, increasing cylindrical compression strength reduces the abrasion rate (Huovinen S., 1990). The primary shear loading of ice is the result of compression stress at microscopic inclinations on the concrete surface. Large compression stresses in brittle ice failure causes shear stresses due to the hydrodynamic flow regimes from a combination of frictional heat and pressure melting of the interface layer. Lower compression stresses cause shear stresses due to a granular flow. Liquefaction of the flow reduces the adhesion bonding (Saeki H., 2010).

Secondary order of resistance: Secondary order abrasion resistance include resistance to indirect effects on the abrasion rate for example like fracture initiation, propagation or chemical intrusion. These local failures immediately reduce the primary abrasion resistance, but won't cause concrete abrasion due to itself. Secondary order abrasion resistance might consist of resistance to freeze-thaw cycles, thermal stresses and chemical resistance. The secondary order resistance is of increasing concern over time, but commonly negligible on short timespans. Although the approach originates on a probabilistic background, the deterministic approach would for example combine the effects in one equation. The abrasion criteria proposal is:

Abrasion resistance (R) < Abrasion loading (L)

The criteria is valid on macroscopic scale as to globally estimate the abrasion rate, but also on microscopic scale to describe the abrasion mechanism. The abrasion rate is larger than zero when the abrasion loading (L) exceeds the abrasion resistance (R). The primary order of loading determines the abrasion loading (L) and the secondary order of loading determines the reduction of the abrasion resistance (R). The formulation of the reduction on the abrasion resistance is:

$$R = R_0 * c_r$$

Where R_0 is the initial abrasion resistance dependent on the concrete mixture (for example represent the 30-day concrete abrasion resistance) and c_r is the reduction coefficient smaller than one dependent on the secondary order of loading.

5.2.2 EXPERIMENTAL ABRASION

FIGURE 85 CONCRETE ABRASION ON THE HIGH PERFORMANCE CONCRETE SAMPLE (LEFT) AND LOW PERFORMANCE CONCRETE SAMPLE (RIGHT) OVER A TEST SEQUENCE. THE LOCATION IS AT THE STARTING POINT OF THE TEST RUNS AS SHOWN WITH THE CROSS IN FIGURE 66. THE LOADING ON THE HIGH PERFORMANCE CONCRETE SAMPLE IS MUCH HIGHER THAN FOR THE LOW PERFORMANCE CONCRETE SAMPLE. THE GRID LINES (20 MM DISTANCE) PROVIDE REFERENCE.

Figure 85 shows initial traces of abrasion at the start location ($z_{ab} = 94\ mm$) over a test with crushing and sliding that exhibited stick-slip behaviour. The abrasion damage is minor in comparison to field studies (Janson J., 1988). The abrasion loading was over W_n = 2.6 J/mm² and W_s = 0.2 J/mm² for the HP concrete and less for the low performance concrete (see section 4.3). The high performance concrete sample shows less abrasion than the low performance concrete sample, the silica fume particles seem to increase the matrix strength and improve the abrasion resistance. Also, the surface reveals smaller aggregates already exposed, indicating the cement layer is wearing. The concrete surface evolves over longer ice sliding distances and exposes, in a later stage, larger diameter aggregates (Itoh Y. et al., 1988; Huovinen S., 1990). Thus, Figure 85 shows the cement properties govern the initial abrasion rate.

The tangential force for two identical sequential tests didn't show any significant variation. The surface texture measurement device could only measure a maximum surface elevation of 160 μm, thus we can state the local abrasion of the high performance concrete sample is larger than 160 μm. The calliper helps to describe the surface visually.

Concrete abrasion is in reality always a set of primary and secondary order mechanisms. Also, the abrasion factors are able to strength or weaken each other, through some interaction (Jacobsen J. et al., 2010). For example frost action (freeze-thaw cycles) can strengthen the effect of chemical intrusion (chlorides and carbonation) and reduce the concrete abrasion strength. Second example is fracture initiation due to thermal stresses, often at the matrix bonding (between cement and aggregates) and fracture propagation due to cyclic stick-slip loading. The interaction between failure mechanism has been part of the studies of (Jacobsen J. et al., 2010), but are a gap of knowledge still.

Weakening is often the cause, but strengthening is also possible. The same studies suspect a positive effect of micro bacterial attack due to carbonation and pH changes in the concrete material. Micro bacterial effects are not part of the scope, because they are not causing major effects if they already are in place. Possibly the compression stresses due to ice action reduce any tension stresses in the concrete and might reduce fracturing effects.

The three interactions previously complicate the abrasion estimation, because other unidentified interactions possibly contribute to the overall abrasion. Further research should indicate the relevance of the interaction between failure mechanisms and if so, correlate them.

5.2.3 Interface layer processes

The interface layer is the layer between the undamaged ice and concrete and involves a mixture of crushed ice and concrete particles. The crushed ice particles originate from flaking ice during sliding due to micro shearing. The concrete particles originate from flaking concrete due to microshearing, but also due to adhesion with the ice. The mass flow on the interface under high pressure exhibits a hydrodynamic character and under lower pressures shows a more solid granular character (Jordaan I., 2001). The liquefaction of ice is due to a combination of pressure and frictional heat. The ice surface layer will immediately absorb frictional heat for melting a very thin surface sub-layer and during refreezing release the latent heat. Figure 67 shows enclosure of concrete particles after recrystallization of the ice surface (shown by the fine crystalline ice structure) and Figure 81 shows evidence of heat traces. Also, Figure 67 shows the ice impurity content increases due to the enclosure of abraded concrete particles, and thus the abrasion rate increases in a similar manner as in (Itoh Y. et al., 1988) due to the effect of sand particle content in the ice.

Fast moving ice generates frictional heat as is shown in (Tijsen J. et al., 2013). With increasing melting of ice, hydrodynamic characteristics at the contact dominate over asperity contact in governing the characteristics of the interface layer and thus abrasion rates. Lower temperatures imply less melting and increasing dry friction over wet friction. The ambient temperature during testing was -10 (+-1.5) $^\circ$C and shortly after interaction temperature increments of +10.3 $^\circ$C were measured as shown in Figure 81. The heat traces indicate very local liquefaction of the ice interface material.

Temperature increments on the interface will also reduce the adhesive bonding (Saeki H., 2010) and thus tend to increase the stick-slip frequency. Large local temperature gradients due to heat generation can also introduce thermal stresses in the concrete surface. Thermal stresses reduce the strength of the concrete surface and will increase the probability on local abrasion.

Also, decreasing ice temperature increases the abrasion rate (see section 2.4.3). Few thoughts on that:

- Ice temperature directly affects the crystal structure of ice and ice temperatures down to approximate -22 Celsius the crystal structure remains the same type, but becomes stiffer. The force under constant deformation rate increases faster than at higher temperatures and induces most likely a higher contact pressure with increasing abrasion rate.
- Decreasing ice temperature reduces the thickness of the liquid like layer (LLL) on the interface. Decreasing ice temperature thus reduces viscous friction (lubrication) and increases dry friction. Dry friction might increase the concentration of high local peak stresses at asperity level on the concrete surface and thus sensitivity to abrasion.

Concluding, the interface temperature affects the abrasion rate through two ways. Firstly, the ice contact material behaves stiffer and less liquid under decreasing temperature and increases the abrasion load. Wintertime involves the coldest temperatures and thus most likely largest abrasion rates. Frictional heat mitigates the effect of decreasing temperature, but the effect is often negligible in brittle ice velocities due to continuous generation of new crushed ice material. Secondly, frictional heat induces local temperature gradients (10 Celsius over a few millimetres) and decreases the abrasion resistance of concrete.

5.3 Abrasion risk control

5.3.1 ABRASION THREAT

The threat definition is degradation of the inner bearing strength of the concrete material due to ice abrasion, indications are exposure of lower surface layers of concrete and reinforcement to ice, air and (sea) water. The abrasion only develops when

Abrasion resistance (R) < Abrasion loading (L)

The specification of the ice abrasion loading (L) depends on the extreme values within the environmental conditions. The abrasive loading factors are according to section 2.4:

- Ice movement
  - Direction
  - Distance
- Ice contact pressure
  - Ice type (growth history)
  - Ice velocity
- Ice temperature
  - Air temperature
  - Sea water temperature
- Ice impurity content
  - Salinity
  - Sediment inclusions
- Abrasion depth
- Ice thickness

A preliminary study to the local ice conditions for an offshore structural design is crucial in order to specify the threat and make an ice abrasion resistant design. The study involves measurements preferable over a long period of time to make good predictions of the factors. Although, the effects of the factors are not entirely clear, they can provide an indication of abrasion severity relative to previous studies. The uncertainty of factors in relation to concrete abrasion is worth of further examination.

The impact (different than the threat) on concrete structures at remote offshore locations depends on the structural design. Ice abrasion removes structural material but also exposes the lower layers of the concrete, including reinforcements. Exposure to ambient conditions deteriorates the reinforcement steel and reduces the reliability of the structure until an unacceptable level. The abrasion depth should maintain within safe boundaries over the service lifetime of the structure. The abrasion depth is an excellent parameter to quantify the threat. An increasing abrasion depth increases the threat to the structure. The concrete type B70 might provide already a reasonable reference abrasion rate (section 2.6) under controllable condition and makes rough calculation in concept or basic design phase possible.

5.3.2 ABRASION RELIABILITY

The reliability of the abrasion loading and resistance still involves a high level of uncertainty, because of the lack of data. An improvement of the reliability would involve a 20 year real scale abrasion depth registration at a standard concrete. Also, an increasing number of concrete tests would improve the reliability of the design abrasion rate.

Ultimately designers like to prove the reliability of an abrasion resistant design. For example, the design abrasion depth will only occur with a probability of occurrence of 1% (return period 100 years).

5.3.3 MITIGATION: TECHNIQUES

Two mitigation techniques are known:

- Geometrical consideration, for example conical shape
- Material consideration, for example a protective layer

The first mitigation technique not only reduces the concrete abrasion, but also reduces the external loading, is application of a conical shape at the waterline. The ice sheet will not fail due to crushing, but to bending. The reduction of local stresses directly reduces the abrasion rate.

The second mitigation technique focus on material application: Implementation of ice abrasion resistance in concrete material or in a protective layer. An efficient design reduces the risk as is shown in Figure 86

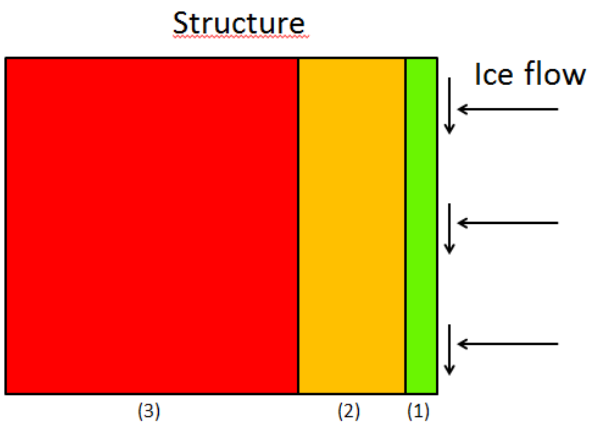

FIGURE 86 ABRASION DEPTH LIMITS: (1) PRIMARY PROTECTION LAYER, EASY REPLACEABLE MATERIAL; (2) SECONDARY PROTECTION LAYER, ABRASION RESISTANCE CONCRETE COVERAGE; (3) INNER CONCRETE WITH BEARING FUNCTION

The primary protection layer (1) is the first layer of material to abrade off due to ice movement. The layer should function between two maintenance windows and protect the inner layers (2) and (3). The regular replacement requires constant fabrication of new material and makes cost efficiency an important consideration. Also, the material shall function maintenance friendly and won't require expensive equipment to handle. The thickness of the layer depends on the acceptable probability of exceedance of the abrasion depth to layer (2). The ISO19906 section 7.2.2.2 provides in this case a probability of exceedance smaller than 10^{-1} in the service limit state. The consideration of material choice for the primary layer will include two materials for demonstration purpose. The best abrasion resistant material other than concrete treatment according to section 2.6 is Low Density Propy Ethylene (LDPE), a thermoplastic. The material is also costly (LDPE: 1000 – 2000 USD/metric ton) and difficult to repair during damage. Steel on the other hand is twice as cheap as LDPE (Steel: <500 – 1000 USD/metric ton) and easily replaceable or attachable after any damage occurrence. The abrasion rate of LDPE is 0.022 mm/km per MPa on lab scale and of steel 0.030 mm/km per MPa. The thickness of the primary layer is proportional to the weight, thus Steel (45.4k – 90.9k USD/metric ton*abrasion rate) is more cost effective than LDPE (<16.6k – 33.3k USD/metric ton*abrasion rate) which makes steel the more cost efficient material. Still, the additional weights of the layer requires a check upon bearing capacity. The density of LDPE is 0.910 mt/m^3 and is much lower than steel 0.785 mt/m^3 and may be more decisive in structural weight considerations.

The secondary protection layer does not fail during the lifetime and mainly functions as buffer to the critical layer (3) in the case the primary layer fails. Regular replace-ability is thus less important than for the first layer. The thickness of layer (2) depends on the acceptable probability of exceedance of the abrasion depth after failing of layer (1). Layer (2) should reduce the probability of exceedance of abrasion depth from layer (1) until layer (3) and depends on the consequences what level is acceptable. For example exposure of layer (2) is only applicable in the case of an extreme ice event. ISO19906 section 7.2.2.3 suggests a value smaller than 10^{-2}, but should balance out with the threat to the structural integrity. Identification of exposure of layer (2) during inspection shall initiate an extra alert state of maintenance and potential repair of layer (1). The secondary layer may be a concrete type highly resistant to ice abrasion and integral part of the structural bearing capacity. The concrete improvement can be for example steel (up to 1%) / basalt fibre content. The improvement is about 40% on the abrasion rate according to section 2.6, the addition of fibres is only profitable if the secondary layer gets to thick or heavy, but mainly complements the primary layer as ice abrasion protection.

Layer (3) is the structural layer and includes reinforcement steel. The layer is integral part of the bearing strength and correspond to a minimum (acceptable) tolerance of ice abrasive damage. Also, regular inspection of the concrete surface above and below water prevent damage on this layer and shall be integral part of the operations. Excessive concrete abrasion without adequate counter measures can potentially lead to a reduction of structural integrity and thus an immediate threat to operations.

The design of an abrasion resistant design complicates when the location of the structure involve year-round ice conditions. Maintenance is very expensive and dangerous in that case, thus the solution requires an reliable abrasion resistant material during its lifetime. Possibly replaceable protection layer (1) is no option anymore and protection layer (2) requires extra improvement (like fibre reinforcements) and safety margin.

5.4 Abrasion case study

The ice abrasion risk on concrete is manageable, but requires sufficient effort in design or maintenance phase. The section demonstrates how to reduce, but also manage the risk on ice abrasion on concrete over a lifetime by means of a fictive case study.

5.4.1 Abrasion challenge

A client intends to construct a concrete oil platform onto a remote Arctic location for 20 years and involves four legs of 22 meter diameter, similar to the structure as is shown in Figure 87. The nearest harbour is 350 km away and makes logistics hard with an ice-free window of 6 weeks. The local ice conditions involve first year level ice and about 700 km of ice movement each winter with an average ice velocity of 0.1 m/s and an ice thickness of 2.0 meter. The direction of movement is predominantly 225˚ southwest (20% of the movement), 180˚ south (45%), 135˚ southeast (25%) and 90˚ east (10%) according to measurements over a long period. The air temperature varies between -35 and 5 degrees Celsius. The tidal fluctuation vary diurnal between MSL -2.0 m and MSL+2.0 m.

FIGURE 87 SAKHALIN PLATFORM IN ICE INFESTED WATERS (SHELL WEBSITE)

The environmental information on location is crucial to make an effective risk control plan. Secondly, the critical area of exposure of the platform depends on two environmental phenomena, the lateral on ice movement and vertical on water level fluctuation. Lateral location is on the perpendicular face in the 180˚ south direction, the perpendicular face involves largest local pressures due to ice crushing and will abrade fastest. The vertical location depends solely on the tidal fluctuation in this specific case. The upper boundary is MSL +2.0 m plus the ice above water level, physically an average ice density of 0.920 kg/m^3 over sea water density 1030 kg/m^3 (0.11x ice thickness), but as conservative value 0.2x ice thickness (>0.11x). The upper boundary of the area of exposure is MSL +2.4 m. The lower boundary is MSL -2.0 minus the ice below water level with a conservative value (>0.91x) of 0.95x the ice thickness. The lower boundary of the area of exposure is MSL -5.90 m. The critical area is thus 8.30 m height and 574 m^2 per leg. The water level fluctuation has a favourable effect of spreading of the abrasion rate and reduce the local abrasion rate, but the report makes a conservative assumption that the abrasion rate is constant over the vertical height and thus contributes to the safety margin.

Third step, the critical location determines the design abrasion rate. The 20 years lifetime result into an ice movement of 14000 km assuming the full movement at one direction. Standard concrete for offshore platforms is the B70 and correspond to an empirical abrasion rate without real-scale verification of 0.05 mm/km under 1 MPa global normal pressure (Section 2.6). The global contact pressures is average over the sliding distance is 0.5 MPa (Vershinin S. et al., 2006) and the actual abrasion rate is thus half 0.025 mm/km. The theoretical abrasion depth will result into 350 mm after 20 years without any measures.

Field observations suggests maximum abrasion measurements of 11.6 mm/year under similar conditions as on location (700 – 800 km ice movement) which correspond to 232 mm after 20 years. The theoretical abrasion depth is 1.5 times more than has been observed for the Sydostbrotten lighthouse. Conservative assumptions explain the difference.

5.4.2 MITIGATION: APPLICATION

The extra coverage for a 20 year design is thus 350 mm and requires a minimum addition of 1000 tons of extra concrete. The client prefers a solution with less additional weight. A steel protective layer with a repair period of 5 years (3500 km ice sliding distance) requires a conservative minimum thickness of 6 mm (100 tons additional weight).

6 NUMERICAL MODEL OF ABRASION

Research not only focus' on preliminary answers but meanwhile, already explores new questions. The report examines the phenomenon ice abrasion through experimental glasses but also defy curiosity by trying on numerical glasses. Existing ice and concrete models may already describe ice-structure interaction behaviour pretty well, but don't include enhancements on concrete abrasion processes yet.

The purpose of the numerical approach is model interaction between two heterogeneous materials and consequently generates concrete abrasion. The numerical model does not require expensive facilities to ensure sufficient significance like for physical models, but only require a few validation tests. The development of the numerical model consist of the following steps:

1. Develop a model of the ice material including failure conditions
2. Develop a model of the concrete material including failure conditions
3. Introduce interface conditions between ice and concrete (including abrasion resistance limits)
4. Numerically simulate surface abrasion as outcome of ice-concrete interaction

The determination of numerical method commonly depends on the availability of models and the philosophy of the developer. The lattice model is potentially able to model the ice and concrete material, then, interesting is to combine the two models and model abrasion due to ice-concrete interaction. The extensive scope will mainly touch upon the potential of the lattice model and briefly glaze over the existing probabilistic model.

6.1 LATTICE MODEL AND PROBABILISTIC MODEL

(Bekker A. et al., 2012) describes a probabilistic macro-scopic approach on the ice-concrete abrasion process and treats the parameters describing the ice conditions as random variables. The stochastic parameters of the ice feature are width, drift velocity, interaction diameter with structure, temperature and cohesion. The input on a not specified algorithm calculates the ice force, dimensions of contact zone on structure and path length of interaction (i.e. indentation). Then, the (normal) ice force leads to the (global) compression stress exertion on the structural face by dividing the force by the area of interaction. An illustration of the structure is shown in Figure 88. The macro-scopic approach describes the abrasive processes on macro level and skips the physical representation of the abrasion processes still.

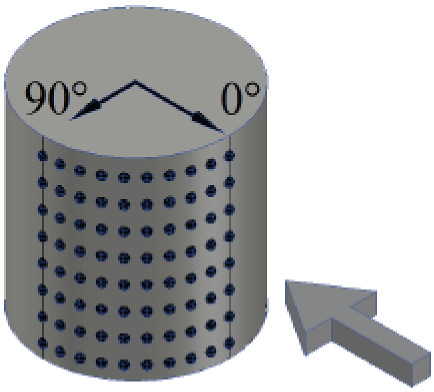

FIGURE 88 GRID OF DESIGN POINTS FOR THE PROBABILISTIC NUMERICAL MODEL (BEKKER A. ET AL., 2012)

The disadvantage of the probabilistic model is that it models the abrasion events as a chaotic process, but does not need to include the physical mechanism. The probabilistic model requires all stochastic variables to be independent and the general applicability on all ice-concrete abrasion problem is thus still an issue to address.

(Dorival O. and Metrikine A., 2008) develops a lattice model for ice crushing against a rigid structure, Figure 89 illustrates the model. The lattice model consists of a set of elements in a truss shape network and is capable to describe ice behaviour in high detail. Highly interesting is the ability to also describe the material behaviour on meso- and micro-level. The lattice model also exists for concrete material. The ability to zoom in onto the micro-level for ice and concrete at interfacial zone makes the combination of lattice model very suitable to implement abrasion criteria.

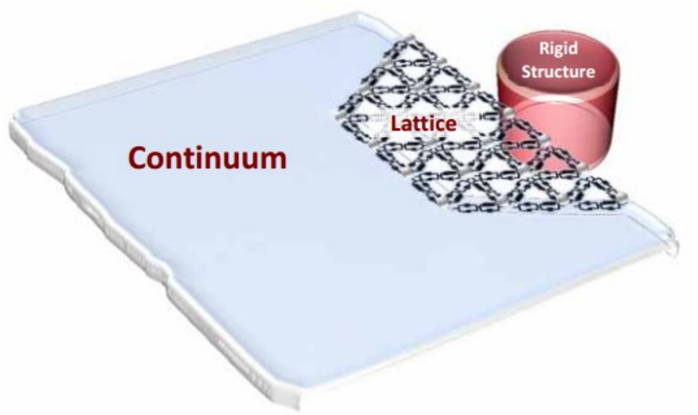

FIGURE 89 LATTICE MODEL OF ICE DURING ICE-STRUCTURE INTERACTION (DORIVAL O. AND METRIKINE A., 2008; READ IN HOVING J., 2014)

6.2 STEP 1: ICE MODELLING

The elements of the lattice numerical model involves a hexagonal shape and are part of a network through viscoelastic connections. The element represents the mass within the borders of the hexagonal. The boundary conditions depends on the structure and will result into a normal force (n) and tangential force (t). The lattice moves in the network in x and y direction (see Figure 90) through two force equations:

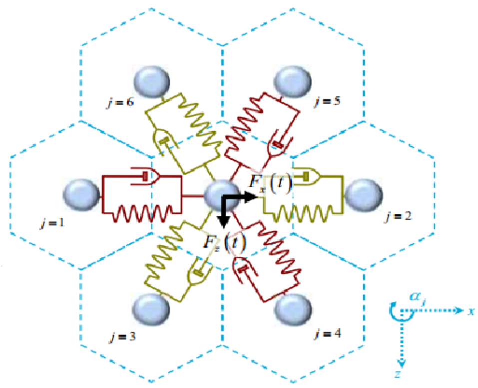

FIGURE 90 VISCOELASTIC HEXAGONAL LATTICE (HOVING J., 2014)

The connection between two elements deletes if the force will exceed the force limit on that connection. In other words a crack will initiate. The propagation of cracks is strongly mesh dependent, because the fracture propagates through the weakest connections (fracture increases strain, exceedance of force limits and deletes the connection). A regular mesh won't describe crack propagation very naturally for a heterogeneous material as ice, because it will just propagate straight along the borders with the most strain of nearby elements. Randomizing the mesh reduces homogeneity and improve the model on fracturing behaviour.

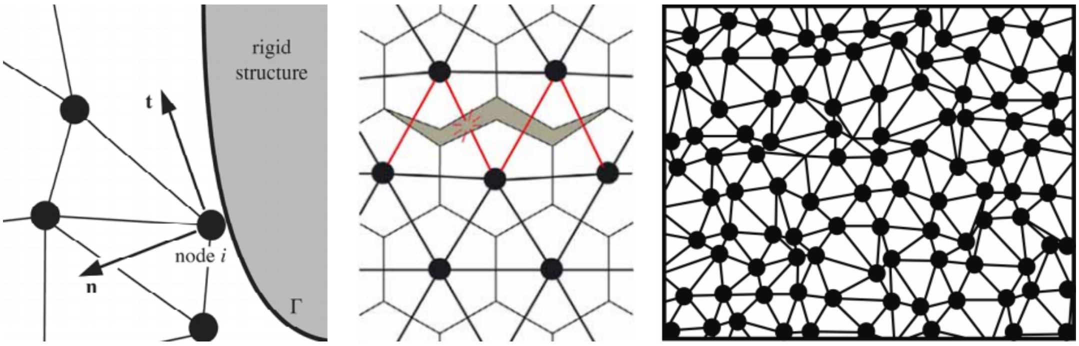

FIGURE 91 MESH GRID INTERFACE FORCES (LEFT), ELEMENT CONNECTIONS AND CRACK INITIATION (MIDDLE), AND RANDOMIZED MESH GRID (RIGHT) (HOVING J., 2014)

The lattice model of ice can model a range of ice features, but the report did only describes micro level structures of the lattice models yet. The model of ice features consist on macro level of several mesoscopic bodies as shown in Figure 92.

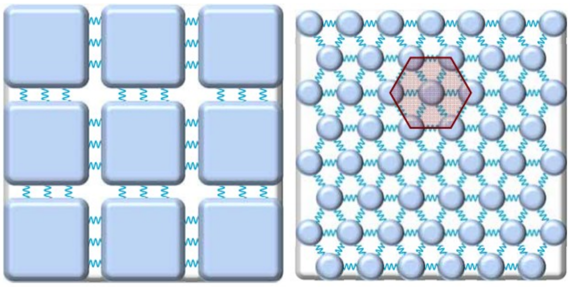

FIGURE 92 (LEFT) MESOSCOPIC BODIES IN MACROSCOPIC ICE FEATURE AND (RIGHT) SINGLE MESOSCOPIC BODY (HOVING J., 2014)

An individual mesoscopic body might consist of a continuum with its own properties and thus improves the inhomogeneity of the macroscopic model. The relation between the mesoscopic bodies depends on their relative motion (kinematics). The interaction between two lattices in a mesoscopic body (see Figure 92) depends on kinematic relations (see Figure 93).

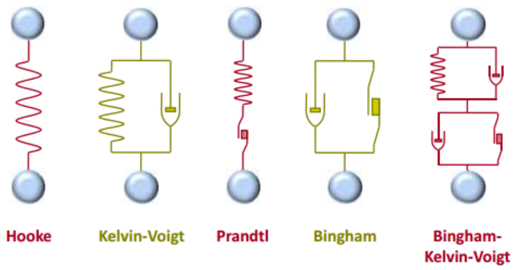

FIGURE 93 KINEMATIC RELATIONS BETWEEN TWO PARTICLES (HOVING J., 2014)

The implementation of microscopic bodies into mesoscopic bodies just requires each particle or set of particles at meso level to represent another microscopic body. The level of detail will increase, but microscopic detail enables simulation of microstructural interaction, and may allow simulation of microstructural processes as ice abrasion.

6.3 STEP 2: CONCRETE MODELLING

The concrete material models also exist in a diverse variety, but the report only treats the concrete lattice model intentionally to explore the coupling of the ice-concrete lattice models. Figure 94 shows the lattice model.

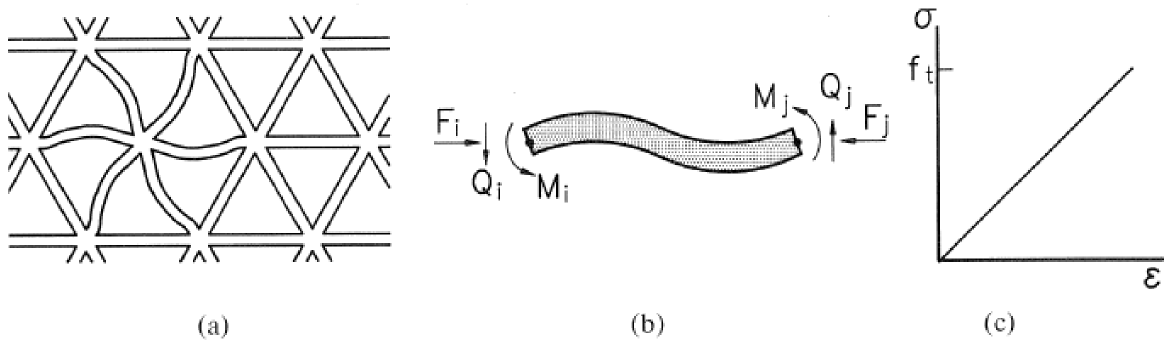

FIGURE 94 CONCRETE LATTICE MODEL. (A) SHOWS A TRIANGULAR SHAPE, (B) SHOWS THE TRANSFER OF AXIAL AND SHEAR FORCES AND BENDING MOMENTS, (C) LINEAR ELASTIC STRESS-STRAIN RELATION OF A SINGLE BEAM ELEMENT (SCHLANGEN E., 1993)

The lattice model describes crack propagation by removing the connection with the highest tensile stress relative to its tensile strength. The linear elastic relation of stress-strain is a large simplification on real concrete material and only illustrates crack behaviour through lattice networks.

Also, heterogeneity is a challenging property to implement. True heterogeneity is very hard to model, but with realisation of inhomogeneity the model approximates the heterogeneous properties. A method to do that is to vary the properties of the beam elements , for example the strength of the beam elements. One is able to put a statistical distribution over the property, for example a normal distribution but other distributions are also possible.

The concrete lattice model involves understanding of the physical concrete material: Cement, aggregate embedding and macroscopic behaviour of the material. A three-tier approach as is shown in Figure 95 provides a solution. Micro level involves the hardened cement paste, meso level the pore inclusions, cracks and interfaces, and macro level relates to the structural element.

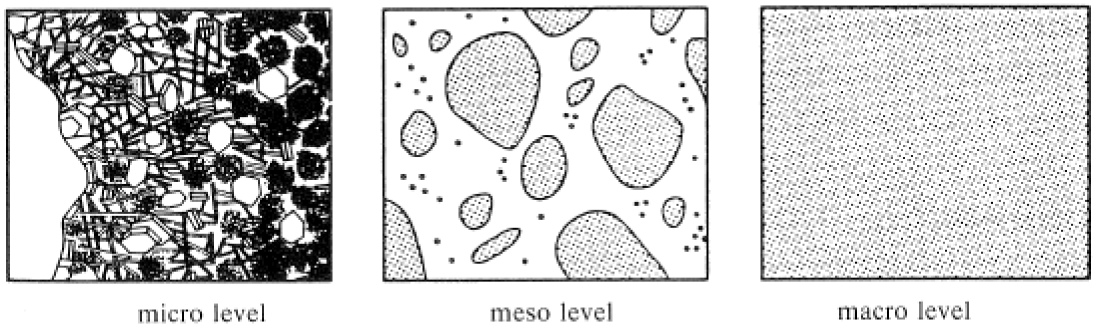

FIGURE 95 THREE TIER APPROACH ACCORDING TO (WITTMAN, 1984; READ IN SCHLANGEN E., 1993)

The model considers as a two-phase material consisting of varying sizes aggregates embedded in a cement matrix. The heterogeneity of the model improves by implementing the grain structure. First, the model generates the grain structure and second implement the grain circles. The grains are assumed to be perfect circles, but require a diameter distribution since not all grains are of equal sizes. (Schlangen E., 1993) suggests the application of a fuller curve in combination with a cumulative distribution function for a certain concrete mix. The circles may not overlap.

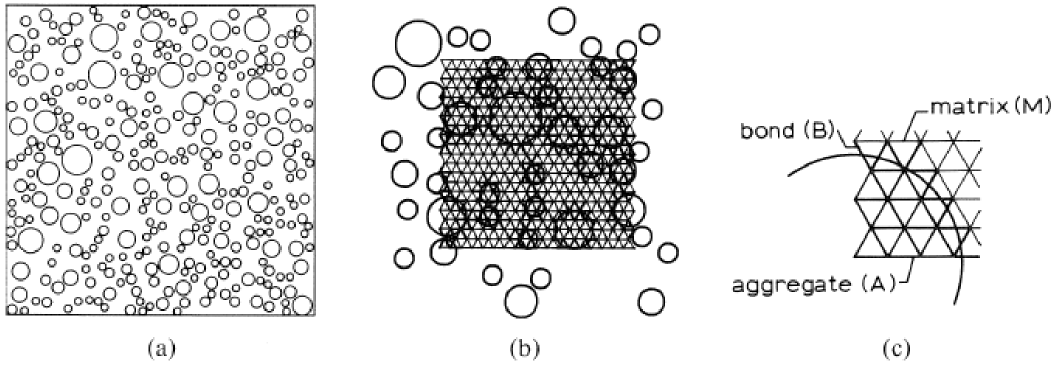

Figure 96 Grain implementation in lattice model. (a) shows the grain structure, (b) shows the grain projection on the lattice model and (c) shows the definition of aggregate, bond and matrix beams (Schlangen E., 1993)

Figure 96 (c) shows the three beam elements with different properties. The cement matrix gets the matrix strength, the aggregate the strong aggregate strength and stiffness, and the beam element on the border between aggregate and cement gets a low bond strength. The disorder of the model still not suffices, but methods to improve the disorder are not relevant for the report as it intends to only describe the global model structure.

6.4 Step 3: Interface conditions

The lattice model of ice and concrete make logically use of different links between lattices. The ice model uses kinematic relations as the concrete model uses the constitutional relations. The validation procedure of each material model will involve experimental material testing and thorough tuning of the models. Major challenge is to couple the models and simulate an ice-concrete abrasion process. The interface requires a fundamental description for further development. The ice-concrete lattice model is not part of the scope, but the fundamental description may enable new research to enhance the models.

The stronger concrete probably shows low deformation in comparison to the ice. The ice feature will locally deform viscoelastic during slow interactions and viscoplastic during fast interactions. Figure 97 illustrates this on a concrete asperity with an height in the order of μm and involves during interaction large viscoplastic deformation of the ice before crushing.

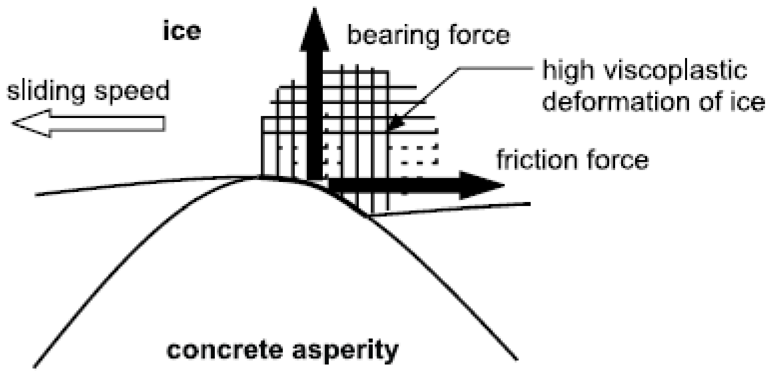

Figure 97 Contact forces due to ice action (Fiorio B. et al., 2002)

The lattice model of the ice allows viscoelastic deformation through lattice connection elements, but only fail under exceedance of a tensile stress limit. Also, the concrete asperity consisting of possible aggregate, cement and/or additives and the asperity of other microscopic feature on the concrete surface may deform during interaction. Structural deformations will occur by force application through interconnected lattices. The problem is how to connect ice and concrete material.

Firstly, the model should define surface roughness' on interface between the concrete and ice. The interface consist of the outer boundaries of the ice and concrete material. For example the maximum height of a concrete asperity may originate from a probabilistic basis as the surface roughness measurement devices uses (see section 2.1) or a physical basis from cement and aggregate compositions. The surface texture is a function of the granular structure and becomes rougher under lack of small granular material. Irregular surface texture with asperities is crucial to induce shear stresses. Concrete mechanics on microscopic level can roughly indicate the failure mechanism and reveal the failure mechanisms. The ice material is a relative flexible material and will easily deform over the irregular surface of the concrete. The surface texture of ice is thus less important than the stronger surface texture of the concrete. The ice impurity content only becomes relevant during very cold ice temperatures (stiffer and stronger ice behaviour). Impurities are salts and sediment materials. Impurity modelling forms another enhancement of the lattice model of ice. The ice and concrete surface are of primary importance to define an interface.

Secondly, the model requires adhesion criteria to model stick-slip processes. The adhesion criteria may originate from a phenomenological coulomb criteria or from a physical criteria. The physical criteria should involve a time factor into account to deal with varying ice velocities. The adhesion in combination with surface contact events cause tangential forces. The contact points on microscopic level are very critical.

Thirdly, a model enhancement is to include thermodynamic effects. The macroscopic temperature distribution through the ice thickness directly relates to local strength and stiffness of the ice and concrete. Local means here on microscopic level, probable as a discrete distribution. The thermodynamic boundary conditions (air and sea water temperature) ultimately fluctuate over time. Last thermodynamic enhancement would be the effect of frictional heat. A combination of heat and pressure softens and even liquefies the surface layers of ice and reduces the abrasion strength of concrete. The addition of a thermodynamic dimension enables recrystallization of ice during fracture.

Fourthly, a model enhancement is expansion from one or two dimensional model to the third geometrical dimension. Fifth, a model enhancement is to include the effect of water content on the interface, for example sea water or local melting. Sea water may increase the impurity contents on the interface.

6.6 Lattice model: Potential

Chapter 6 explores the lattice models on potential to simulate the abrasion processes. Such a model would be very useful for further simulation and understanding of ice-concrete interaction in general, but involve hard challenges to overcome as the contact definition. A high detail (microscopic) numerical simulation of ice running into concrete allows to study a microstructural process like concrete abrasion. The microscopic model also allows the user to study the inside interface during interaction which is almost impossible during experimental testing. The inside interface reveals answers on ice mechanical questions of high pressure zone development, but also on surface texture development over abrasion depth.

The drawback of a microscopic lattice model is the computational intensity. The system has to solve for every time step an incredible amount of equations and requires a significant amount of resources.

7 Conclusions and recommendations

7.1 Conclusions

7.1.1 Location of abrasion

The abrasion phenomenon occurs commonly under large movements of level ice (see section 2.4) and the abrasion depth increases proportionally to the movement. The perpendicular face of the structure to the ice flow direction involves the extreme abrasion depth. The vertical location of the extreme abrasion depth of a homogeneous ice sheet is on the lowest and most upper borders of the water level fluctuation as the tide slows down and turns there. Also, the water fluctuation spreads out the abrasion damage which allows less conservative approximations of the abrasion depth.

The study distinguishes region I: 'Crushing and extrusion' ($a \approx 0°$), region II: 'Stick-slip' ($0° < a < 90°$) and region III: 'Slip' ($a \approx 90°$) according to section 3.1.1, because adhesion effects introduces stick-slip. The stick-slip characteristics depends on ice velocity (v_{ice}) and the angle of contact (a). Each region involve another abrasion loading (L). Region I: 'Crushing and extrusion' experiences largest level of abrasion rate from all regions.

7.1.2 Abrasion mechanism

Abrasion occurs when the abrasion loading (L) exceeds the abrasion resistance (R) from fundamental point of view (section 5.1). The L over R ratio depends on local spatial parameters. Macroscopic abrasion covers the phenomenon in the abrasion resistant design and depends on direct parameters like ice sliding distances, but the microscopic abrasion explains the mechanisms and justifies the macroscopic design methodology. The mechanism of abrasion fall under three separate categories: Mechanical, physical and chemical mechanisms. The most important mechanisms are crushing (high shear stress) and sliding (low shear stress) in combination with adhesion (section 2.2 and 5.2), and freeze-thaw cycles due to expansion of ice in pores (section 2.5.4). Some of the mechanisms are also capable to strengthen or weaken each other (section 5.2). Abrasion loading (L) consist of primary and secondary order of loading. The primary order of loading directly exceeds the abrasion resistance (R) and the secondary order of loading reduces the abrasion resistance (R). Typical first order of loading are compression and shear stress. Typical secondary order of loading are freeze-thaw cycles or local temperature gradients. The abrasion loading is often expressed as abrasion rate.

Ice contact pressure, ice temperature and impurity content on the ice are most important factors on the abrasion rate. Increasing contact pressure increases the abrasion rate (L) proportionally (see section 2.4.1). Locally, the crushing pressure can obtain values over 70 MPa for a short duration also known as high pressure zones. The high pressure zones causes dry and wet friction processes of crushed ice and concrete material. Friction under very high compression stress is also known as extrusion and involves large shear stresses on the concrete. Decreasing temperature increases the abrasion rate (L) (see section 2.4.3). The spatial temperature variation indicate the abrasion rate is larger on top of the ice sheet (with lowest temperature) and lower on the bottom of the ice sheet (with highest temperature). Increasing impurity content on the interface increases the abrasion rate (L). The abrasion rate increases with increasing impurity content at the interface like sediment or salt contents, but also concrete particles. The hard particles function like sandpaper on the concrete surface.

The initial concrete abrasion resistance (R) of concrete increases with very fine particle content like Silica Fume - the bonding strength of the internal cement structure and cement-aggregate structure increases. The concrete abrasion resistance reduces due to secondary order effects (see section 5.1), for example like freeze-thaw cycles, temperature fluctuations due to water level changes and chemical intrusion. Concrete abrasion resistance (R) increases with concrete surface treatment like polyurethane lining and with steel fiber or basalt content up to 1.0%.

7.1.3 Experiment

The experimental set-up is suitable for simulation of two-dimensional ice-structure interaction on and examination of local material processes like ice abrasion. The most important advantage is the ability to simulate interaction at a predetermined point of contact dependent on angle (a) , see section 3.1.1 for the definition. The most important drawback is the limitation of not being able to easily achieve large ice sliding distances.

Observations from the preliminary laboratory tests discussed here indicate that:

- The component of local static bonding during a sliding test on the high performance concrete sample can be up to half of the compression force.
- Adhesion introduces a cyclic load on the concrete surface due to stick-slip under low ice velocities (v_{ice})
- The stick-slip cycle depends on real contact area. Ice fracture and spalling reduces adhesion bonding due to reduction of real contact area.
- The areal size of region II: 'Stick-slip' reduces with increasing ice velocity (v_{ice})
- Static bonding increases with decreasing concrete surface roughness. Surface characteristics of concrete like roughness depend on the concrete mixture composition: cement type or additives like silica fume.,

On micro scale processes:

- Secondary order abrasive ice loading is only important on long sliding distances,, which is often seen in lifetime design offshore structures.
- Frictional heating in combination with contact pressure significantly increases the temperature of the ice-concrete interface. The local temperature gradients affect the character of the local shear loading (hydrodynamic flow versus granular solid flow)
- Frictional heat generation introduces local thermal stresses within the concrete surface and reduces the abrasion resistance.
- The ice surface material crushes and recrystallizes an ice-concrete mixture during interaction.
- The ice impurity content increases due to enclosure of concrete particles in the ice surface.
- The high performance concrete sample showed a better abrasion resistance than the low performance concrete sample, most likely due to an improved binding strength by the addition of silica fume.

7.1.4 NUMERICAL MODEL

A numerical model for ice abrasion on concrete may consist of a lattice model for concrete and for ice and involve great opportunities to study the inside of the interface for example during crushing. The implementation of an abrasion criteria on the concrete seem feasible (static/dynamic shear limits), but the microscopic interface between ice and concrete impose harder challenges to overcome. The interface model requires the ice and concrete to interact through several contact points, and requires to define a surface roughness' and adhesion criteria for stick-slip behaviour from a physical understanding. The surface roughness of concrete is of more importance than the surface roughness of ice due to the difference in strength. The numerical model may determine ice velocity and angle of contact as shown in section 3.1 in order to define the macroscopic situation. Enhancement of the model may include temperature or impurity modelling.

7.1.5 RELIABILITY

The risk of severe damage at a concrete design is high without considering the concrete abrasion threat in ice infested waters. Ice abrasion threatens the structural integrity and thus the direct function of the structure. The abrasion depth can achieve several centimetres over a structural lifetime and deteriorates the inner concrete layers away and abrade the reinforcements off. The designer may wish to implement sufficient abrasion resistance in the concrete design or apply mitigation, for example steel protection layers. Concluding, the ice abrasion phenomenon is indispensable but requires further investigation in the physical abrasion process or amount of abrasion data to estimate a reliable abrasion loading (L) for design. The abrasion resistance (R) requires further investigation in abrasion resistant materials or treatments like impregnation. The reliability of an abrasion resistant design depends on the frequency on which the abrasion loading (L) exceeds the abrasion resistance (R). The recommendation section will discuss possible follow-up.

7.2 RECOMMENDATIONS

The ice-concrete abrasion theory requires to refine. The general perception of ice abrasion is incomplete, because the underlying microscopic processes are not well understood yet. The current assumption is: Increasing global contact pressure increases the abrasion rate, but the assumption does not include a high detail about the mechanism and also speculates about the presence of shear stresses. Important goals are developing standard testing or numerical modelling of the problem in order to test or evaluate abrasion resistant materials. The study of a standard test requires to provide a clear indication of the concrete surface changes during ice loading for a reliability assessment.

7.2.1 MEASURING CONCRETE ABRASION

Prior to new testing, the choice of a representative surface texture measurement technique is very important. The techniques in this report won't suffice anymore, because the measurement techniques don't provide any reliable quantification of abrasion. Reliable means here large uncertainty in measurements which only allows a qualitative description. The technique should only include measurements over the area of contact and quantify at least the following spatial characteristic.

- Abrasion depth: Average change of surface texture (R_a)
- Roughness: Asperity characteristic like maximum asperity peak height (R_p)

A measurement technique which may suit the requirements is a non-contact device with a microscopic sensitivity (order of µm) up to mesoscopic features (order of mm) according to section 2.1.

7.2.2 SETUP IMPROVEMENTS

The largest drawback of the apparatus is the absence of the ability to slide long distances of ice along the concrete surface, because significant damage in the current setup is hard to achieve. The ice supply intends to remain under constant contact under compression and shear, thus the system requires another degree of freedom to refresh the ice supply and maintain force control.

Abrasion conditions offshore often involves water content at the interface. The setup should include some way to insert water content at the interface as simulation of an offshore situation.

The effect of the structure in cyclic loading for example stick-slip can also decrease by increasing the stiffness of the structure of the experimental setup. The structure was built around the MTS machine, one can possibly integrate the structure in the cold room support structure and increase the stiffness of the setup.

7.2.3 FOLLOW UP TESTING

The microscopic processes in region I, II and III (see section 5.1) are not well understood. The specific character of compression, shear and adhesive loading requires some effort like:

- Ice shear stress requires investigation under high and low compression stress.
- High pressure zones requires investigation on fracture and recrystallization
- Adhesion bonding requires investigation and effect on cyclic loading build-up (adhesion versus shear)
- Interface layer requires investigation during ice-concrete interaction.

The second order type of loading require an sensitivity analysis on ice-concrete abrasion. For example, freeze-thaw loading induces micro cracks on the concrete surface which accelerate the abrasion rate by some percentage. Test 3 or more beams on a varying number of freeze-thaw cycles and apply identical loading schemes on them. The description or model of ice concrete abrasion requires verification on real scale. Field tests should be integral part of the verification procedure.

Also, the reliability of an abrasion resistant design is insufficient and requires multi-year tests at several location. Ice abrasion testing methods and thorough understanding of the microscopic processes will enable industry to develop abrasion resistant concrete materials. Or develop measures to mitigate the risk on ice abrasion. Also, other lines of technology benefit from the results concerning abrasion, for example cold road design.

LIST OF FIGURES

LIST OF TABLES

Bibliography

A., Bekker, Gomolskiy S., Sabodash O., Kovalenko R., Uvarova T., en Pomnikov E. 2010. „Physical and Mechanical Properties of Modeling Ice for Investigation of Abrasion Process on Ice-Resistant Offshore Platforms." *Proceedings of the Twentieth (2010) International Offshore and Polar Engineering Conference.* Beijing, China.

A., Bekker, Uvarova T., en Kim S. 2003. „Abrasion Effect of Ice Cover on Supports of Hydraulic Engineering Structures in Conditions of Sakhalin Island Shelf." *Proceedings of the Thirtheenth (2003) International Offshore and POlar Engineering Conference.* Honolulu, Hawaii.

A., Bekker, Uvarova T., en Pomnikov E. 2012. „Numerical Simulation of Ice Abrasion on Offshore Structures." *21st IAHR International Symposium on Ice.* Dalian, China.

—. 2010. „The Registration of Temperature during Calculation of the Ice Abrasion." *Proceedings of the Ninth (2010) ISOPE Pacific/Asia Offshore Mechanics Symposium.* Busan, Korea.

A., Bekker, Uvarova T., Pomnikov E., Farafonov A., Prytkov I., en Tyutrin R. 2011. „Abrasion, Experimental Study of Concrete Resistance to Ice." *Proceedings of the Twenty-first (2011) International Offshore and Polar Engineering Conference.* Maui, Hawaii.

B., Fiorio. 2004. „Wear Characterisation and Degradation Mechanisms of a Concrete Surface under Ice Friction." *Construction and Building Materials 19 (2005).* Elsevier. 366-375.

B., Fiorio, Meyssonnier J., en Boulon M. 2002. „Experimental Study of the Friction of Ice over Concrete under Simplified Ice-Structure Interaction Conditions." *NRC Research Press Web.*

B., Zuber, en Marchand J. 2000. „Modeling the deterioration of hydrated cement systems exposed to frost action." *Cement and Concrete Research Vol. 30.* 1929-41.

C., Daley, en Colbourne B. 2012. *Lecture slides Arctic Engineering.* St. John's: Memorial University of Newfoundland.

D., Campbell. 2013. „Effects of Ice Loads on the Confederation Bridge." *Journal of Undergraduate Engineering Research and Scholarschip.* St. John's, NL, Canada: Memorial University of Newfoundland.

D., Masterson, Frederking R., Jordaan I., en Spencer P. 1993. „Description of multi-year ice indentation tests at Hobson's Choice Ice Island." *Proceedings, 12th International Conference on Offshore Mechanics and Arctic Engineering, Vol. 4.* Glasgow, Great-Brittain. 145-55.

E., Moen, Hoiseth K., Leira B., en Hoyland K. 2014. „Experimental study of Concrete Abrasion due to Ice Friction - Part I." *Cold Regions Science and Technology.* Elsevier.

E., Moen, Jacobsen S., en Myhra H. 2007. *Ice abrasion data on concrete structures.* Trondheim, Norway: SINTEF Building and Infrastructure.

E., Sistonen, en Vesikari E. 2008. *Effect of Interacted Deterioration Parameters on Service Life of Concrete Structures in Cold Environments.* Espoo, Finland: VTT.

F., Hara, Ohshima K., Hanada M., Ujihira M., Tachibana H., en Saeki H. 1997. „Design Method to Counter the Abrasion of Hydraulic Structures Due to Ice Sheet Movements." *The 9th Workshop on River Ice.* Fredericton, N.B.

H., Justnes. 1998. „A review of chloride binding in cemintitious systems." *Nordic Concrete Research Publication.* 16.

H., Saeki. 2010. „Mechanical Properties between Ice and Various Materials Used in Hydraulic Structures." *International Journal of Offshore and Polar Engineering Vol. 21, No. 2.* 81-90.

I., Glen, en Blount H. 1984. „Measurements of ice impact pressures and loads onboards CCGS Louis S. St. Laurent." *Proceedings, 3rd Offshore Mechanics and Arctic Engineering Symposium, Vol. III.* New Orleans, USA. 246-52.

I., Jordaan. 2001. „Mechanics of ice-structure interaction." *Engineering Fracture Mechanics 68.*

J., Janson. 1989. „Report of Field Investigation of Ice Impact on Lightweight Aggregate Concrete - Results from the winter season 1986-1987." *VBB.* Stockhold, Sweden.

J., Kirkhaug. 2013. *Ice Abrasion and Bond Testing of Repair Mortars and High Performance Concrete.* Trondheim, Norway: NTNU.

J., Marchand. 1993. *Contribution to the study of the de-icer salt scaling deterioration of concrete.* Ph.D. dissertation, France: École Nationale des Ponts et Chaussées.

J., Marchand, Jacobsen S., en Gerard B. 1998. *Concrete cracks I: Durability and self healing - a review.* London, U.K.

J., Marchand, Jolin M., en Machabée Y. 2005. „Influence of the supplementary cementing materials on the de-icer salt-scaling resistance: Ten years of field performance." *Cement Combination for Durable Concrete.* Thomas Telford. 579-90.

J., Marchand, Sellevold E., en Pigeon M. 1994. „The de-icer salt scaling deterioration of concrete - An overview." *ACI-SP-145.* 1-46.

K., Saetre. 2014. *Ice Abrasion on Fiber Reinforced Concrete.* Trondheim, Norway: NTNU.

L., Kim. 2012. „Kinematic Analysis of the Ice Flow around Offshore Structures." *14th International Conference on Computing in Civil and Building Engineering.* Moscow, Russia.

M., Hanada, Ujihira M., Hara F., en Saeki H. 1996. „Abrasion Rate of Various Materials Due to the Movement of Ice Sheets." *Proceedings of the Sixth (1996) International Offshore and Polar Engineering Conference.* Los Angeles, USA.

M., Valentinovna, en Vasilyevna P. 2013. „Abrasion Wear of Heterogeneous Materials." *Applied Mechanics and Materials Vol. 248 (2013).* 355-360.

N., Greaker. 2014. *Laboratory Measurements of Ice-Concrete Abrasion with Different Types of Ice Quality.* Trondheim, Norway: NTNU.

N., Kabay. 2014. „Abrasion resistance and fracture energy of concretes with basalt fiber." *Construction and Building Materials 50.* 95-101.

O., Bohn. 2012. *Ice abrasion of concrete, background theory and testing at the NTNU laboratory.* Trondheim, Norway: NTNU.

P., Moslet, en Myhra H. 2009. „Probabilistic modelling of Concrete Abrasion due to Moving Sea Ice." *Proceedings of the 20th International Conference on Port and Ocean Engineering under Arctic Conditions (2009).* Lulea, Sweden.

R., Frederking, Jordaan I., en McCallum J. 1990. „Field tests of ice indentation at medium scale: Hobson's choice ice island." *Proceedings, 10th International Symposium on Ice 2, IAHR.* Espoo, Finland. 931-44.

R., Helmuth. 1961. „Dimensional changes of hardened Portland cement pastes caused by temperature changes." *Highway Research Board Proceedings Vol. 40.* 315-336.

R., Hooton, en Boyd A. 1997. „Effects of finishing, forming and curing on de-icer salt scaling resistance of concretes." *Frost Resistance of Concrete.* London, U.K. 174-83.

R., Kobrick, Klaus D., en Street Jr. K. 2011. „Validation of proposed metrics for two-body abrasion scratch test analysis standards." *Wear.* 815-22.

S., Bruneau, Dillenburg A., en Ritter S. 2011. *Ice Specimen Fabrication Techniques and Indentation Experiments.* St. John's, NL, Canada: Memorial University of Newfoundland.

S., Huovinen. 1990. „Abrasion of Concrete by Ice in Arctic Sea." *Rakenteiden mekani ikka, Vol. 23 No.1 1990.* 23-35.

—. 1992. „Abrasion of Concrete Structures by Ice." *Cement and Concrete Research, Vol. 23.* 69-82.

S., Jacobsen, Bekker A., Uvarova T., Pomnikov E., Kim L., en Fossa K. 2012. „Concrete ice abrasion: Deterioration mechanisms, testing and modelling." *International Congress on durability of concrete.*

S., Jacobsen, Kim L., en Pomnikov E. 2012. „Concrete Destructure due to Ice-Indentation Pore Pressure." *Proceedings of the twenty-second (2012) International Offshore and Polar Engineering Conference.* Rhodes, Greece.

S., Jacobsen, Sistonen E., Huovinen S., Marchand J., en Tremblay M. 2006. „Abrasion and scaling of concrete by ice, studded tires and frost-salt: Interaction and service-life modeling." *RILEM proceedings PRO 51.*

S.A., Vershinin, Truskov P., en Kuzmichev K. 2006. *Sakhalin Island - Offshore Platform Structures - The Impact and Influence of Ice.* Moscow.

T., Powers, en Helmuth R. 1953. „Theory of Volume Changes in Hardened Cement Paste During Freezing." *Proceedings of the Highway Research Board Vol. 32.* 285-297.

T., Sanderson. 1988. *Ice Mechanics, Risks to Offshore Structures.* London, U.K.: Graham and Trottman.

T., Sebok, en Stranel O. 2004. „Wear resistance of polymer-impregnated mortars and concrete." *Cement and Concrete Research 34 (2004).* Pergamon. 1853-1858.

T., Takeuchi, Kioka S., en Saeki H. 2006. „Significance of Tidal Change on Abrasion Area of Structures due to Sea Ice Movement." *Proceeding of the 18th IAHR International Symposium on Ice.*

T., Takeuchi, Nakazawa N., Mikami T., Watanabe Y., en Saeki H. 2005. „Abrasion of Offshore Structure due to Sea Ice Movement." *Proceedings of the Fifteenth (2005) International Offshore and Polar Engineering Conference.* Seoul, Korea.

Y., Asai, Itoh Y., Kante S., en Sakai M. 1994. „Study on the Characterisitcs of High-Strength Lightweight Concrete for Icy Waters." *Proceedings of the Fourth International Offshore and Polar Engineering Conference.* Osaka, Japan.

Y., Itoh, en Tanaka Y. 1994. „Estimation Method for Abrasion of Concrete Structures due to Sea Ice Movement." *Proceedings of the Fourth International Offshore and Polar Engineering Conference.* Osaka, Japan.

Y., Itoh, Tanaka Y., en Delgado A. 1996. „Abrasion Depth Distribution of a Cylindrical Concrete Structure due to Sea Ice Movement." *International Journal of Offshore and Polar Engineering, Vol. 6, No. 2.*

—. 1995. „Abrasion Mode of A Circular Cylindrical Concrete Structure." *Proceedings of the Fifth (1995) International Offshore and Polar Engineering Conference.* The Hague, The Netherlands.

Y., Itoh, Yoshida A., Tsuchiya M., Katoh K., Corp. T., Sasaki K., Saeki H., en Hokkaido U. 1988. „An Experimental Study on Abrasion of Concrete Due to Sea Ice." *OTC.*

Z., Grdic, Curcic G., Ristic S., en Despotovic M. 2012. „Abrasion resistance of concrete micro-reinforced with polypropylene fibers." *Construction and Building Materials 27.* 305-312.

APPENDIX I: MATLAB CODE OF SINGLE TEST

```
%The vertical axis of the MTS machine is reffered to as normal direction or
%x-axis. The horizonal axis is reffered to as sliding or tangential axis or
%z-axis. The sideward length of the beam has been defined as the y-axis.

%Absolute is defined as the distances set in the driving software of the
%apparatus where +77mm is the lowest point and -77 mm the highest point.
%Relative distances may be calculated from it.

%---------IMPORT------------
specimen = dlmread('specimen_1a.dat','',6,0);

%---------INPUT-------------

alfain = 2.6;              %Initial angle of swing arm (deg) relative to
z-axis
L      = 1.36;             %Length along z-axis (m) swing arm from turning
point to the perpendicular line of the tip of the ice cone
l      = 0.28;             %Length along x-axis (m) between centre line
swing arm to tip ice cone
xin    = specimen(1,2);    %Initial x position (mm)
zin    = specimen(1,4);    %Initial z position (mm)

%---------PROCESS-----------
% i) Correction of contact area due to swing arm angle
XPathAbsolute       = specimen(:,2);
IndentationRelative = -XPathAbsolute+xin*ones(length(XPathAbsolute),1);
%Ice indentation reference (set x starting point on 0)

XTurningAbsolute    = xin - L*sin((alfain/180)*pi);
%Determination of the absolute vertical position of the turning point of
the swing arm
D0                  = 2*IndentationRelative/tan((30/180)*pi());
%Diameter contact area during true normal crushing
alfa                = asin((XPathAbsolute-XTurningAbsolute)/(L*10^3));
%Angle of swing arm (positive values counterclockwise)
D1                  = abs(2*sqrt((D0/2).^2+(D0.*sin(alfa)).^2));
%Valid for alfa positive AND negative (symmetry)
ContactArea_rev_1a = 0.25*pi()*D0.*D1;
%Corrected contact area for angle of swing arm

% ii) Induction of moment due to eccentricity
dFv = (l/L)*tan(alfa).*specimen(:,3);       %Force difference between force
applied and measured due to eccentricity
M_1a= l * sin(alfa).*dFv;                   %Moment due to eccentricity

% v) Start point determination
Flowerlimit = 990; %[N] - Weight of the swing arm and attached parts,
should be subtracted from the force measurements
i           = 500; %Initial sample number in order to make sure that the
starting point is not based on other factors than first contact.
dFlimit     = -1;  %Tolerance to own weight

while dFlimit < 0;
    i       = i + 1;             %Row or sample number
    Fv      = abs(specimen(i,3));   %[N]
    dFlimit = Fv - Flowerlimit;
end
```

```
n=1;
x=IndentationRelative(1,1);
while x < 42.2;
    n       = n + 1;                %Row or sample number
    x      = IndentationRelative(n,1);    %[mm]
end

% vi) Correction of horizontal force measurements
Fs1 = specimen(:,5)-specimen(1,5);
Fs2 = specimen(:,6)-specimen(1,6);

NSR = i:n;
IndentationRelative_1a = IndentationRelative(NSR,1);
specimen_rev_1a = [specimen(NSR,1:2)
specimen(NSR,3)+Flowerlimit*ones(length(NSR),1) specimen(NSR,4) Fs1(NSR)
Fs2(NSR)];
ContactArea_revr_1a = ContactArea_rev_1a(NSR,1);
SlidingRelative_1a = specimen_rev_1a(:,4) -
specimen_rev_1a(1,4)*ones(length(specimen_rev_1a(:,4)),1);
```

APPENDIX II: MATLAB CODE OF FORCE-TO-WORK CALCULATION

```
clc;clear all;clf;

%----Input-----
TestSequence0 = ['1a '; '1b '; '2  '; '3  '; '4  '; '5  '; '6  '; '7  '; '8
'; '9a '; '10a'; '10b'; '11 '; '12 '; '13 ';'14 ';'15 ']; %Test run 9b has
been rejected as outlyer
TestSequence1 = ['1a '; '2  '; '3  '; '4  '; '5  '; '6  '; '7  '; '11 ';
'12 '; '8  '; '14 '; '13 '; '9a '; '10a'; '15 ';'1b ']; %Test run 9b and
10b has been rejected as outlyer
s1 = 'specimen_rev_';

%----Process----
for k = 1:1:16 %Run each dataset as named in TestSequence1
    %---Input of variables
    strcat(s1,TestSequence1(k,:))
%Shows which test is on the go during running of the script
    ProcessScript = strcat('ProcessScript_',TestSequence1(k,:),'.m');
%Select right ProcessScript file per test run
    sp = fullfile(ProcessScript); run(sp);
%Run ProcessScript and obtain data into workspace
    specimen_rev = eval(strcat(s1,TestSequence1(k,:)));
%Select right data matrix per test run
    ContactArea = eval(strcat('ContactArea_revr_',TestSequence1(k,:)));
%Select right corrected Contact area per test run

    %---Essential parameters
    n = length(specimen_rev(:,1));
%Length or last sample number in data vector
    vf = (specimen_rev(n,4)- specimen_rev(1,4))/(specimen_rev(n,1)-
specimen_rev(1,1)); %Average sliding velocity over test run
    vc = (specimen_rev(n,2)- specimen_rev(1,2))/(specimen_rev(n,1)-
specimen_rev(1,1)); %Average indentation velocity over test run
    Fs = specimen_rev(:,5) + specimen_rev(:,6);
%Tangential force (measured by two load cells)
    ps = Fs./ContactArea;
%Nominal shear stress
    pc = specimen_rev(:,3)./ContactArea;
%Nominal compression stress

    %---Integration of forces to work
    Ec_pre = zeros(n,1);Ecsum_pre = zeros(n,1);Ef_pre =
zeros(n,1);Efsum_pre=zeros(n,1);
%Create vectors for loop (as optimization)
    for i = 1:n-1
%Iteration steps - Last sample minus one due to integration requirements
        Ec_pre(i,1) = ((specimen_rev(i+1,1)-
specimen_rev(i,1))*((specimen_rev(i+1,3)+specimen_rev(i,3))/2)*vc)/ContactA
rea(i); %Normal work per area between sample points i and i+1
        Ecsum_pre(i+1,1) = Ec_pre(i) + abs(Ecsum_pre(i,1));
%Cumulative normal work on i+1
        Ef_pre(i,1) = ((specimen_rev(i+1,1)-
specimen_rev(i,1))*((Fs(i+1)+Fs(i))/2)*vf)/ContactArea(i);
%Tangential work per area between sample point i and i+1
        Efsum_pre(i+1,1) = Ef_pre(i) + abs(Efsum_pre(i,1));
%Cumulative tangential work on i+1
    end
```

```
    %---Storage of work variables (Work per integration step and cumulative
work)
    Ec{:,k} = {Ec_pre};
    Ecsum{:,k} = {Ecsum_pre};
    Ef{:,k} = {Ef_pre};
    Efsum{:,k} = {Efsum_pre};
end


%Output for general use
Ec1a = cell2mat(Ec{:,1});     Ecsum1a = cell2mat(Ecsum{:,1});   Ef1a =
cell2mat(Ef{:,1});     Efsum1a = cell2mat(Efsum{:,1});
Ec2 = cell2mat(Ec{:,2});      Ecsum2 = cell2mat(Ecsum{:,2});    Ef2 =
cell2mat(Ef{:,2});      Efsum2 = cell2mat(Efsum{:,2});
Ec3 = cell2mat(Ec{:,3});      Ecsum3 = cell2mat(Ecsum{:,3});    Ef3 =
cell2mat(Ef{:,3});      Efsum3 = cell2mat(Efsum{:,3});
Ec4 = cell2mat(Ec{:,4});      Ecsum4 = cell2mat(Ecsum{:,4});    Ef4 =
cell2mat(Ef{:,4});      Efsum4 = cell2mat(Efsum{:,4});
Ec5 = cell2mat(Ec{:,5});      Ecsum5 = cell2mat(Ecsum{:,5});    Ef5 =
cell2mat(Ef{:,5});      Efsum5 = cell2mat(Efsum{:,5});
Ec6 = cell2mat(Ec{:,6});      Ecsum6 = cell2mat(Ecsum{:,6});    Ef6 =
cell2mat(Ef{:,6});      Efsum6 = cell2mat(Efsum{:,6});
Ec7 = cell2mat(Ec{:,7});      Ecsum7 = cell2mat(Ecsum{:,7});    Ef7 =
cell2mat(Ef{:,7});      Efsum7 = cell2mat(Efsum{:,7});
Ec11 = cell2mat(Ec{:,8});     Ecsum11 = cell2mat(Ecsum{:,8});   Ef11 =
cell2mat(Ef{:,8});     Efsum11 = cell2mat(Efsum{:,8});
Ec12 = cell2mat(Ec{:,9});     Ecsum12 = cell2mat(Ecsum{:,9});     Ef12 =
cell2mat(Ef{:,9});     Efsum12 = cell2mat(Efsum{:,9});
Ec8 = cell2mat(Ec{:,10});     Ecsum8 = cell2mat(Ecsum{:,10});   Ef8 =
cell2mat(Ef{:,10});     Efsum8 = cell2mat(Efsum{:,10});
Ec14 = cell2mat(Ec{:,11});    Ecsum14 = cell2mat(Ecsum{:,11});  Ef14 =
cell2mat(Ef{:,11});    Efsum14 = cell2mat(Efsum{:,11});
Ec13 = cell2mat(Ec{:,12});    Ecsum13 = cell2mat(Ecsum{:,12});  Ef13 =
cell2mat(Ef{:,12});    Efsum13 = cell2mat(Efsum{:,12});
Ec9a = cell2mat(Ec{:,13});    Ecsum9a = cell2mat(Ecsum{:,13});  Ef9a =
cell2mat(Ef{:,13});    Efsum9a = cell2mat(Efsum{:,13});
%Ec9b = cell2mat(Ec{:,14});    Ecsum9b = cell2mat(Ecsum{:,14});  Ef9b =
cell2mat(Ef{:,14});    Efsum9b = cell2mat(Efsum{:,14});
Ec10a = cell2mat(Ec{:,14});   Ecsum10a = cell2mat(Ecsum{:,14}); Ef10a =
cell2mat(Ef{:,14});   Efsum10a = cell2mat(Efsum{:,14});
%Ec10b = cell2mat(Ec{:,15});   Ecsum10b = cell2mat(Ecsum{:,15}); Ef10b =
cell2mat(Ef{:,15});   Efsum10b = cell2mat(Efsum{:,15});
Ec15 = cell2mat(Ec{:,15});    Ecsum15 = cell2mat(Ecsum{:,15});  Ef15 =
cell2mat(Ef{:,15});    Efsum15 = cell2mat(Efsum{:,15});
Ec1b = cell2mat(Ec{:,16});    Ecsum1b = cell2mat(Ecsum{:,16});  Ef1b =
cell2mat(Ef{:,16});    Efsum1b = cell2mat(Efsum{:,16});
```

APPENDIX III: MATLAB CODE OF ABRASION LOAD (J/MM²) PER SLIDING DISTANCE

```
clear g
%----Input-----
TestSequence0 = ['1a '; '1b '; '2  '; '3  '; '4  '; '5  '; '6  '; '7  '; '8 
'; '9a '; '10a'; '10b'; '11 '; '12 '; '13 ';'14 ';'15 ']; %Test run 9b has 
been rejected as outlyer
TestSequence1 = ['1a '; '2  '; '3  '; '4  '; '5  '; '6  '; '7  '; '11 '; 
'12 '; '8  '; '14 '; '13 '; '9a '; '10a'; '15 ';'1b ']; %Test run 9b and 
10b has been rejected as outlyer
astart = 0;
astep = 1;
aend = 900;
s1 = 'specimen_rev_';
di = 1;
dj = 1;

%----Process----
i=1;a1=1;Wc=zeros(length(astart:astep:aend),1);Wf=zeros(length(astart:astep
:aend),1);dWc=zeros(18,1); dWf=zeros(18,1);
for a = astart:astep:aend %Defined length z (over beam), from z=astart to 
z=aend with dz = astep
    for k = 1:1:16 %Run each dataset as named in TestSequence1
        %strcat(s1,TestSequence1(k,:)) %Shows which test is on the go 
during running of the script
        TestNr = eval(strcat(s1,TestSequence1(k,:))); %Select right matrix 
originating from corresponding test run
        Ecsum = eval(strcat('Ecsum',TestSequence1(k,:))); %Select right 
work due to crushing vector
        Efsum = eval(strcat('Efsum',TestSequence1(k,:))); %Select right 
work due to friction vector
        i=1; %Restart number of indice in lower boundary for each vector
        j=length(TestNr(:,4))-1; %Restart number of indice in upper 
boundary for each vector
        z1 = TestNr(1,4);
        z2 = TestNr(j,4);
        g(k,1)= a;
        g(k,2)= a+astep;
        g(k,3) = z1;
        g(k,4) = z2;
        %Start value estimation
        %v  = (TestNr(length(TestNr(:,4)),4)-TestNr(1,4))/
(TestNr(length(TestNr(:,1)),1)-TestNr(1,1)); %Average sliding velocity over 
entire test run
        %i = round(((TestNr(1,4) - a) / v ) * 
(length(TestNr(:,4))/TestNr(length(TestNr(:,1)),1))) ;  %Estimated start 
value of indice of lower boundary
        %j = round(((a + astep - TestNr(1,4)) / v) * 
(length(TestNr(:,4))/TestNr(length(TestNr(:,1)),1))) + 10^4; %Estimated 
start value of indice of upper boundary

        if z1 < a
            if z2 > a
               if z2 < a + astep
                   %2 Start indice lower than lower boundary, end indice
                   %between lower and upper boundary
                   while z1 < a
                       z1 = TestNr(i,4);
                       i = i+di;
```

```
                    end
                    j = length(TestNr(:,4))-1;
                else
                    %6 Start indice lower than lower boundary, end indice
                    %higher than upper boundary
                    while z1 < a
                        z1 = TestNr(i,4);
                        i = i + di;
                    end
                    while z2 > a + astep
                        z2 = TestNr(j,4);
                        j = j - dj;
                    end
                end
            else
                %1 Start indice lower than lower boundary, end indice lower
                %than lower boundary
                i = length(TestNr(:,4))-1;
                j = length(TestNr(:,4))-1;
            end
        else
            if z2> a + astep
                if z1 < a + astep
                    % 4 Start indice between lower and upper boundary, end
                    % indice greater than upper boundary
                    i = 1;
                    while z2 > a + astep
                        z2 = TestNr(j,4);
                        j = j - dj;
                    end
                else
                    % 5 Start and end indice greater than upper boundary
                    i = length(TestNr(:,4))-1;
                    j = length(TestNr(:,4))-1;
                end
            else
                %3 Start and end indice between lower and upper boundary
                i = 1;
                j = length(TestNr(:,4))-1;
            end
        end

        g(k,5) = TestNr(i,4);
        g(k,6) = TestNr(j,4);

        dWc(k) = Ecsum(j) - Ecsum(i); %Generated work due to crushing in
vector k
        if length(TestNr(:,4)) == length(Efsum); %No frictional work
vectors available
            i = i; j=j;
        else
            i = 1; j = 1;
        end
        dWf(k) = Efsum(j) - Efsum(i); %Generated work due to friction in
vecotr k
        g(k,7) = dWc(k)*10^-6;
        g(k,8) = dWf(k)*10^-6;
    end
    Wc(a1) = sum(dWc); %Exerted work due to crushing on interval a1
    Wf(a1) = sum(dWf); %Exerted work due to friction on interval a1
    a1 = a1 + 1; %Postive increment of interval space parrallel with a
```

```
end

clf;
plot(astart:astep:aend,Wc*10^-3);
hold on;
plot(astart:astep:aend,Wf*10^-3,'r');
xlabel('Absolute sliding distance (mm)');
ylabel('Work (J/mm2 per sliding mm)');
hleg1 = legend('Work due to normal load','Work due to tangential load');
set(hleg1,'Location','NorthEast');
axis([0 900 0 0.3])
saveas(gcf, 'Loading on concrete surface - Test 1a', 'png' )
```

Appendix IV: Abrasion of high performance concrete

The description of the abrasion process is shown in this appendix. The left side data shows the photographic documentation of the concrete beam and the right hand side data the ice loading in Work per area (J/mm²) along the sliding distance. The letters on the side mark the location and make comparison possible.

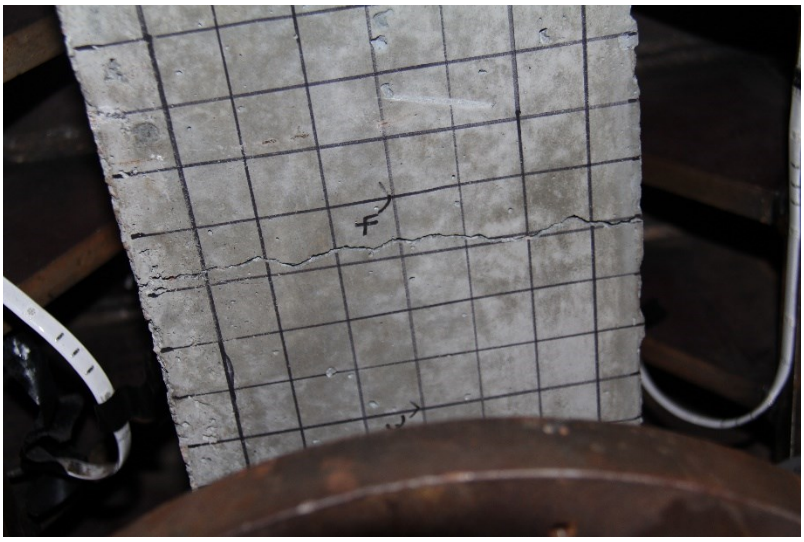

Figure 98 Concrete surface prior to a test sequence

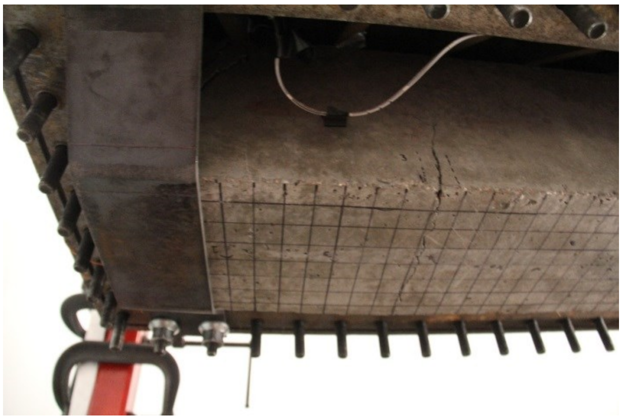

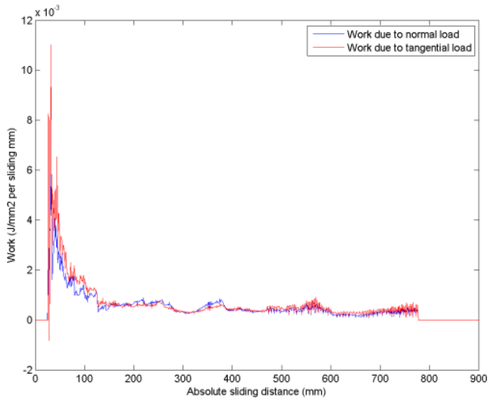

Figure 99 Concrete surface after test run 1a - Starting point - Slight colour change on the middle of the beam, no significant damage

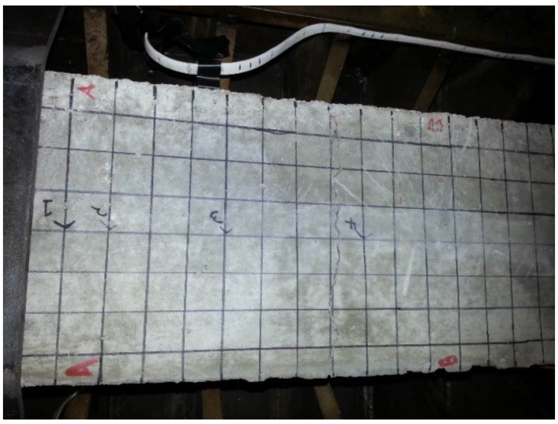

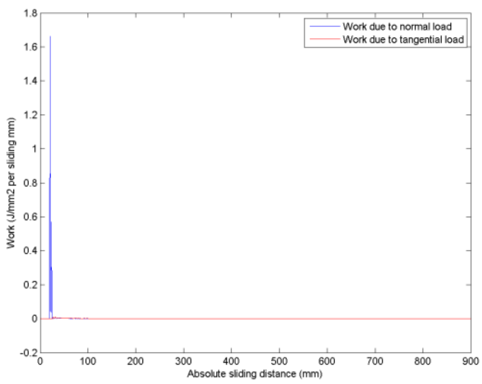

Figure 100 Concrete surface after test run 2 - Starting point

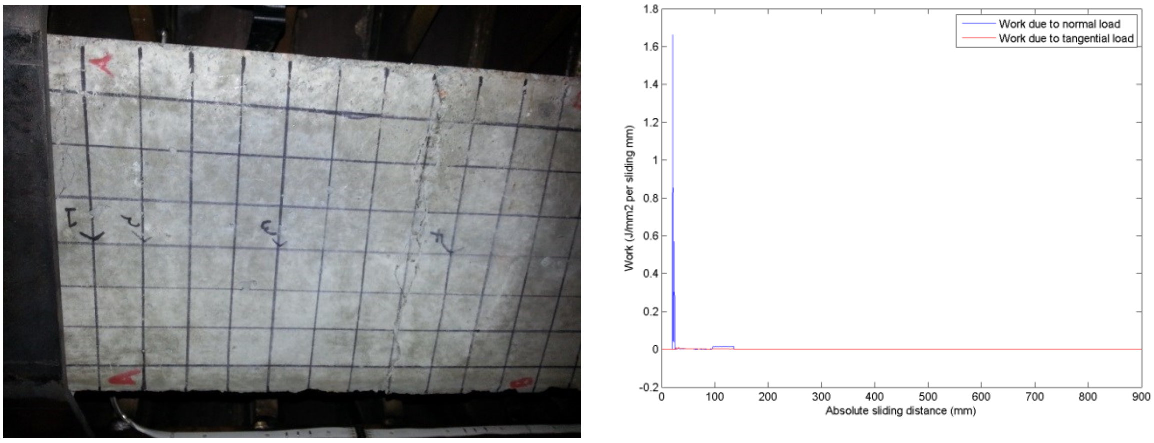

FIGURE 101 CONCRETE SURFACE AFTER TEST 3 - STARTING POINT

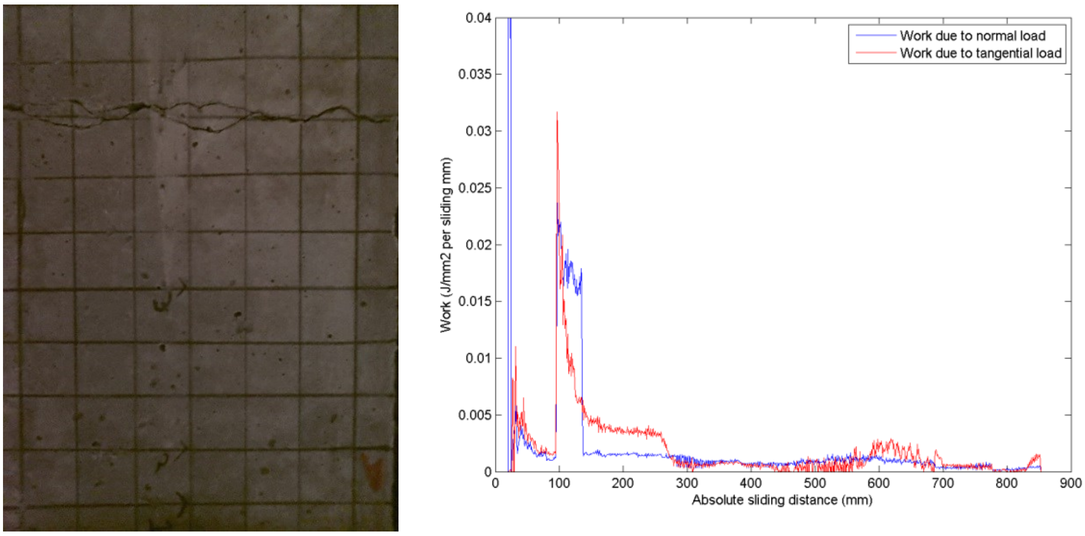

FIGURE 102 CONCRETE SURFACE AFTER TEST RUN 4 - STARTING POINT

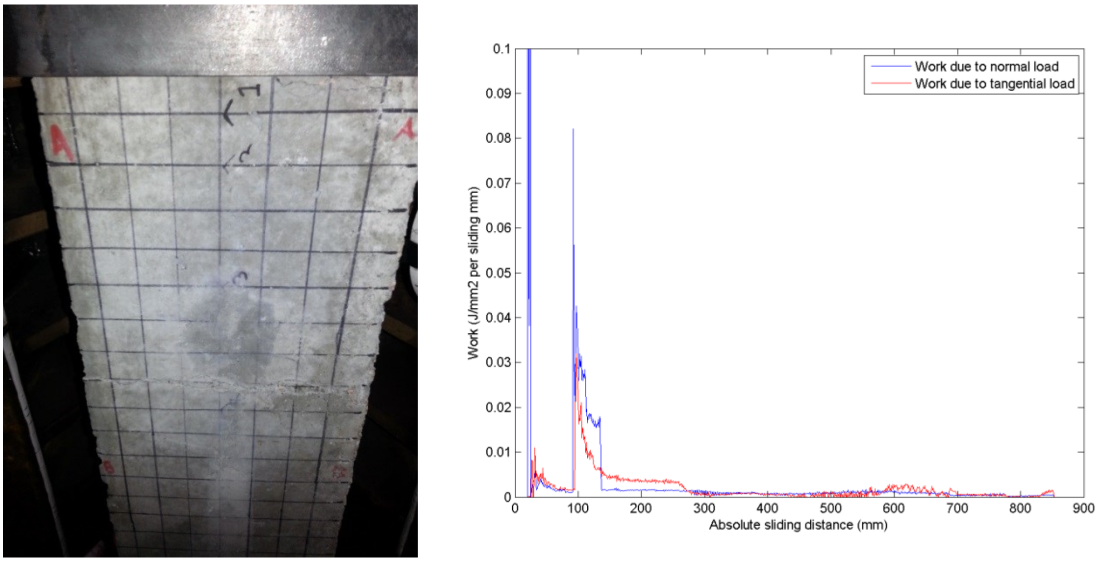

FIGURE 103 CONCRETE SURFACE AFTER TEST RUN 5 - STARTING POINT - SMOOTHENING OF SURFACE

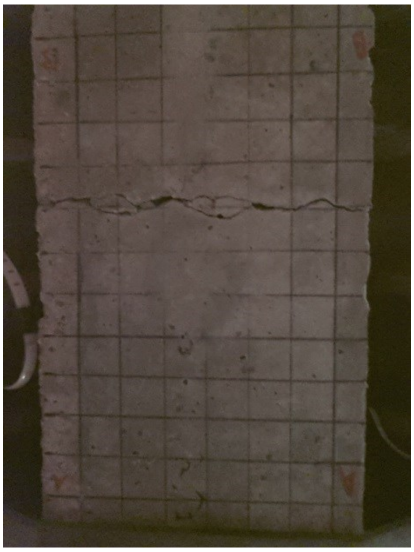
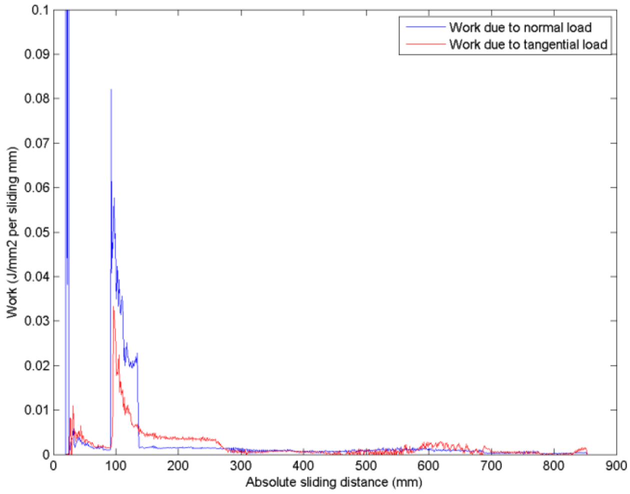

FIGURE 104 CONCRETE SURFACE AFTER TEST RUN 6 - STARTING POINT - SMOOTHENING OF SURFACE

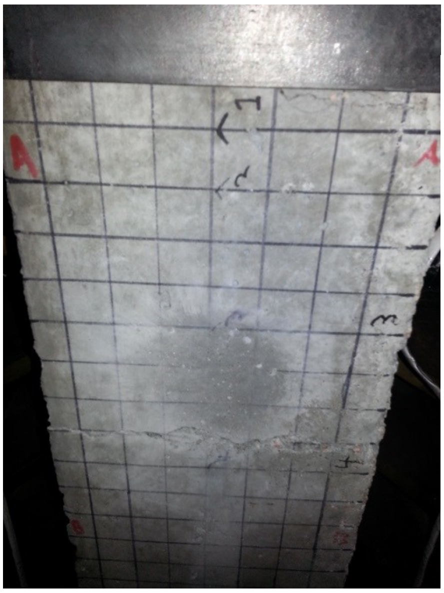
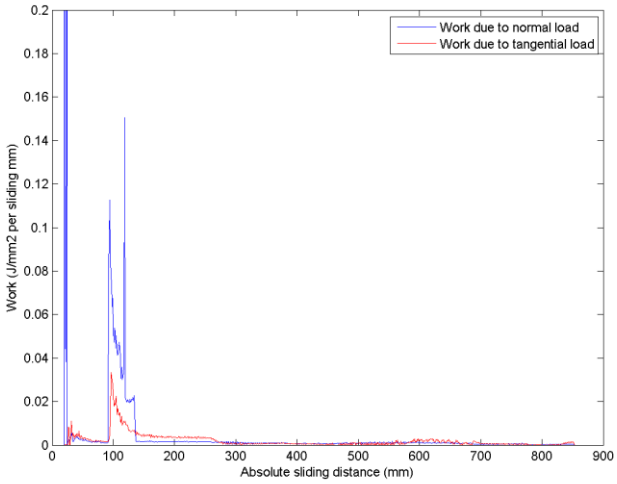

FIGURE 105 CONCRETE SURFACE AFTER TEST RUN 7 - STARTING POINT - SMOOTHENING OF SURFACE

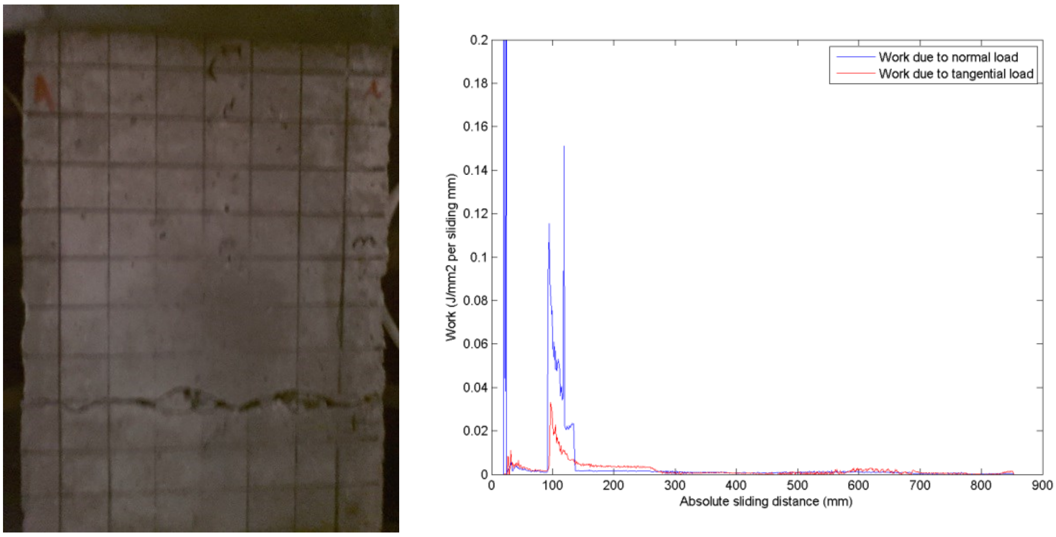

FIGURE 106 CONCRETE SURFACE AFTER TEST RUN 11 - STARTING POINT - SMOOTHENING OF SURFACE

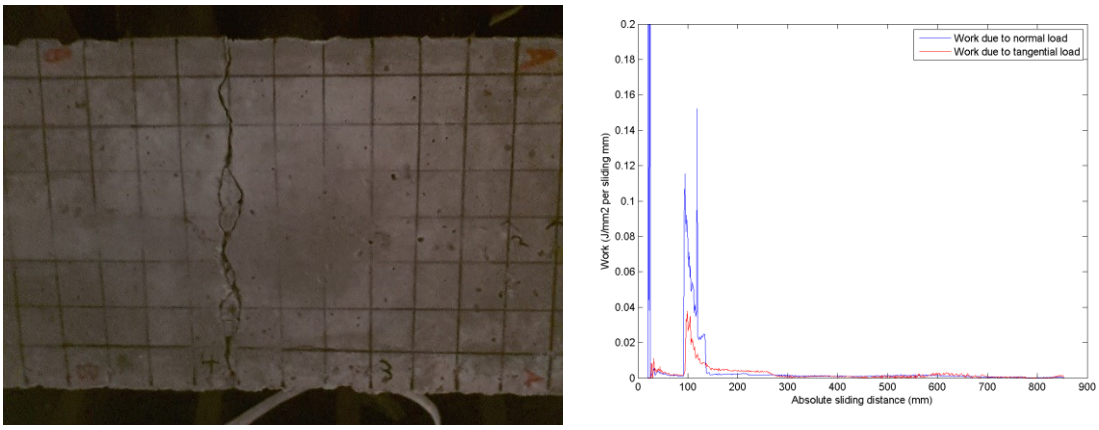

FIGURE 107 CONCRETE SURFACE AFTER TEST RUN 12 - STARTING POINT

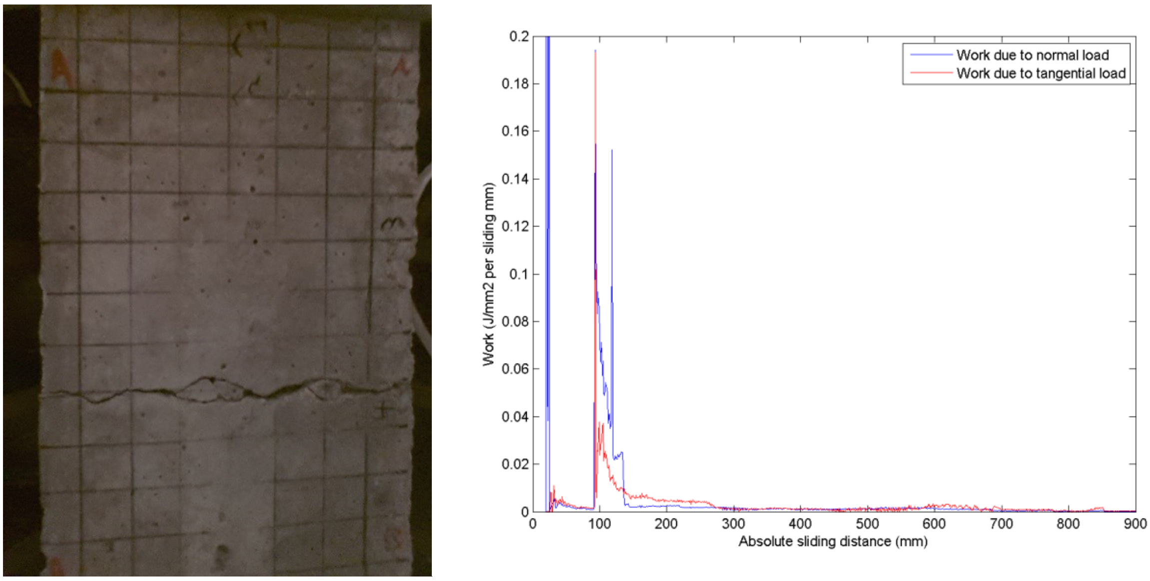

FIGURE 108 CONCRETE SURFACE AFTER TEST RUN 8 - STARTING POINT

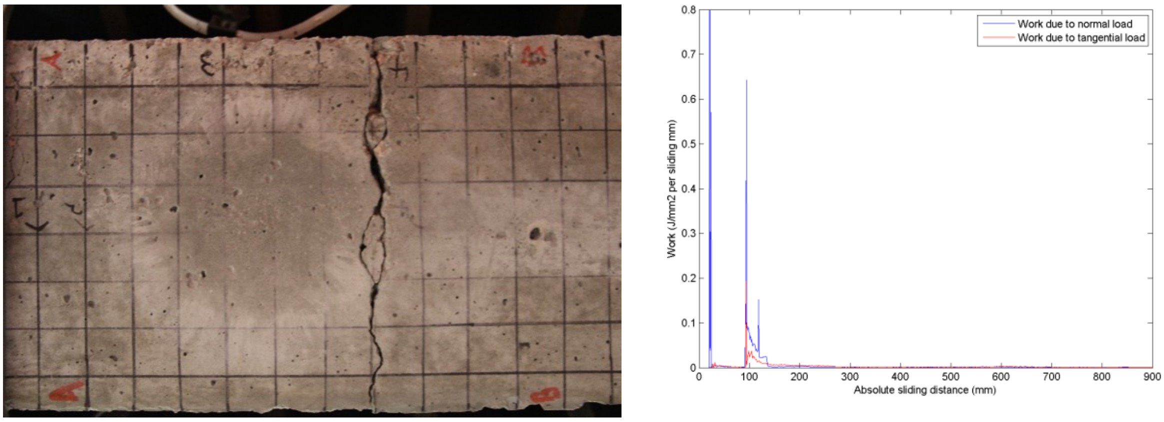

FIGURE 109 CONCRETE SURFACE AFTER TEST RUN 14 - STARTING POINT

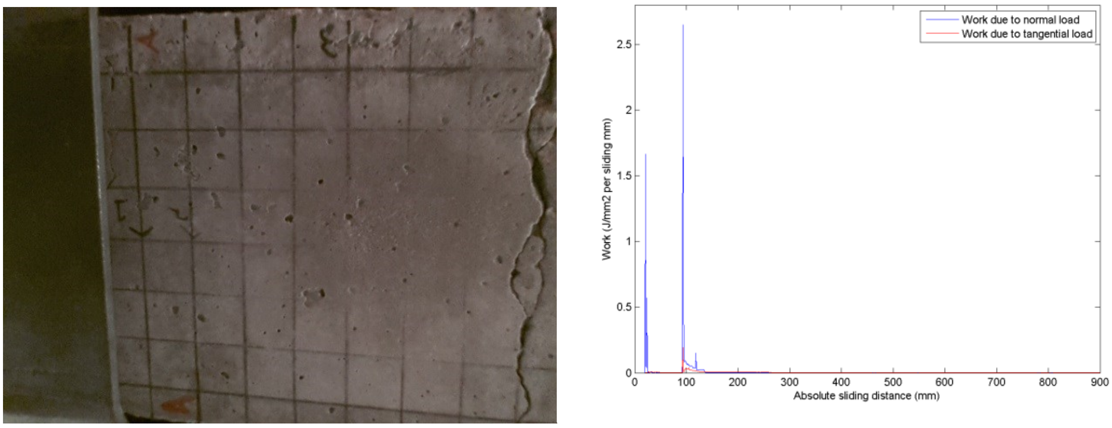

FIGURE 110 CONCRETE SURFACE AFTER TEST RUN 13 - STARTING POINT

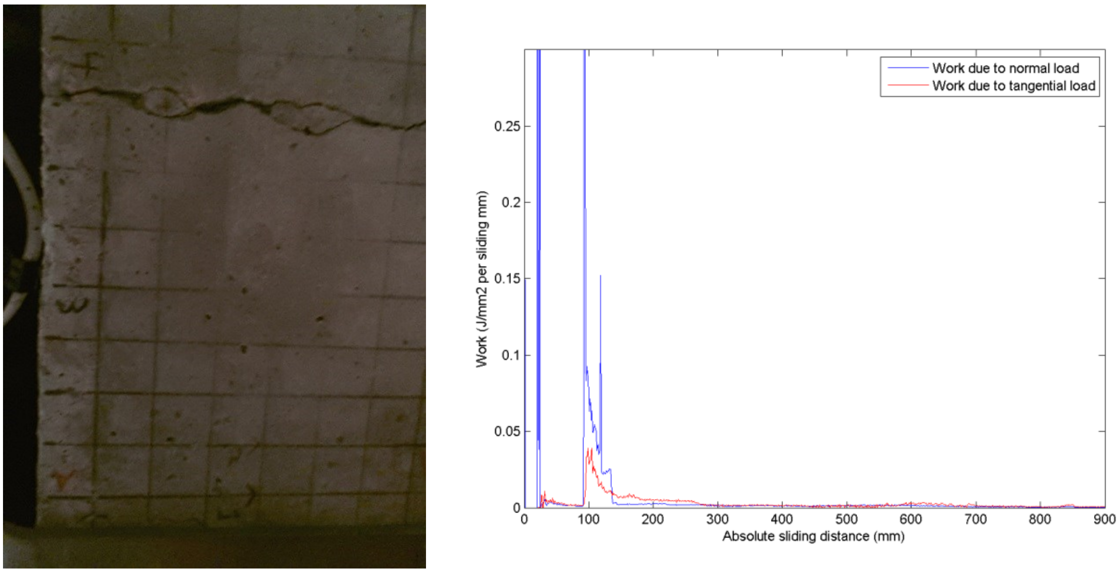

FIGURE 111 CONCRETE SURFACE AFTER TEST RUN 9A - STARTING POINT

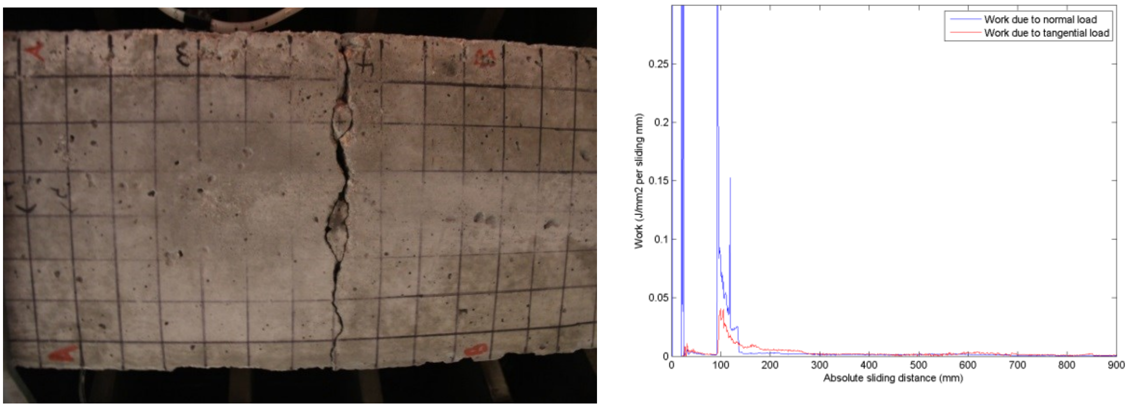

FIGURE 112 CONCRETE SURFACE AFTER TEST RUN 10A - STARTING POINT

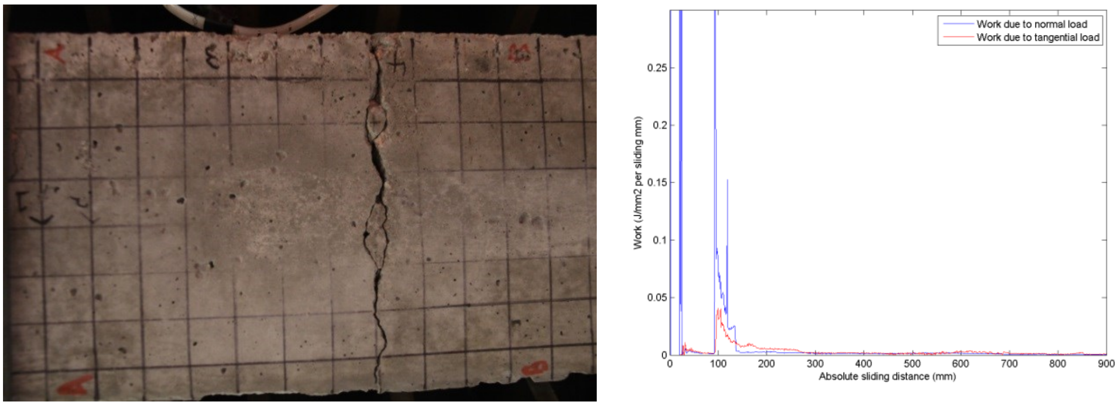

FIGURE 113 CONCRETE SURFACE AFTER TEST RUN 15 - STARTING POINT

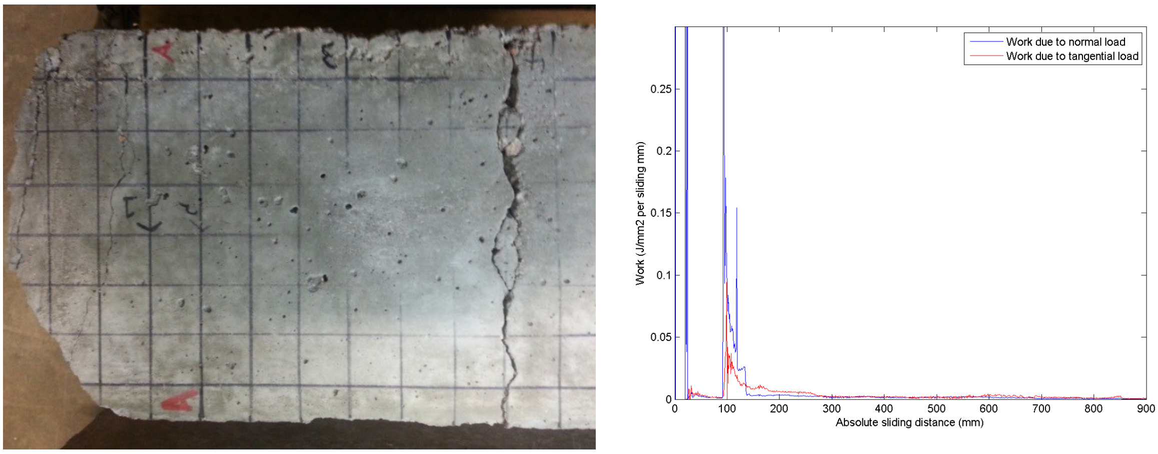

FIGURE 114 CONCRETE SURFACE AFTER TEST RUN 1B (POST TEST SEQUENCE) - STARTING POINT

APPENDIX V: ICE SAMPLE FABRICATION

The ice fabrication procedures are designed in the STePS[2] group. The ice sample (Figure 115) fabrication is a very delicate process. Freezing without precautions most likely leads to high internal stresses and fracturing as result. The second reason to control the process strictly is to keep a consistent ice quality among all samples in a test sequence. The fresh water ice grade is closest to natural iceberg grade, but generally even stronger. The analysis of the data always requires some consideration on the comparison with natural ice.

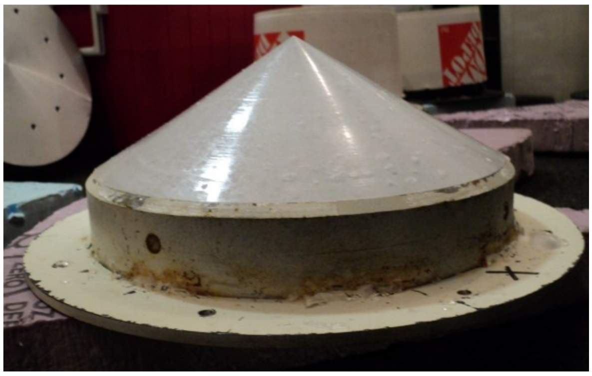

FIGURE 115 CONICAL ICE SAMPLE

The details of the fabrication process are shown in (Bruneau S. et al., 2011). The ice sample is made of sieved ice grains, from 4 – 10+ mm and treated water. The ice grain size distribution is consistent for all ice samples. The grain distribution is reasonable consistent over the experimental program due to careful sieving procedures. The grains and sieving is shown in Figure 116.

FIGURE 116 UNSIEVED GRAINS (LEFT), SIEVING (MIDDLE) AND POURING OF THE SAMPLE PRIOR TO FREEZING (RIGHT)

The water is distillated, deionized, de-aerated and chilled to approximately 0 degrees Celsius before mixing. After addition in the bucket (in the freezer) the ice is thoroughly shaken to compact them and topped off with treated water. Figure 117 shows the schematic of the unidirectional growth of ice samples. Note the isolation layer on of the bucket, similar isolation has also been folded around the bucket. The temperature gradients starts thus coldest from bottom to warmest on top. Water can thus always escape upwards and fracturing due to enclosure of higher density water most likely won't happen. In other words unidirectional growth reduces the risk on high internal stresses and cracks.

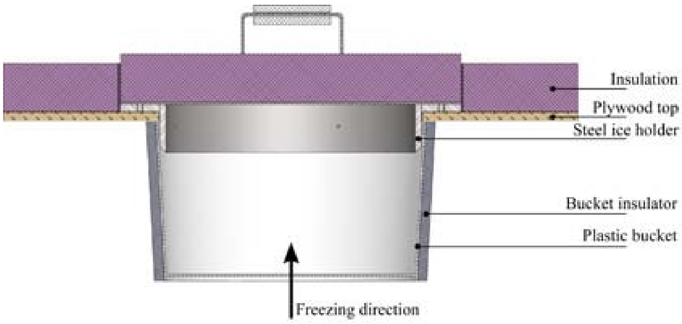

FIGURE 117 UNIDIRECTIONAL GROWTH OF ICE

The crystal structure depends the grain size variation and water treatment procedure as is shown in the polarization of ice slices (Figure 118).

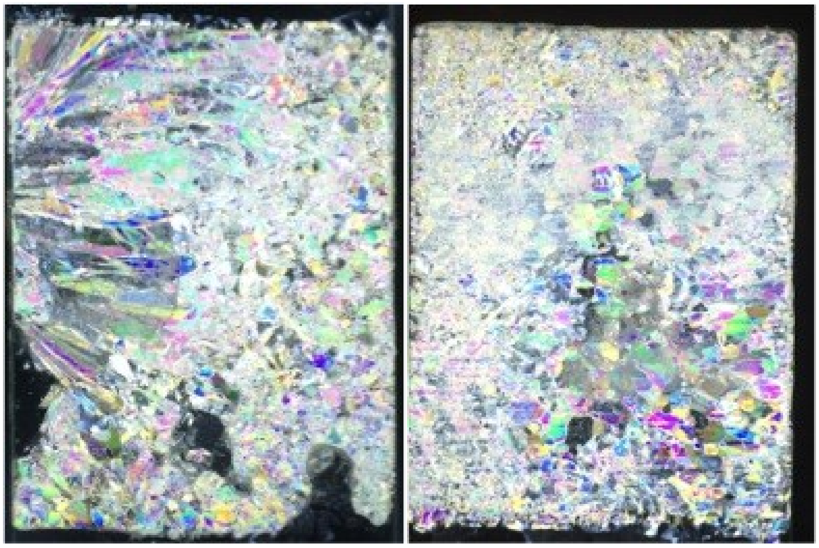

FIGURE 118 POLARIZED IMAGES OF ICE SLICES, THE VARIOUS COLOURS INDICATE THE ORIENTATION OF THE ICE CRYSTALS (C-AXIS). LEFT PHOTO SHOWS A 'DIRTY' ICE SLICE WITH JUST TAP WATER AND NO SIEVING. THE RIGHT PHOTO SHOWS AN ICE SLICE AFTER A CAREFUL FABRICATION PROCEDURE (PHOTOS TAKEN BY JAKE HARRIS)

Environmental temperature is an important parameter and preferably kept constant over time. Large temperature differences between ice and environments leads to temperature gradients in the ice and may cause fracturing. The temperature has been set onto -10 Celsius in two large cold rooms in the laboratory. Ice samples always get time to acclimatize and settle down thermal stresses over at least 24 hours after change of room temperature. Acclimatization procedures are crucial for an excellent ice grade.

The last step is shaping of the ice sample to a cone form (30 degree cone angle), this is done by an ice shaping apparatus as is shown in Figure 119. The apparatus uses a rotating plate and a blade to shape slowly the cone. Main concern is to minimize the internal stresses and the risk on cracks in the sample. In other words one should avoid to shape (or shave) too fast and introduce high torsional stresses. Also, the bottom of each ice sample require equalization of the surface in order to avoid local stresses during bolting onto the support structure of the bi-axial apparatus.

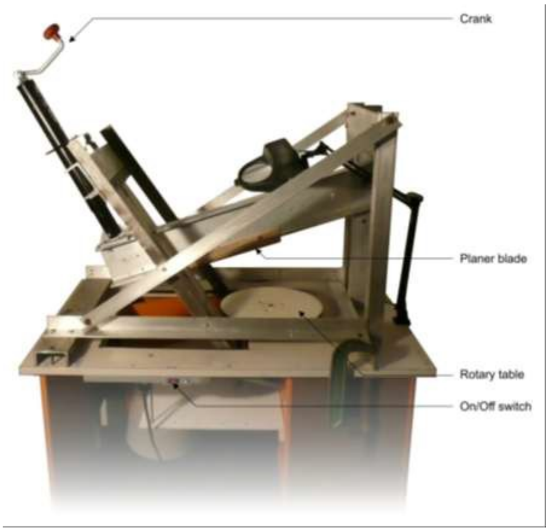

FIGURE 119 ICE CONE SHAPER

Appendix VI: Concrete samples

The carriage of the bi-axial apparatus determines the shape of the concrete beams. The dimensions have been chosen such that it matches the roof of the carriage and can be tensioned in the moving direction. The dimension are: 1495x195x207mm (LxWxH). The concrete sample must further resemble to a concrete grade in an offshore structure at an ice exposed environment. The concrete samples are a 70 MPa marine grade concrete and a reference grade 40 MPa concrete. The concrete samples include one reinforcement bar in order to prevent it falling apart concerning the safety and practicality.

Table 4 shows the mixture of the high and low performance concrete sample. The C60/70 mixture function as reference.

Table 4 Concrete mixtures

	Mix I (High perform.)	**Mix II (Low perform.)**	**PA-B C60/70 (Kvaerner)**
Component			
Air volume	3 – 5%	3 – 5%	4 – 6%
SCM	8%	0%	
Binder	500	300	
C/F	1.2	1.2	
W/B	0.33	0.5	0.37
Absorption	0.01	0.01	
Cement	(460)	(300)	(454)
Portland cement	460	300	-
Norcem standard cement	-	-	227
Norcem Anlegg cement	-	-	227
SF	40	0	5.5%
C.A (8 – 16 mm)	952.09	1070.39	879
F.A (0 – 8 mm)	793.41	891.99	783
W	165	150	
TW	182.46	169.62	

Mixture I contains silica fume and a lower w/c ratio which positively affects the compression strength (see section 2.5.3). Mixture II contains more aggregates than mixture I and according to literature (Itoh et al, 1988) aggregates have a good abrasion resistance compared to surface abrasion of cement. The low performance concrete beam (mixture II) enters the stable abrasion region faster than high performance concrete (mixture I).

The validation of compression strength requires to test three cylindrical validation samples. The mixture ingredients are shown in Figure 120

FIGURE 120 SOME INGREDIENTS MIXTURES - FINE AGGREGATES (UPPER LEFT), SILICA FUME (UPPER MIDDLE), COURSE AGGREGATES (UPPER RIGHT), CEMENT (LOWER LEFT), ALL PROPORTIONS READY (LOWER MIDDLE), WEIGHTING SCALE (LOWER RIGHT).

The determination of the amount per ingredient goes by weighing scale. The mixing itself occurs by help of a concrete mixer as is shown in Figure 121.

FIGURE 121 MIXER AND MIXING PROCESS

The addition of super plasticizer during mixing and make sure the mixture gets ready for pouring. Then, pouring. Important is to vibrate the concrete during pouring as it distributes the material more equally over the beam. A stick vibrates the mixture in the beam holder and a similar procedure for the validation samples as they were put at a vibration table.

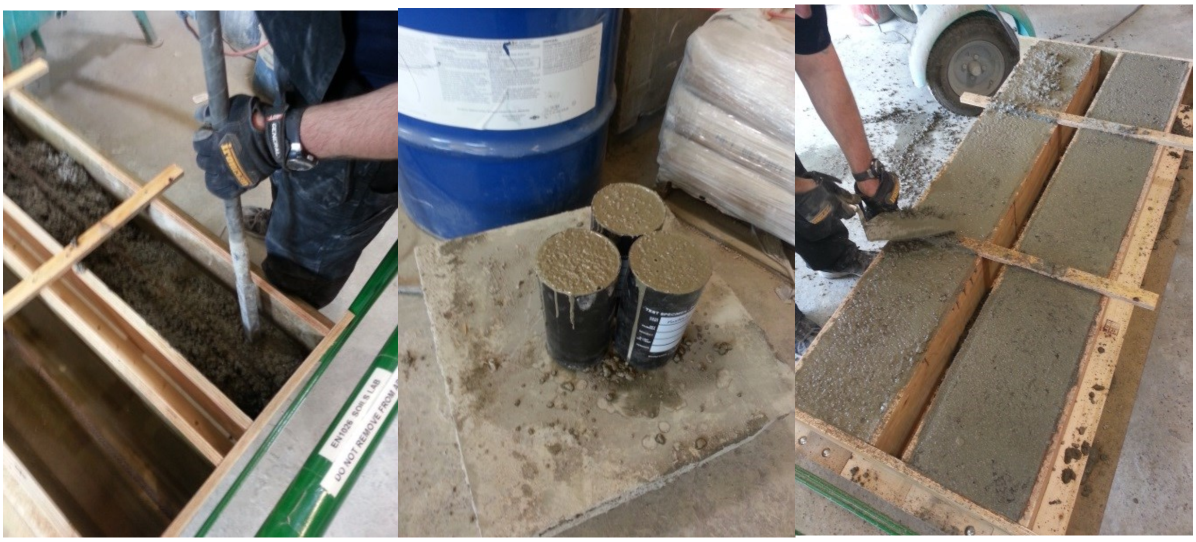

FIGURE 122 VIBRATION OF CONCRETE HIGH (LEFT). (70 MPA) AND LOW (40 MPA) PERFORMANCE BEAM AFTER POURING (RIGHT)

The two concrete samples got 28 days rest after pouring and have been checked regularly upon hardening. Three days before testing (at 25th day) the concrete beams have been taken from the holder and moved into the cold room at a room temperature of -10 ˚C. The acclimatization procedure took place for both concrete beams and cylindrical validation samples.

The validation tests have been conducted at a concrete temperature of -10 Celsius and varying age. Results of validation of the compression tests of each beam are shown in Table 5 and Table 6.

TABLE 5 VALIDATION TEST MIX I (HIGH PERFORMANCE)

Day	f_{cm} (MPa)
28	74.5
30	72.9
33	71.5
Average	73.0

TABLE 6 VALIDATION TEST MIX II (LOW PERFORMANCE)

Day	f_{cm} (MPa)
35	41.1
36	39.9
37	41.0
Average	40.7

Last, the concrete beams have been marked with a grid. The dimensions of each area in the grid is 25x25mm. A letter marks each 250 mm, from A to F. The purpose is to simplify linking visual data with data based upon displacement measurements of the system.

Appendix VII: Test schedule

The appendix shows the test sequence design. Tests 1 – 15 are on the high performance concrete sample. Tests 16 – 30 on the low performance concrete sample. The notes describes the notes during testing.

				Vnorm	Vsliding	Fnormal	Tprior	Note
				[mm/s]	*[mm/s]*	*[kN]*	*[s]*	
Date	**Time**	**Test i**	**Sub**					
11-jun	14:45	1	a	1	18	-	-	Three cracks in beam. Two cracks halfway propagated in the middle of the length of the beam without external normal load, perhaps due to a combination of bending and vibrations. The crack in the front is due to excessive normal load and sheared through the beam. The latter one is due to the wrong starting settings. Position along line of sliding of the tip: Crack 1: 446.6 mm (absolute) Crack 2: 773.7 mm (absolute) Crack 3: 176.4 mm (absolute) Horizontal start: 21,7 mm (absolute) Horizontal end: 1200 mm (absolute)
11-jun	16:45	2		0,1	0,05	-	-	Steel straps intervened during test by crushing partly into the concrete and partly into the steel Two go-pro's: Front and back {REJECT}
12-jun	11:45	3		0,1	0,1	-	-	Visual - Concrete surface intact, dust after test. No abrasion holes, mark lines washed away at higher distances. After test the surface pores seem te grow. After attempting to lower the ice cone. The entire cone and swing arm kept adhered to the concrete surface.
12-jun	14:15	4		0,1	1,8	-	-	Visual - Seems like a lot of holes with increasing size. A very low frequency stick/slip. High speed recording has overwritten the beginning. After 10s adhesion, lowering with 10 mm/s.
12-jun	16:30	5		1	0,5	-	-	Visual - Number of holes seems to increase and the size as well. Just cementary surface layer is affected so far. After 10s adhesion, lowering with 10 mm/s.
13-jun	12:10	6		1	1	-	-	Visual - Clear wear of surface (roughened) compared to the no touched zone, including a few large holes. Hole concentration does increase. Angle of carriage prior to test: 2.6. deg. After 10s adhesion, lowering with 10 mm/s.
13-jun	14:36	7		1	1	-	-	Visual - Prior to test concrete surface measurements around B and C of hole depths. Between 1 and 2 mm. Cracks in cone due to tighten it up with bolts. After 10s adhesion, lowering with 10 mm/s.
13-jun	15:45	11		10	10	-	-	Visual - Concrete surface wear seems to be different (less holes at the crushing interface and the retracting interface), more holes at the sliding interfaces. 2.6 deg starting angle swing arm. After 10s adhesion, lowering with 10 mm/s.
13-jun	16:25	12		10	180	-	-	Almost no adherence. Smooth slide. After 10s adhesion, lowering with 10 mm/s.
16-jun	11:30	8		-	1,8 / FC / other	10	15	Visual - Suspicion of growing holes on the surface. Verification by photos. High speed: 71 fps. Indentation of sample prior to testing. Second test at 5 mm/s and no cleaned concrete surface. Third test 3.6 mm/s and no cleaned concrete surface (7.5 P gain, I 0.5 gain, D and others are 0 gain). Fourth test 5 mm/s and no cleaned concrete surface (Changing control parameters). 5 run. 6 th run force contr. 7th run
16-jun	14:50	14		1	-	-	-	Visual - Several holes up to 2.5 mm. Beam seems to be worn off halfway.
16-jun	16:30	13		0,1	-	-	-	At the crushing interface of the initial position of only crushing differing surface textures have been identified. Directly in the center several small aggregates are noticed and more to the outer crushing interface there has been radial tangential trails. Angle of swing arm 2.7 deg.
17-jun	10:30	9	a	-	1,8	10	45	Glinstering surface behind cone after thorough cleaning of surface (may be silica)
17-jun	12:30	9	b	-	180	10	45	Second run of ice cone, with cleaned concrete surface. Visual - Concentrations of silica glinstering on start position of ice cone and at the end position of ice cone (~991 mm). Other silica is showing up on the track from beginning to end, but less wide and spread out. Small agregates starts to reveal themselves as well.

17-jun	14:20	10	a	-	1,8	10	90	Angle of swing arm 2.6 deg
17-jun	14:50	10	b	-	FC	10	90	Hor. Force controlled with 5 kN at hor. Load sensor 1. Angle of swing arm 1.8 deg
17-jun	09:45	15		10	-	-	-	Visual with Calipers - Measured at initial crushing surface of the concrete hole depths of up to 3.4 mm.
17-jun	15:35	1	b	1	18	-	-	Visual - Halfway the beam there reveals some small agregates on the surface. Angle of swing arm: 2.7 deg
18-jun	14:15	16	a	1	18	-	-	Heavy stick slip already on 18 mm/s. Could be influenced by a too little warming up. Angle of swing arm 2.6 deg. No cracks or inital surface damage observed. No vertical force data due to unplugged wire. After 10s adhesion, lowering with 10 mm/s.
18-jun	16:00	19		0,1	1,8	-		Angle of swing arm 2.8 deg, No vertical force data due to unplugged wire. After 10s adhesion, lowering with 10 mm/s.
19-jun	10:00	22	a	-	1,8	10	15	Visual - The sliding trail seems to smooth the concrete surface. No bouncing back as we saw with the high performance beam
19-jun	11:00	22	b	-	180	10	15	The end of the test after stopping, there was a slippage (probably in position). Hearing shifting/fluctuating sound, similar to stick/slip sound
19-jun	14:30	30		10	-	-	-	Visual - Hole sizes on track seems to increase in radius.
19-jun	15:08	27		10	180	-	-	Visual - Concrete surface on initial position due to previous crushing test seems to feel porous/rougher than original concrete surface. Two movies of one go-pro seems to not work properly. After 10s adhesion, lowering with 10 mm/s.
19-jun	16:00	28		0,1	-	-	-	Pieces of concrete fall off.
20-jun	11:00	23	a	-	180	10	45	Should have been 1.8 mm/s, but due to setting issue not.
20-jun	12:30	23	b	1	18	-	-	Truncated cone due to previous normal load test. Defrost mode. Higher frequency vibration on the later part in the test. Two movies from one go-pro, no pics of post concrete surface (apparantly it went well without memory card in slr). Film crew recording. After 10s adhesion, lowering with 10 mm/s.
20-jun	13:20	29		1	-	-	-	Visual - Small hole forming in the middle of the beam. Hole lips seems to headed towards the sliding direction. The hole concentration of smaller holes seems to increase significantly.
20-jun	14:45	24	a	-	1,8	10	90	On the initial position the concrete surface starts to glinster (suspicion of the fine grains becoming visible). High speed 60 fps. 2 go pros instead of 3
20-jun	15:30	24	b	-	FC	10	90	Visual - Holes seems to increase in size halfway the beam and small holes appears. High speed 70 fps. Hor. Force controlled 5 kN on hor load cell 1 (10 kN/s loading rate).
20-jun	16:05	16	b	1	18	-	-	No high speed footage due to sideways thermal imagery. After 10s adhesion, lowering with 10 mm/s.

APPENDIX VIII: PUBLICATION (POAC'15)

Manuscript is under review (Half feb-15).

LABORATORY EXAMINATION OF ICE LOADS AND EFFECTS ON CONCRETE SURFACES FROM BI-AXIAL COLLISION AND ADHESION EVENTS

Jochen Tijsen [1], Steve Bruneau and Bruce Colbourne [2]
[1]Delft University of Technology, Netherlands
[2] Memorial University Newfoundland, Canada

ABSTRACT
Concrete structures in marine environments subject to sea ice interaction are at risk of erosion and damage. Industry is interested in characterizing the ice abrasion phenomenon so that abrasion risk can be managed. The experiments conducted in this work have an exploratory character in order to identify the abrasion phenomenon and qualitatively observe the corresponding processes. The tests are a simulation of micro scale ice-structure interaction and involve the translation of concrete samples while subject to lateral impingement of conical ice samples. Loads in both axes are measured so that tangential and normal force relationship can be examined while the ice samples are catastrophically crushed. The paper divides the interaction into abrasive loading regions and loading orders intentionally to facilitate analysis of the abrasion process. The wear of the concrete surface is described using visual observation and surface feature measurements Concrete of varying mixtures has been examined and the effects on the concrete surfaces from repeated static ice-bonding and bond-breakage is analysed.

INTRODUCTION
Ice abrasion is known to induce wear on concrete offshore structures in the cold environment. The outer layers of concrete can be abraded or protection layers can be torn off by hundreds of kilometres of ice movement each year in sub- and high Arctic regions. Reinforcement and inner bearing strength of the concrete structure are thus under threat. At present, the severity of the problem is not well understood, although some studies have been conducted (Janson J., 1989; Huovinen S., 1990). It is worthwhile to achieve an improved fundamental understanding of the elements of the ice-concrete abrasion process, on the one hand abrasive ice loading and the other hand concrete abrasion resistance. The paper describes an experimental approach and touches upon the knowledge gaps remaining.

EXPLORATORY EXPERIMENT
Ice-structure simulation
The experiment is an exploratory 2D simulation of an ice-structure interaction. The lab scale apparatus provides a simple and controllable analog of the full scale interaction as shown in Figure 1. The entire apparatus is located in a large coldroom at constant ambient temperature of -10 °C.

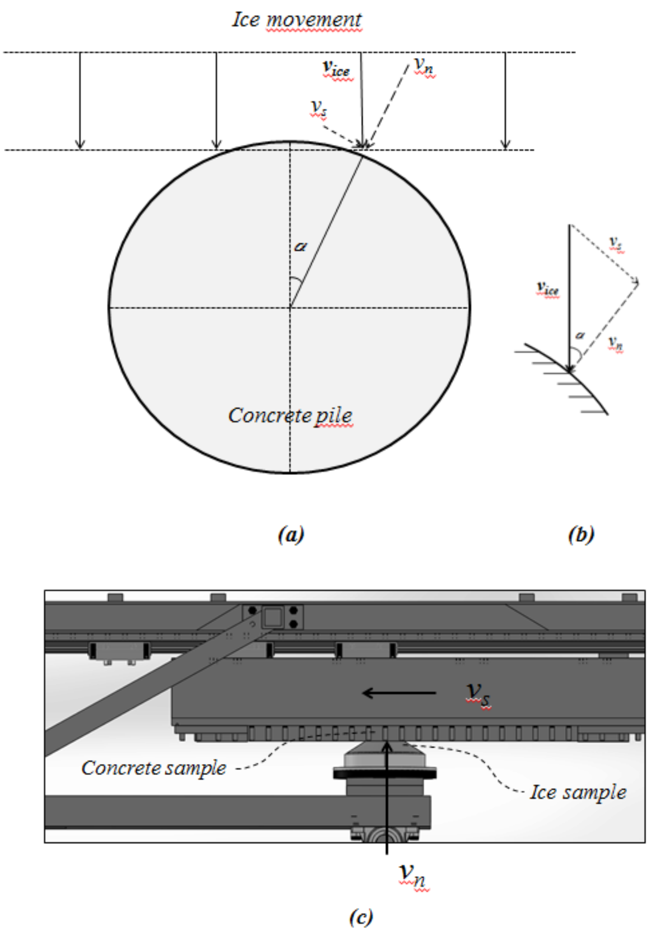

Figure 1 Ice-structure interaction (a) and (b), simulation in the laboratory (c).Figure (a) shows an incoming sheet of level ice with ice velocity (v_{ice}) into a circular concrete pile at a point of contact. (b) shows an schematization on local level. The system has two degrees of freedom: ice velocity (v_{ice}) and angle of contact (α) , together define the normal velocity (v_n) and sliding velocity (v_s). Figure (c) shows the impingement of the conical ice sample (v_n) and simultaneous sliding of the concrete sample (v_s).

The input for the test settings consist of a normal and sliding velocity. The definition of the normal velocity (v_n) is:

$$v_n = v_{ice}\cos(a) \tag{1}$$

The definition of the sliding velocity (v_s) is:

$$v_s = v_{ice}\sin(a) \tag{2}$$

Each individual test run involves impinging a 30 degree conical ice sample on concrete material and in some tests simultaneously sliding the concrete. The description of the ice fabrication procedure is shown in (Bruneau S. et al., 2012). The experiment involves two concrete samples, one high performance and one low performance mixture. The experiment consists of two concrete samples of 1495x195x207 mm. An high performance and a low performance concrete grade according to the concrete mixtures in Table 1. The high performance (HP) concrete sample consists of a marine concrete grade ($\sigma_c \approx 70$ MPa). Silica fume is part of the HP mixture and result into a larger matrix strength. The pore spaces fills up with the very fine silica fume particles and increases the cohesion of the concrete. The finish of the silica fume causes a very smooth surface. The low performance (LP) concrete sample is a lower concrete grade ($\sigma_c \approx 40$ MPa). The surface of the LP concrete was rougher than that of the HP concrete despite the same level of formwork being used to fabricate the concrete grades. The intention of the LP concrete sample is to make it abrasion sensitive and use the output data as reference concrete.

Table 1 Concrete mixtures

	HP Concrete Sample	**LP Concrete Sample**
Air volume	3 – 5%	3 – 5%
SCM	8%	0%
Binder	500	300
C/F	1.2	1.2
W/B	0.33	0.5
Absorption	0.01	0.01
Portland cement	460	300
SF	40	0
C.A (8 – 16 mm)	952.09	1070.39
F.A (0 – 8 mm)	793.41	891.99
W	165	150
TW	182.46	169.62

The test sequence for each concrete sample involves solely crushing (v_{ice} = 0.1; 1.0 and 10.0 mm/s), solely sliding (v_{ice} = 1.8 and 180.0 mm/s / normal force F_n = 10 kN) and simultaneous crushing and sliding for three chosen angles of contact.

Data logging

Load cells log forces and displacement sensors log the displacements in the normal and sliding directions. A SLR camera, three video cameras (front, side and back) and a High-speed camera (side view / 50 – 150 FPS) record the concrete surface and ice samples during testing. Also, a thermal image record behind the interaction gives the signature of heat traces after interaction on the concrete surface.

There is currently no standard definition or measure of concrete abrasion due to ice action. This paper defines abrasion as concrete surface texture change due to mass loss. This study explores four ways of quantification of concrete abrasion:

- Visual data by video and photo camera
- Surface roughness measurement device (up to 160 µm)
- Two identical test runs before and after a test sequence. Identify potential change of tangential forces due to the change of surface texture.
- Calliper (hole characterization)

RESULTS AND DISCUSSION

General: Point of Contact

The test sequences align with the idea of three typical adhesive regions as shown in Figure 2, because three typical abrasive ice loading regimes occur over varying angles of contact (α).

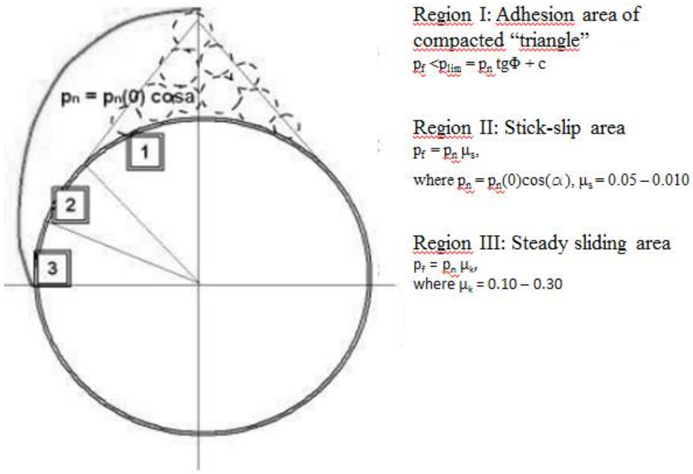

Figure 2 Contact regions with different abrasion mechanisms according to (Jacobsen et al., 2012)

The abrasion mechanisms globally consist of three categories as is shown in Figure 2: Solely crushing ($\alpha \approx 0^{\circ}$), crushing and sliding ($0^{\circ} < \alpha < 90^{\circ}$) and solely sliding ($\alpha \approx 90^{\circ}$) . These regions correspond to the three following modes of interaction:

- Region I 'Crushing and extrusion'
- Region II 'Stick-slip'
- Region III 'Slip'

The type of loading gets even more interesting on micro scale level, because each loading type may contribute in its own unique manner to concrete abrasion. (Itoh Y. et al., 1988; Huovinen S., 1990; Bekker A. et al., 2010; Sistonen E. and Vesikari E., 2008; Jacobsen et al., 2012) and a few others already identifies 9 abrasive loading types, all contributing to abrasion according to one of the following orders:

- Primary order of loading: Direct exceedance of abrasion strength by loading and physical deterioration of material surface occurs: Shear stress due to tangential forces (friction and adhesion).
- Secondary order of loading: Reduction of abrasion resistance and thus increasing the probability of physical deterioration of material surface: Stick-slip cycles, indentation pore pressure, freeze-thawing cycles, concrete shrinkage, thermal gradients, chloride migration, dissolving of lime.

Region I 'Crushing and extrusion':

The location associated with Region I abrasion is around the structural face perpendicular to the ice movement and involves most critical ice abrasion on offshore structures (Janson J., 1989; Hara F. et al., 1995). The largest local compression (Bekker A. et al., 2003) and shear stresses occur in this region and result into exceedance of the abrasion resistance of the concrete. The local compression stress under brittle ice failure may reach, for very short periods, up to 60 MPa for multiyear sea ice (Masterson D. et al., 1993) or in small-scale laboratory conditions over 100 MPa at areas of a few mm^2 (Mackey T. et al., 2007) and corresponding friction processes can thus induce large shear stresses. The observation of eruption of spalls during fast tests *(v_n > 1.0 mm/s)* resembles an extrusive processes under extreme compression stress (Jordaan I., 2001).

The abrasive ice loading quantity in this paper is work (or energy), because (Itoh Y. et al., 1988) shows, through empirical data, proportionality between concrete abrasion on the one hand and normal pressure and ice sliding distance on the other hand. Work includes force and displacement through a proportional relation and is thus able to indicate a global abrasive load. Also, one is able to determine the cumulative loading and compare it to the abrasion depth. The formula for work in normal direction is:

$$W_n = \int_0^x F_n(x)\,dx \approx \sum_i^{n-1}(x_{i+1} - x_i)\left(\frac{F_{n,i+1}+F_{n,i}}{2}\right) \quad (3)$$

Where x is the indentation (mm), F_n the normal force (kN) and i the index number of a chosen sample. The discrete approximation of the continuous integral is the trapezoidal integration rule. The formula for work in the sliding direction is:

$$W_s = \int_0^x F_s(x)\,dx \approx \sum_i^{n-1}(z_{i+1} - z_i)\left(\frac{F_{s,i+1}+F_{s,i}}{2}\right) \quad (4)$$

Where z is the sliding distance (mm), F_s the tangential force (kN) and i the index number of a chosen sample. The work is spread over the contact area such that it normalizes the loading. The unit of the abrasive loading is J/mm^2 per mm absolute sliding distance, where absolute means the apparatus' reference system. Figure 3 shows the change of surface texture and loading data shows the change of cumulative abrasive loading from tests that correspond to Region I loading. In these cases the ice was crushed against the concrete sample without lateral sliding.The change in cumulative loading and abrasion reveals aspects of the abrasion process.

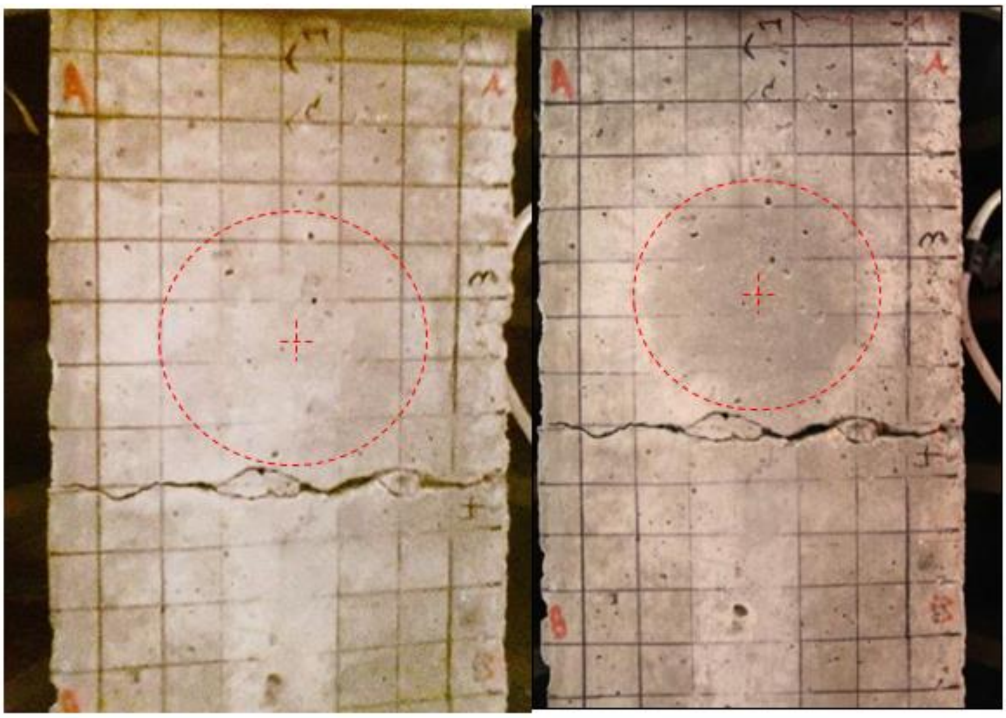

Figure 3 Surface of high performance concrete sample before (left) and after (right) slow crushing test (v_{ice} = 0.1 mm/s / $\alpha \approx 0^{\circ}$). The abrasive loading over only one test run is about 1.95 J/mm^2 normal loading at the reference cross. The loading correspond to a nominal compression pressure of about 20 MPa. The concrete after the test shows scour like traces radial on the concrete surface and also involves exposure of small aggregates.

Region II 'Stick-slip'

The stick-slip region doesn't abrade the concrete in an early stage, but will reduce the concrete abrasion resistance over long time scales. Figure 4 shows a stick-slip cycle and indicates static friction up to half (5 kN) the normal force (10 kN). The stick-slip region can abrade the concrete surface due to local fatigue issues (Huovinen S., 1990). Stick-slip loading falls thus under the secondary order of abrasive loading, because it doesn't exceed the nominal surface abrasion resistance but does tend to reduce it over time.

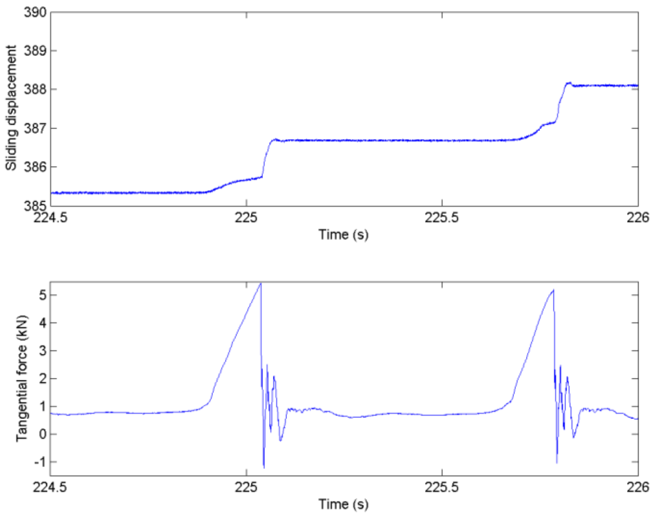

Figure 4 Stick-slip cycle for 1.8 mm/s sliding rate under 10 kN normal load – High performance concrete sample

Figure 5 shows that the stick-slip character depends on ice velocity and the stick-slip region thus reduces with increasing ice velocity. Slow ice velocities v_{ice} are of increasing importance for the local fatigue strength of the concrete surface.

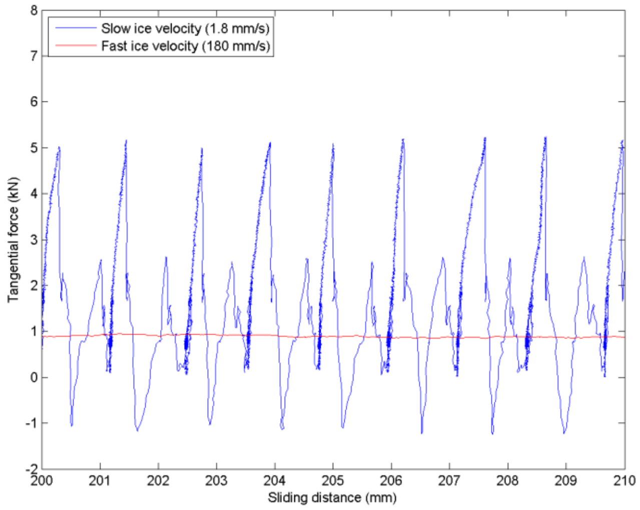

Figure 5 Tangential force for slow (v_s=1.8 mm/s) and fast sliding (v_s=180 mm/s) under 10 kN normal load – High performance concrete sample. The fast ice velocity is a very smooth sliding process in comparison with the slow ice velocity. The scatter of data points originates from the overshoot of the position in sliding direction. Figure 4 correspond with the slow ice velocity and illustrates the stick-slip cycle over time instead.

The stick-slip cycle period not only depends on the ice velocity (v_{ice}) and angle of contact (α), but also on the concrete type. Note the stick-slip period also depends on the stiffness of the apparatus, but is the same for all tests. Figure 6 and Figure 7 are FFTs of the tangential loading in identical tests, but the two figures compare high performance and low performance concrete. The peak frequency and active frequencies vary (HP Concrete grade: f_{peak}≈0.7 Hz / LP Concrete grade: f_{peak}≈0.78 – 0.85 Hz), the LP concrete involve higher active frequencies than the HP concrete and indicate a variation in adhesive properties of the two concrete types. The (smooth) high performance concrete sample is more sensitive (lower active frequencies) for adhesion than for the (rough) low performance concrete sample. Adhesive bonding depends mainly on real contact area (Saeki H., 2010) and increases with increasing roughness. The adhesive forces seem to be larger on a smooth surface than rough surface over a test run, corresponding to observations on confinement in (Dragt R., 2013) for varying roughness' in ice-steel crushing tests. Ice seems to adhere between two asperities on the rougher surface and thus reduce the real contact area.

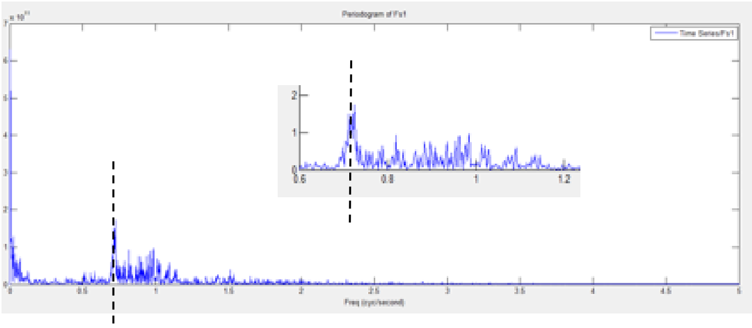

Figure 6 High performance concrete sample – FFT of tangential force under slow ice velocity (v_{ice}= 1.8 mm/s) at α=86.6 degrees, from 0 – 5 Hz. The peak frequency concentrates about 0.7 Hz.

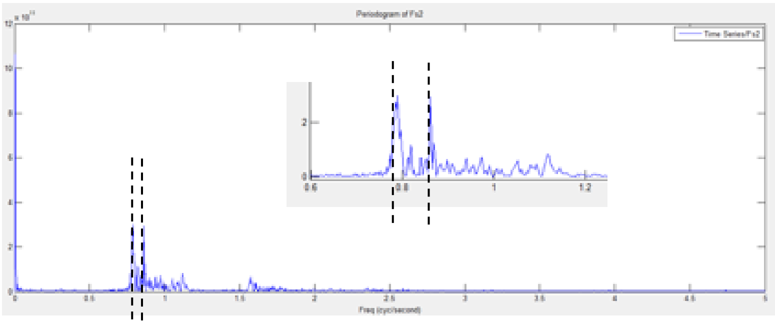

Figure 7 Low performance concrete sample – FFT of tangential force under slow ice velocity (v_{ice}=1.8 mm/s) at α=86.6 degrees, from 0 – 5 Hz. The peak frequency concentrates at about 0.78 – 0.85 Hz.

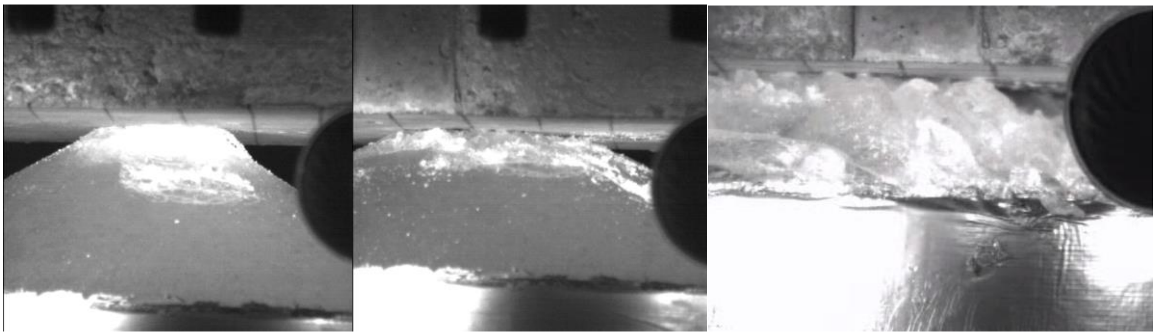

Figure 8 High speed imagery at varying contact areas, the screenshots show beginning test 1.5 Hz (left photo), halfway test 0.9 Hz (middle photo) and at the end of the test 1.1 Hz (right photo).

Figure 8 shows that the stick-slip period depends on fracture and thus on real contact area. High frequency motions correspond with low static binding and low frequency motions with high static binding. The ice sample in the right photo shows reduced real contact area due to fracture and spalling, and the stick-slip frequency is thus increased.

Region III 'Slip'

The slip region doesn't critically affect the abrasion risk of the concrete significantly. Low stresses and large sliding velocities characterize the region barely leaving any abrasion traces behind. However if we consider that the first two regions should not govern the design abrasion loading, then ice sliding can cause abrasion over long sliding distances as is shown in (Itoh Y. et al., 1988) and (Bekker A. et al., 2011). The lower stress cases do require sufficient localized compression stress to induce abrading effects, for example due to enclosed ice spalls and rubble at the free surfaces between ice sheet and structure. The slip region only has to overcome the dynamic ice-concrete friction during large ice velocities and the tangential force consists of a combination of wet and dry friction. The slip region changes into a stick-slip region for lower ice velocities.

Observations of ice abrasion

Figure 9 Concrete abrasion on the high performance concrete sample (left) and low performance concrete sample (right) over a test sequence. The location is at the starting point of the test runs as shown with the cross in Figure 3. The loading on the high performance concrete sample is much higher than for the low performance concrete sample. The grid lines (20 mm distance) provide reference.

Figure 9 shows initial traces of abrasion at the start location (z_{ab} = *94 mm*) over a test with crushing and sliding that exhibited stick-slip behaviour. The abrasion damage is minor in comparison to field studies (Janson J., 1988). The abrasion loading was over $W_n = 2.6$ J/mm^2 and $W_s = 0.2$ J/mm^2 for the HP concrete and less for the low performance concrete. The high performance concrete sample shows less abrasion than the low performance concrete sample, the silica fume particles seem to increase the matrix strength and improve the abrasion resistance. Also, the surface reveals smaller aggregates already exposed, indicating the cement layer is wearing. The concrete surface evolves over longer ice sliding distances and exposes, in a later stage, larger diameter aggregates (Itoh Y. et al., 1988; Huovinen S., 1990). Thus, the cement properties seem to govern the initial abrasion rate in Figure 9.

The tangential force for two identical sequential tests didn't show any significant variation. The surface texture measurement device could only measure a maximum surface elevation of 160 μm, thus we can state the local abrasion of the high performance concrete sample is larger than 160 μm. The calliper helps to describe the surface visually, with more details in (Tijsen J., 2015).

Interface layer

The interface layer is the layer between the undamaged ice and concrete and involves a mixture of crushed ice and concrete particles. The crushed ice particles originate from flaking ice during sliding due to micro shearing. The concrete particles originate from flaking concrete due to microshearing, but also due to adhesion with the ice. The mass flow on the interface under high pressure exhibits a hydrodynamic character and under lower pressures shows a more solid granular character (Jordaan I., 2001). The liquefaction of ice is due to a combination of pressure and frictional heat. The ice surface layer will immediately absorb frictional heat for melting a very thin surface sub-layer and during refreezing release the latent heat. Figure 10 shows enclosure of concrete particles after recrystallization of the ice surface (shown by the fine crystalline ice structure) and Figure 11 shows evidence of heat traces. Also, Figure 10 shows the ice roughness increases during interaction due to the enclosure of concrete particles, and thus the abrasion rate increases in a similar manner as in (Itoh Y. et al., 1988) due to the effect of sand particle content in the ice.

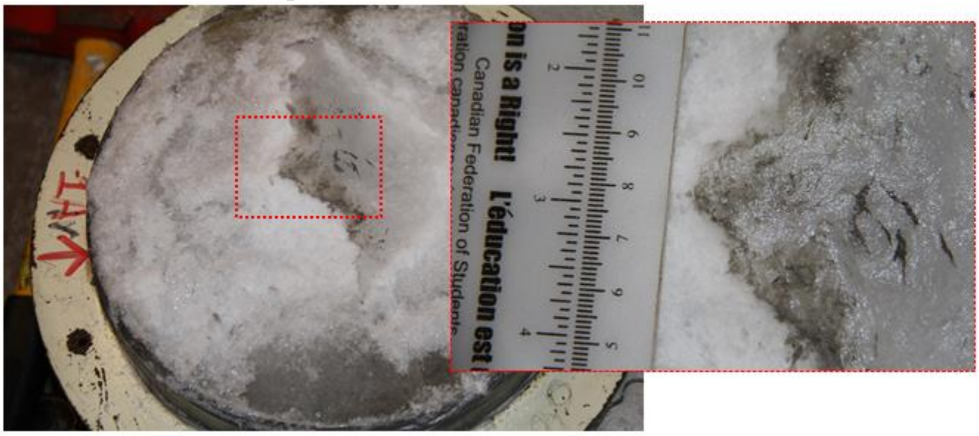

Figure 10 Concrete dust and particles enclosure under recrystallized ice after test 1a (v_n = 1.0 mm/s / v_s = 18.0 mm/s) at the high performance concrete sample

Fast moving ice generates frictional heat as is shown in (Tijsen J. et al., 2013). With increasing melting of ice, hydrodynamic characteristics at the contact dominate over asperity contact in governing the characteristics of the interface layer and thus abrasion rates. Lower temperatures imply less melting and increasing dry friction over wet friction. The ambient temperature during testing was -10 (+-1.5) $^\circ$C and shortly after interaction temperature increments of +10.3 $^\circ$C were measured as shown in Figure 11. The heat traces indicate very local interaction and possible liquefaction of the ice interface material.

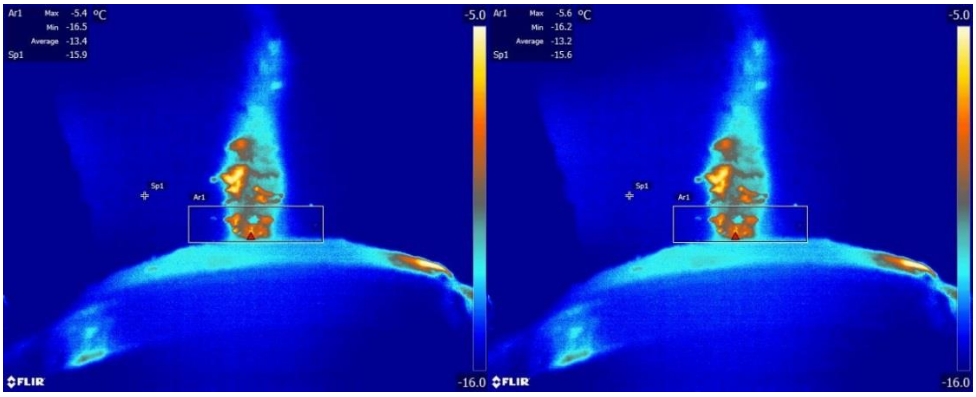

Figure 11 Thermal image of a crushing and grinding test (at α=86.6 deg and ice velocity 18 mm/s) concrete (emittance = 0.92 – left picture) and for ice (emittance = 0.96 – right picture) temperature data

Temperature increments on the interface will also reduce the adhesive bonding (Saeki H., 2010) and thus tend to increase the stick-slip frequency. Large local temperature gradients due to heat generation can also introduce thermal stresses in the concrete surface. Thermal stresses reduce the strength of the concrete surface and will increase the probability on local abrasion.

CONCLUSIONS

The experimental set-up is suitable for simulation of two-dimensional ice-structure interaction on and examination of local material processes like ice abrasion. The most important advantage is the ability to simulate interaction at a predetermined Point of Contact dependent on angle (α). The most important drawback is the limitation of not being able to easily achieve large ice sliding distances.

Observations from the preliminary laboratory tests discussed here indicate that:

- The type of abrasive ice loading depends on ice velocity (v_{ice}) and Angle of Contact (α) (AoC). The paper distinguishes Region I: ‘Crushing and extrusion’ ($\alpha \approx 0^\circ$), Region II: ‘Stick-slip’ ($0^\circ < \alpha < 90^\circ$) and region III: ‘Slip’ ($\alpha \approx 90^\circ$).
- Region I: ‘Crushing and extrusion’ experience the highest level of abrasion from all regions.

On adhesion:

- The component of local static bonding during a sliding test on the high performance concrete sample can be up to half of the compression force.
- Adhesion introduces a cyclic load on the concrete surface due to stick-slip under low ice velocities (v_{ice})
- The stick-slip cycle depends on real contact area. Ice fracture and spalling reduces adhesion bonding due to reduction of real contact area.
- The areal size of region II: ‘Stick-slip’ reduces with increasing ice velocity (v_{ice})
- Static bonding increases with decreasing concrete surface roughness. Surface characteristics of concrete like roughness depend on concrete mixture composition, for example cement type or additives like silica fume.

On micro scale processes:

- Secondary order abrasive ice loading only becomes of importance on long sliding distances, which is often the case with lifetime design in offshore structures.
- Frictional heating in combination with contact pressure significantly increases the temperature of the ice-concrete interface. The local temperature gradients can affect the character of the local shear loading (hydrodynamic flow versus granular solid flow)
- Frictional heat generation introduces local thermal stresses within the concrete surface and reduces the abrasion resistance.
- The ice surface material crushes and recrystallizes an ice-concrete mixture during interaction.
- The ice roughness increases due to enclosure of concrete particles in the ice surface.
- The high performance concrete sample shows a better abrasion resistance than the low performance concrete sample, most likely due to an improved binding strength due to the addition of silica fume.

Thus, the experimental setup is able to provide valuable data on microscopic processes. The authors refer for the interested reader to the underlying master of science thesis (Tijsen J., 2015) for more details.

ACKNOWLEDGEMENTS
The authors are thankful to the STePS^2 group within Memorial University Newfoundland (MUN) for funding. Second, to the team of lab technicians of MUN to provide best support possible in building and operating the tests. Last, appreciation goes to the Arctic group within Delft University for providing fruitful discussion on underlying master thesis work.

REFERENCES

- Bekker A. et al., 2003, Abrasion Effect of Ice Cover on Supports of Hydraulic Engineering Structures in Conditions of Sakhalin Island Shelf, Proceedings of the Thirteenth International Offshore and Polar Engineering Conference
- Bekker A. et al., 2011, Experimental Study of Concrete Resistance to Ice Abrasion, Proceedings of the Twenty-first International Offshore and Polar Engineering Conference
- Bruneau S. et al., 2013, Laboratory indentation tests simulating ice-structure interactions using cone-shaped ice samples and steel plates, Proceedings of the 22nd International Conference on POAC'13.
- Dragt R., 2013. The collision of cone-shape ice samples against steel plates of varying surface roughness, chapter 2. Submission of master of science thesis to the Delft University of Technology, The Netherlands
- Hara F. et al., 1995, Prediction of the degree of abrasion of Bridge Piers by Fresh water ice and the Protective
- Huovinen S., 1990, Abrasion of Concrete by Ice in Arctic Sea, Rakenteiden mekani ikka, Vol. 23 No. 1 1990 s. 23-35
- Huovinen S., 1992, Abrasion of Concrete Structures by Ice, Cement and Concrete Research, Vol. 23, p. 69-82
- Itoh Y. et al., 1988, An Experimental Study on Abrasion of Concrete Due to Sea Ice, OTC
- Jacobsen S. et al., 2012, Concrete Destructure due to Ice-Indentation Pore Pressure, Proceedings of the Twenty-second International Offshore and Polar Engineering Conference

- Janson J., 1987, Results from the winter seasons 1988 – 1989. Conclusion after the three winters 1986 – 1989. Joint Industry Study, Field investigation of Ice Impact on Lightweight Aggregate Concrete
- Janson J., 1989, Report of field investigation of ice impact on lightweight aggregate concrete – results from the winter season 1986 -1987, VBB, Stockholm, Sweden
- Jordaan I., 2001, Mechanics of ice-structure interaction, Elsevier – Engineering Fracture mechanics 68.
- Mackey T. et al., 2007, Experiments on the fracture of polycrystalline ice. Proceedings of POAC 2007
- Masterson D. et al., 1993, Description of multi-year ice indentation tests at Hobson's choice ice island, Proceedings, 12th International conference on offshore mechanics and arctic engineering, vol. 4, Glasgow, p. 145-55
- Saeki H., 2010, Mechanical Properties between Ice and Various Materials Used in Hydraulic Structures: The Jin S. Chung Award Lecture, International Journal of Offshore and Polar Engineering Vol. 21, No. 2, pp. 81 – 90
- Tijsen J. et al., 2013, Use of Thermal Imagery to assess Temperature Variation in Ice Collision Processes, Proceedings of the ICETECH'13 conference.
- Tijsen J., 2015, Ice-concrete abrasion, Submission of a master of science thesis to the Delft University of Technology, The Netherlands.